UNIVERSITÀ
DEGLI STUDI
DI PADOVA

Sede Amministrativa: Università degli Studi di Padova

Dipartimento di Principi e Impianti di Ingegneria Chimica (DIPIC)

SCUOLA DI DOTTORATO DI RICERCA IN : Ingegneria Industriale
INDIRIZZO: Ingegneria Chimica
CICLO: XXII

ENGINEERING THE REACTION OF HYDROGEN PEROXIDE DIRECT SYNTHESIS

Direttore della Scuola: Ch.mo Prof. Paolo Bariani
Coordinatore d'indirizzo: Ch.mo Prof. Alberto Bertucco
Supervisore: Ch.mo Prof. Paolo Canu

Dottorando : Pierdomenico Biasi

Index

Chapter 2

Experimental Reactors and preliminary data

Chapter 3

Batch and semi-batch reactors data and modelling

Chapter 4

Direct Synthesis of hydrogen peroxide in a Trickle Bed Reactor (TBR).

Chapter 5

Direct Synthesis of hydrogen peroxide in a Trickle Bed Reactor (TBR): comparison among Pd-based catalysts

Chapter 6

Direct Synthesis of hydrogen peroxide in a Trickle Bed Reactor (TBR): bimetallic catalysts and H_2 concentration

Chapter 7

Conclusions and future perspectives

Appendix

Vapor-liquid equilibrium in multi-component systems

Foreword

This work was made possible thanks to many people and institutions that the author would like to gratefully acknowledge. Part of the research activity was carried out at the Department of Chemical Engineering Principle and Practice (DIPIC), University of Padova, Italy, under the supervision of Prof. Paolo Canu, to whom great esteem and consideration goes. Experimental studies were also conducted at the Åbo Akademi Process Chemistry Centre, Turku, Finland, under the supervision of Prof. Tapio Salmi, precious advisor and life teacher. Financial support during the staying in Finland from Åbo Akademi Foundation (Johan Gadolin Scholarship) is gratefully acknowledged.
Valuable help and advices were received by many people during the development of this project, particularly: Dr. Kari Eränen, Prof. Dmitry Murzin, Prof. Francesco Pinna and Dr. Federica Menegazzo, Dr. José Hernandez Carucci, MSc. Nicola Gemo, and Lucio Gelmi.

Abstract

Hydrogen peroxide (H_2O_2) is a versatile environmentally friendly oxidizing agent that has many practical applications. H_2O_2 has countless qualities and it is one of the world's most important bulk inorganic chemicals. Most of the world's H_2O_2 is produced by auto-oxidation process (AO). The AO process involves indirect oxidation of H_2 to yield H_2O_2. The first commercial anthraquinone (AQ) process was operated by I.G. Farbeinindustrie in Germany during the second world war. The AO process is successfully used to produce most of the world's H_2O_2 because it avoids explosive H_2/O_2 gas mixture.

However AO process suffers from several drawbacks, such as the use of a complex and toxic solvent system, the periodic replacement of costly quinone-derivative due to non-selective hydrogenation, the deactivation of the hydrogenation catalyst, high requirements of energy and intensive process steps for the removal of organic impurities. Also, it is known to have high capital and operating costs, thus it economically viable only for large scale productions (>4*104 tons per year). Therefore, H_2O_2 is produced in few locations and then transported to the customers. Transportation of H_2O_2 creates additional safety concerns since concentrated H_2O_2 can decompose explosively.

A process where H_2O_2 forms from the direct combination of its elements (H_2 and O_2) could be preferred, especially for small scale productions at the end-user site, if control of the sequential hydrogenation can be achieved, but none of the presently available processes has solved the productivity vs. safety dilemma.

Traditionally, the attention of the scientists focused on the identification of an active and particularly selective catalyst, overlooking the impact of safety and multiphase issues. Both aspects may benefit from continuous operations and suitable feeding policies, along with kinetics studies as we are currently investigating.

Three reactor set-ups were developed and realized for hydrogen peroxide direct synthesis: two of them are based on batch reactors of different size to perform catalytic tests and kinetics studies, and one is based on a trickle bed reactor (TBR).

Most of the work presented here is focused on the continuous reactor, far more attractive from an industrial perspective. In the TBR set up different catalysts were chosen to investigate H_2O_2 direct synthesis. A systematic study on operative conditions was performed, varying liquid and gas flow rates (contact time between liquid, gas and solid phases), changing H_2/O_2 ratio, investigating conditions for H_2O_2 decomposition and the effect of pressure. With this work very high values of selectivity were achieved (up to 90%), much improving catalytic performances of the same catalyst compared to those previously obtained in batch reactors. The best results were accomplished with a Pd and Au catalyst supported on sulfated zirconia.

Despite an extensive body of research on the direct synthesis process, very little has been published about kinetic rate expressions of the full reaction network, and in this study experimental kinetics in a batch reactor and their relative modeling are treated for the first time.

Sommario

Il perossido di idrogeno è un ossidante “verde” e non tossico, che non genera sottoprodotti inquinanti per l’ambiente, poiché si decompone a dare solamente acqua ed ossigeno.
Il perossido di idrogeno viene utilizzato principalmente nelle cartiere come sbiancante, nell’industria tessile e metallurgica, come intermedio nella sintesi chimica, come disinfettante e additivo per detergenti, e molto altro.
L’H_2O_2 viene attualmente prodotto con il processo dell’antrachinone, il quale necessita di numerose operazioni per la produzione e la purificazione del prodotto finale, con il conseguente elevato consumo energetico, a cui sono associati notevoli costi di esercizio, e la formazione di sottoprodotti inquinanti.
La sintesi diretta di H_2O_2 è un’alternativa interessante, che si propone di eliminare i sottoprodotti inquinanti e ridurre drasticamente i costi di impianto e di esercizio, per produzioni su piccola scala direttamente in situ presso l’utilizzatore finale. In questo modo sarebbe possibile abbattere anche i costi di trasporto e i rischi ad esso connessi.

Negli ultimi anni particolare attenzione è stata data al processo di sintesi diretta di acqua ossigenata, tuttavia i lavori pubblicati e brevettati vertevano per lo più sullo sviluppo di un catalizzatore che potesse avere delle caratteristiche tali da favorire la formazione di perossido di idrogeno a dispetto delle reazioni di decomposizione e idrogenazione dello stesso, anch’esse facenti parte del network di reazione. Scarso interesse è invece stato rivolto allo studio sistematico delle condizioni operative e allo sviluppo di un processo continuo. Ad esempio, lo studio in reattori batch non è stato mai approfondito con cinetiche di reazione e con lo studio degli equilibri liquido-vapore che si instaurano all’interno del sistema di reazione.

In questo lavoro sono stati sviluppati e realizzati due reattori di tipo batch (di due volumi differenti) e un reattore in continuo: dei due reattori batch, uno è stato utilizzato per testare i catalizzatori e condurre studi preliminari, mentre nell’altro si sono svolti

studi di cinetiche di reazione, che sono stati successivamente utilizzati per sviluppare un primo modello cinetico basato su un'ipotesi di meccanismo superficiale dettagliato. Il reattore continuo, invece, è un reattore a letto fisso con 2 fasi fluide (trickle bed reactor) costantemente alimentate. Solo un operazione in continuo può favorire uno sviluppo industriale. Al tempo stesso, opernado in continuo si possono ottenere prestazioni anche molto diverse (e migliori) che in batch. Perciò in questo progetto è stata data particolare attenzione allo sviluppo di un tale processo, ottimizzandone le condizioni operative per massimizzare la produzione di acqua ossigenata. Numerosi catalizzatori mono- e bi-metallici sono stati studiati, supportati su diversi materiali, sia inorganici che organici, e per ognuno di essi sono state studiate le migliori condizioni operative, che in alcuni casi hanno portato ad ottenere un evidentissimo aumento di prestazioni rispetto al reattore batch, con lo stesso catalizzatore.

Nel Capitolo 1 è presentato lo stato dell'arte della ricerca sulla sintesi diretta del perossido di idrogeno, e viene spiegato come la ricerca effettuata fin d'ora abbia posto l'attenzione sullo studio di un catalizzatore che potesse essere adatto alla sintesi diretta, dando meno importanza allo studio reattoristico.
Nel Capitolo 2 è descritto lo sviluppo dei reattori in seguito utilizzati nella sperimentazione, ed i sistemi di analisi implementati. Vengono presentati gli schemi di impianto e gli studi preliminari condotti sia sui reattori batch, che sul reattore continuo.
Il Capitolo 3 illustra risultati ottenuti in bacth, si formula un modello cinetico di cui si dà una prima applicazione, calibrando i parametri cinetici sui dati disponibili.
Nel Capitolo 4 si è studiato un catalizzatore al palladio su un supporto di ceria sulfatata, con il quale sono stati condotti esperimenti di decomposizione e idrogenazione del perossido di idrogeno. Partendo da questi risultati si è svolto uno studio teso ad identificare le migliori portate di gas e di liquido per ottenere la massima produttività e la massima selettività. Un'altra condizione operativa indagata è stata la pressione ed il suo effetto sulla produzione di acqua ossigenata.
Nel Capitolo 5 sono stati studiati nel reattore continuo 4 catalizzatori a base di palladio, supportati su diversi materiali inorganici. Variando le condizioni operative di sistema si è studiato il comportamento di questi catalizzatori in relazione alla produzione di H2O2 e alla loro selettività. I diversi catalizzatori, a seconda del supporto, hanno proprietà differenti e le condizioni operative ottimali sono distinte.
Il Capitolo 6 tratta lo studio di catalizzatori bimetallici a base di palladio e oro e catalizzatori a base di solo palladio. Diversi supporti inorganici sono stati utilizzati ed è stato introdotto un nuovo supporto organico. I catalizzatori sono stati studiati in reattore

continuo, variando le condizioni operative. È stato inoltre studiato l'effetto della concentrazione di idrogeno immesso come reagente e la sua influenza sulla sintesi diretta di H2O2.
Il Capitolo 7 riassume i migliori risultati ottenuti e fornisce indicazioni relativamente agli sviluppi futuri.
In Appendice è descritto un approccio per la modellazione termodinamica del sistema gas-liquido.

Chapter 1

Introduction

1.1 Green chemistry

Green chemistry is an effective approach for environmental protection which involves the entire product life-cycle, from its design to the application and waste disposal or recycling.

Green chemistry consists of environmentally friendly, sustainable chemicals and processes that result in reduced waste products, improved efficiency (high atom economy, low E-factor), and less hazard to human health and the environment. Green chemistry encourages research and innovation, and promotes those products and processes that attempt to reduce the environmental impact and also are economically sustainable.

The term 'green chemistry' was coined by Paul Anastas in 1991, and later himself and John Warner published the 12 Principles of Green Chemistry (Anastas, Warner, 1998), which provide practical guidelines to implement green chemistry both on a research and industrial level:

1. *Prevention*
   It is better to prevent waste than to treat or clean up waste after it has been created.
2. *Atom Economy*
   Synthetic methods should be designed to maximize the incorporation of all materials used in the process into the final product.
3. *Less Hazardous Chemical Syntheses*
   Wherever practicable, synthetic methods should be designed to use and generate substances that possess little or no toxicity to human health and the environment.
4. *Designing Safer Chemicals*
   Chemical products should be designed to effect their desired function while minimizing their toxicity.

5. *Safer Solvents and Auxiliaries*
   The use of auxiliary substances (e.g., solvents, separation agents, etc.) should be made unnecessary wherever possible and innocuous when used.
6. *Design for Energy Efficiency*
   Energy requirements of chemical processes should be recognized for their environmental and economic impacts and should be minimized. If possible, synthetic methods should be conducted at ambient temperature and pressure.
7. *Use of Renewable Feedstocks*
   A raw material or feedstock should be renewable rather than depleting whenever technically and economically practicable.
8. *Reduce Derivatives*
   Unnecessary derivatization (use of blocking groups, protection/ deprotection, temporary modification of physical/chemical processes) should be minimized or avoided if possible, because such steps require additional reagents and can generate waste.
9. *Catalysis*
   Catalytic reagents (as selective as possible) are superior to stoichiometric reagents.
10. *Design for Degradation*
    Chemical products should be designed so that at the end of their function they break down into innocuous degradation products and do not persist in the environment.
11. *Real-time analysis for Pollution Prevention*
    Analytical methodologies need to be further developed to allow for real-time, in-process monitoring and control prior to the formation of hazardous substances.
12. *Inherently Safer Chemistry for Accident Prevention*
    Substances and the form of a substance used in a chemical process should be chosen to minimize the potential for chemical accidents, including releases, explosions, and fires.

1.2 Hydrogen peroxide

Hydrogen peroxide is considered an inherently green oxidant, one of the cleanest, most versatile chemical oxidants available, since it decomposes to yield only water and oxygen as the reaction products. H_2O_2 is also one of the most efficient oxidizing agents by virtue of its high active oxygen content (about 47%), only next to molecular oxygen.

Hydrogen peroxide was discovered by the French chemist Louis-Jacques Thenard in 1818. Since then to the beginning of the 20th century, 3% H_2O_2 solutions were obtained from the hydrolysis of barium peroxide with sulfuric acid. Several alternative processes, such as electrochemical and chemical (oxidation of isopropanol or methylbenzyl alcohol, or antraquinone oxidation) processes have been developed and are available for the production of H_2O_2.

1.2.1 Uses

Hydrogen peroxide is a versatile oxidant that is effective over the whole pH range with a high oxidation potential (Eo=1.763 V at pH 0, Eo=0.878 V at pH 14) (Campos-Martin 2006).
It is an effective, nonpolluting oxidizing agent, with a wide variety of applications in different fields: (1) Wastewater treatment, (2) Pulp/paper bleaching, (3) Textile industry, (4) Chemical synthesis, (5) Detergents, (6) other uses (metallurgy, electronics -semiconductors, propulsion -satellite and rockets, food etc.).

1.2.1.1 Wastewater and sludge treatment

Hydrogen peroxide is a versatile chemical that can be used in the treatment of a wide variety of industrial wastes and wastewaters, for example for the removal of hydrogen sulfide (H_2S), which forms in sewer pipes. Cyanide, thiocyanate, nitrite, chloride, hypochlorite, and organic matter can be efficiently removed by H_2O_2 treatment (Kosaka 2001). Hydrogen peroxide is also used as a source of hydroxyl radicals in more complex advanced oxidation processes. Hydroxyl radicals are, after fluorine, the second most powerful oxidant available. Oxides of nitrogen and sulfur, mercaptans, and several other toxic odorous components of waste gases can be removed by oxidation with hydrogen peroxide. Hydrogen peroxide can be used as a source of oxygen in the biological treatment of bulking sludges, and for the prevention of denitrification in settling tanks. Hydrogen peroxide has recently been implemented in the in situ bioremediation of contaminated soils. This process combines the injection into the ground of microorganisms and enzymes with hydrogen peroxide as a source of oxygen, saving removal/replacement costs and minimizing worker exposure.

1.2.1.2 Pulp bleaching

One of the most important applications of hydrogen peroxide is its use in pulp and paper bleaching (Hart 1998). It replaces chlorine-based bleaches and therefore avoids halogenated products in waste streams. Alkaline conditions are required to generate the active bleaching species from H_2O_2, the perhydroxyl anion, which improves delignification eliminating various chromophores in the lignin structures, allowing bleaching of chemical pulp to full brightness. For mechanical pulps, where the lignin content is higher, the usual approach is the employment of H_2O_2 together with caustic soda as alkali source, sodium silicate for stabilization and buffering, and a chelant for the sequestering of metal traces in the wood pulp. As well as for colored lignin residues in chemical and mechanical pulp, hydrogen peroxide is also used in the bleaching of recycled paper to increase its brightness. For this process, a combination of H_2O_2 and reductive bleaching steps with sodium dithionite are employed to remove the printing dyes.

1.2.1.3 Textile industry

Hydrogen peroxide is widely used as a bleaching agent in the textile industry as a substitute for hypochlorite and other bleaching agents, especially for the bleaching of cotton and linen (Jones 1999). Hydrogen peroxide acts by creating active oxygen. It has advantages over other alternatives such as sodium hypochlorite and sodium hydrosulfite in that it is suitable for continuous processing, has no severe toxicity or effluent problems, and creates no harmful by-products.

Color-safe laundry bleaches containing hydrogen peroxide have increasingly replaced bleaches containing hypochlorite. In this case, the hydrogen peroxide is used with stable precursors such as sodium percarbonate and sodium perborate, which release hydrogen peroxide when dissolved in water.

1.2.1.4 Chemical synthesis

Hydrogen peroxide is a powerful and environmentally friendly oxidizing agent, with numerous applications in the chemical industry. Due to its low molecular weight, hydrogen peroxide is a more efficient oxidizing agent pound per pound than other common oxidizers, like potassium dichromate or permanganate. It is used in the manufacture of many organic and inorganic chemicals, for example, hydrazine, cyanogen, cyanogen chloride, bromine, iodic acid, high-purity ferric sulfate, perborates, and percarbonates. Typical applications in organic synthesis include

oxidation (Tanev 1994), epoxidation (propene oxide), hydroxylation (plasticizers and stabilizers, aromatic diphenols), oxohalogenation (flame retardants) (Ligtenbarg 2003), and initiation of polymerization reactions (MEK peroxide, benzoyl peroxide, lauryl peroxide). Another interesting use of hydrogen peroxide is for the synthesis of caprolactam, with a process originally developed by EniChem (now Syndial) and commercialised by Sumitomo in 2003 at its Ehime plant in Japan, where cyclohexane is reacted with ammonia and hydrogen peroxide at around 90°C in the presence of a titanosilicate catalyst (Kitamura 2001).

Degussa/Uhde's advanced propylene epoxidation, known as hydrogen peroxide–propylene oxide (HPPO) process, is a single step process with water as the only by-product (Hass 2004). Propylene oxide (PO) is a starting material for polyurethane and also used to produce solvents, chemical intermediates, flame retardants, synthetic lubricants, and textile surfactants. BASF and Dow Chemical have also announced to produce propylene oxide by the HPPO-process.

H_2O_2 would become the ultimate green reagent for the manufacture of many oxygenated fine/bulk chemicals, if its cost of production is reduced than the current process based on antraquinone oxidation.

1.2.1.5 Detergents and disinfectants

Detergent or bleach compositions formulated with sodium percarbonate/perborate have strong stain-removal capabilities, are color safe, and do not lead to yellowing or darkening of the fabric, as opposed to bleaches containing hypochlorite (Campos-Martin 2006).

Among other applications, hydrogen peroxide is used as a disinfectant (commonly as a 3% solution by weight). It is used to treat inflammation of the gums, to clean wounds and to disinfect drinking water. It is also used against excessive microbial growth in water systems and cooling towers.

Hydrogen peroxide is also widely used as a sterilizing agent for drinks, milk etc. The most common process comprises sterilization with concentrated hydrogen peroxide by either immersion-bath or spray method.

1.2.1.6 Other uses

Hydrogen peroxide is involved in a number of applications in mining and metal processing (Jennings 2000). Typical applications in this field include the extraction and purification of uranium, gold recovery, the extraction and separation of

chromium, copper, cobalt, tungsten, molybdenum, and other metals, and metal finishing (etching, stainless steel pickling, non-ferrous metal finishing).
High-purity hydrogen peroxide is used in the electronics industry for the pickling of metal surfaces as well as for the cleaning of silicon wafers in the production of printed circuit boards (Jones 1999). For various electronic and semiconductor applications, high purity hydrogen peroxide is available with total cationic impurity levels below 10 ppb , 1 ppb, 0.1 ppb, and 0.01 ppb.
Hydrogen sulfide, S-containing hydrocarbons, nitrogen oxides, and sulfur dioxide can be removed by hydrogen peroxide from exhaust gases generated in chemical and pharmaceutical syntheses, the production of graphite, titanium dioxide, and sulfuric acid, as well as in the combustion of sulfur-containing fuels.
As a propellant, current uses include hypergolic bi-propellant engines for low-cost launch vehicles, mono-propellant systems to power satellites or helicopters and land-based and submarine applications.

1.2.2 Transport and storage

Hydrogen peroxide can decompose exothermally in the presence of certain catalytically acting impurities, to give oxygen and water.
The stability of hydrogen peroxide solutions is influenced primarily by the temperature, the pH value, and importantly by the presence of impurities with a decomposing effect.
High temperature as well as a high pH value promote the decomposition of H_2O_2. Above pH 5, the decomposition of pure H_2O_2 increases sharply.
The shelf life of hydrogen peroxide is negatively affected by impurities of every type even at very low concentrations (ppm quantities). The decomposition can be induced homogeneously by dissolved ions such as heavy metals like iron, copper, manganese, nickel, and chromium. Hydrogen peroxide is also decomposed through the effect of light as well as by certain enzymes, namely catalase.
Stabilizers are usually added to protect hydrogen peroxide against unavoidable impact during handling and transport.
Hydrogen peroxide of a concentration of less than 8% by wt. is not subject to any transport regulations.
Usually hydrogen peroxide is available in three common concentrations (35, 50, and 70% by wt. aqueous solutions). While transportation costs of hydrogen peroxide decrease with increasing concentration, for the handling of hazards (severity of tissue burns and ease of ignition of combustibles), the costs increase with increasing concentration. Technical grade hydrogen peroxide is stabilized with low levels of tin

based stabilizers and phosphates. Organic based stabilizers are used in hydrogen peroxide grades destined for use in organic synthesis reactions due to possible interference that inorganic stabilizers can cause in some types of metal treatment and for electronic uses.

Another important characteristic of H_2O_2 solutions to be taken into account when handling them, is that they are nonflammable but can ignite flammable materials.

In relation to H_2O_2 storage, only certain materials that do not promote the catalytic decomposition of hydrogen peroxide are suitable for the construction of container and storage equipment. Typically, as construction material for storage tanks, aluminium, polyethylene (up to 60% by wt. H_2O_2) or stainless steel are used.

Hydrogen peroxide is also usually protected from the sunlight and kept cool in roofed, fireproof rooms.

For piping, stainless steel and PVC have proved most safe and effective.

1.2.3 Production

The annual world production of hydrogen peroxide is approximately 2.2 million metric tons, and its demand is growing at a steady pace of around 4% per annum (Campos-Martin 2006). The market is dominated primarily by two companies, Solvay and Degussa, with a share of about 30% and 20% of the market, respectively. Two other companies, FMC and Arkema, own a share above 10%, while all the others are present with a lower share.

The use distribution of hydrogen peroxide is shown in Figure 1.1, but it depends on the market region. The two major areas of application in Europe are chemical synthesis, mainly in detergent manufacturing (43%), and pulp and paper bleaching (41%). The increasing interest on the integrated HPPO (hydrogen peroxide–propylene oxide) process, in which the hydrogen peroxide required for the epoxidation of propylene is produced on site, should lead to a relevant growth in the use of hydrogen peroxide for chemical syntheses .

As well as in Europe, the major areas in Japan are pulp and paper bleaching and chemical synthesis. An increasing use of hydrogen peroxide for chemical synthesis in Japan arises from the implementation of Sumitomo's route to caprolactam. The situation in the US is slightly different. The hydrogen peroxide market is dominated by the pulp and paper bleaching (about 59%), while organic and inorganic synthesis represent only 13% and electronics applications take up approximately 5%.

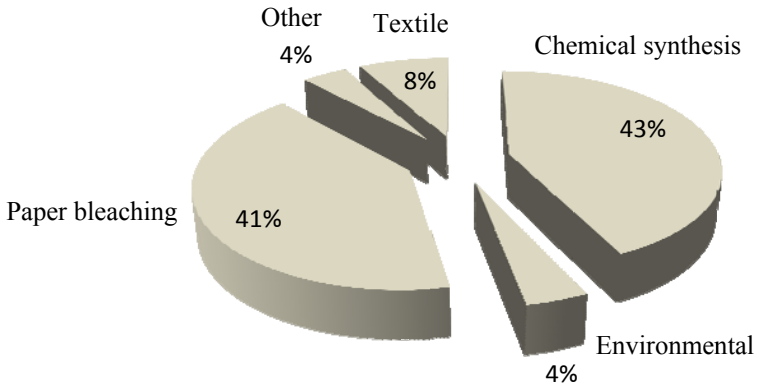

Fig. 1.1. H_2O_2 use worldwide for year 2008.

1.2.3.1 Anthraquinone oxidation (AO) process

Hydrogen peroxide is currently produced almost exclusively with the anthraquinone oxidation (AO) process, which accounts for around 95% of the global H_2O_2 production. The indirect anthraquinone process, developed by Riedl and Pfleiderer in 1939 (Reidl 1939), and introduced by IG Farbenindustrie in Germany in the 1940s, involves the hydrogenation of an anthraquinone derivative (typically 2-ethylantraquinone) using a nickel or palladium catalyst, forming the diol. The subsequent oxidation of anthraquinol with air (or oxygen-enriched air) gives the original anthraquinone back, and produces H_2O_2.

This process was developed from a previous work by Manchot, who noted in 1901 that hydroquinone and hydrazobenzenes undergo auto-oxidation under alkaline solutions producing peroxides.

The hydrogen peroxide obtained with the AO process is then purified and concentrated, and is usually marketed with an added stabilizer as aqueous solutions at concentrations of 35, 50, and 70% by weight.

During the last decades, after the introduction of the original AO process, important improvements were made in each of the four major steps: hydrogenation, oxidation, hydrogen peroxide extraction, and treatment of the working solution. A simplified flow diagram of the process steps is given in Figure 1.2.

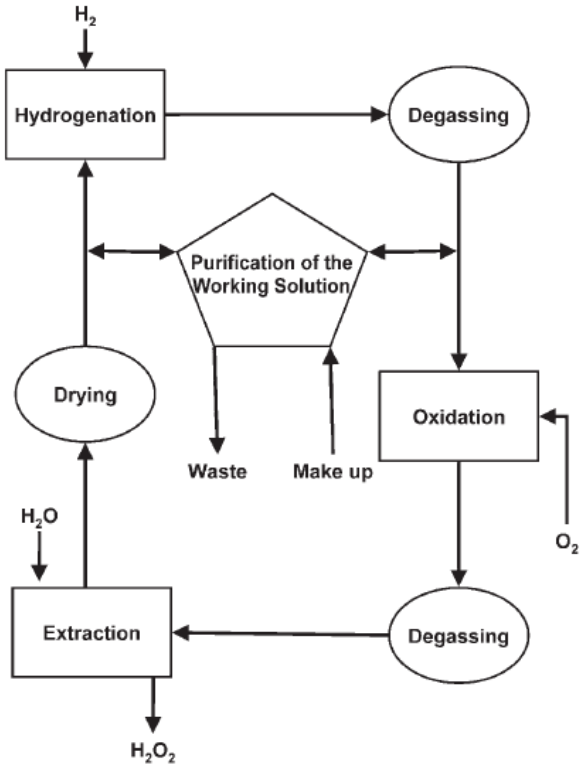

Fig. 1.2. Block diagram of the steps involved in the AO process.

The main reactions involved are shown in Figure 1.3. A 2-alkylanthraquinone (AQ; usually 2-ethylantraquinone) in an appropriate solvent is hydrogenated catalytically to anthraquinol or anthrahydroquinone (AHQ). Unfortunately, a side reaction also occurs, which is the hydrogenation of the aromatic ring with no functional groups to give 5,6,7,8-tetrahydroanthrahydroquinone. The solution containing the AHQ is recovered and then oxidized with air to give the original anthraquinone back, and at the same time produce equimolar amounts of hydrogen peroxide. Demineralized water is used to strip the product from the working solution in a countercurrent column, usually giving a 30% wt. solution of H_2O_2. The aqueous H_2O_2 solution is then distilled to remove impurities and increase the concentration to as high as 70%, and the anthraquinone is recycled. However, many other side reactions can occur during this process, causing a net consumption of the original amount of anthraquinone.

The major advantage of the AO process is the very high yield of hydrogen peroxide, but several disadvantages are also present.

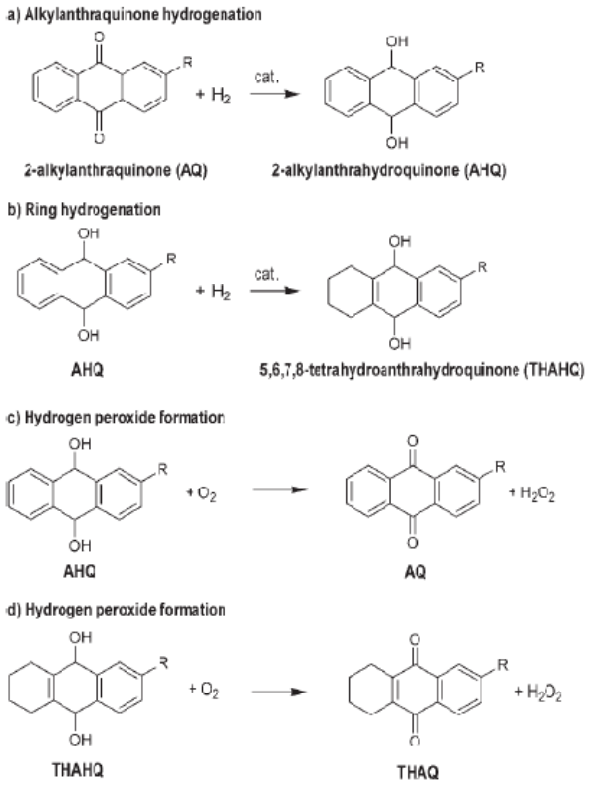

Fig. 1.3. Reactions involved in the AO process.

1.2.3.2 Major drawbacks of the AO process

The AO process has replaced almost completely the other H_2O_2 production processes (primary and secondary alcohol oxidation, electrochemical) and currently accounts for more than 95% of the world's production of H_2O_2. With the AO process H_2O_2 is produced continuously at mild temperatures and safety issues are minor since direct contact of O_2 and H_2 is avoided. However, the AO process has several drawbacks, including mass-transport limitations in the hydrogenation and oxidation steps, organic contamination of H_2O_2 during its recovery by liquid–liquid extraction. The difficulty in controlling the H_2/AQ ratio and the AQ residence time during the hydrogenation step causes by-products formation, such as overhydrogenated AQ, that has to be constantly removed. A further problem is that the partition coefficient of H_2O_2 between water and the organic phase is not the most favorable, therefore distillation of both the concentrated and purified H_2O_2 is required, which makes the process significantly energy intensive.

1.2.3.3 Direct synthesis and other alternatives

Now an increasing number of processes (from chemical to environmental applications) would benefit from a small on site H_2O_2 production, eliminating transport costs and avoiding the hazards connected to the transport of concentrated H_2O_2 solutions. A further advantage is that a highly pure H_2O_2 can be used, since the presence of stabilizers necessary for the transport is not needed.

The AO process is currently being used for large scale production, but for on site smaller productions alternative ways are being explored.

One possible route to H_2O_2 synthesis that avoids the use of AQ is the direct synthesis from hydrogen and oxygen in the presence of a catalyst. A real improvement in H_2O_2 chemistry would be a one-pot process involving the atom efficient direct synthesis of H_2O_2 from its elements, and its immediate application in a subsequent reaction.

This process is described in details in the following section.

Another alternative for producing hydrogen peroxide is the partial oxidation of primary or secondary alcohols, which yields also an aldehyde or ketone as the coproduct (Harris 1949). From 1957 to 1980 Shell Chemical employed this process, with the 2-propanol being oxidized by an oxygen-enriched gas stream at temperatures ranging from 90 to 140°C at a pressure of 10–20 bar. The formation of by-products is limited by keeping the isopropyl conversion below 15%, and the reaction is performed in a series of oxidative steps at decreasing temperatures. The reaction tank is usually made up of passivated steel to avoid the decomposition of the hydrogen peroxide being formed. After the oxidation, the solution containing residual 2-propanol and acetone is passed through an evaporator to collect the hydrogen peroxide produced. Acetone and 2-propanol are then recovered by distillation . The hydrogen peroxide produced by alcohol oxidation shows a poorer quality in comparison to that from the AO process, because of the high solubility of the alcohol in the peroxide containing solution.

Lyondell Chemical and Repsol QuNmica developed in parallel a process for the production of hydrogen peroxide from methylbenzylalcohol (MBA). A catalyst is usually not required for the oxidation of MBA. Typical operative conditions are 120-180°C and 3-10 bar. They declare to achieve with such a process a conversion of 32% and a selectivity for H_2O_2 of 97%, with a hydrogen peroxide content in the final solution of about 7.5% (Leyshon 1993). The latter is then purified and concentrated through extraction and distillation. The distillate is subsequently hydrogenated for the conversion of acetophenone back into methylbenzylalcohol, which is then recycled.

Hydrogen peroxide can also be synthesized by electrolysis of a NaOH containing solution (Dow process). The anodic and cathodic reactions are as follows:

Anode : $2OH^- \rightarrow H_2O + ½O_2 + 2e^-$

Cathode : $H_2O + O_2 + 2e^- \rightarrow HO_2^- + OH^-$

Complete reaction : $NaOH + ½O_2 \rightarrow HO_2Na$

The peroxide is synthesized at an H_2O_2/NaOH weight ratio of 1:1.7 by cathodic reduction of oxygen. The cathode is made up of graphite coated with carbon black, and a fluorocarbon binder to enhance O_2 transfer (Foller 1995). A cell operating at 2.3 V and 62 $mAcm^{-2}$ yields an NaOH/HO_2^- weight ratio of 1.6–1.8:1 at a current efficiency of 90%.

If an ion-exchange membrane is associated, a 2.1%w/w HO_2^- solution in 5.0%w/w NaOH with 95% current efficiency can be achieved (Henricson 1993). This process is more appropriate for pulp bleaching, for example, that is for applications where separating the peroxide from the sodium hydroxide is not required.

A novel method of H_2O_2 synthesis employing H_2/O_2 fuel-cell system has been explored recently (Yamanaka 2003). It is an electrochemical process in which reduction of O_2 to H_2O_2 takes place at the three-phase boundary: gaseous O_2, aqueous electrolyte, and solid cathode. The major advantages are that explosion hazards associated with the direct mixing of H_2 and O_2 is eliminated since O_2 and H_2 are separated by a membrane and also, generation of electric power together with H_2O_2 formation is achieved, but the process is still far away from the commercial exploitation.

1.2.4 Direct synthesis

The direct synthesis of hydrogen peroxide from its elements is theoretically the most straightforward method for producing H_2O_2. As extraction of H_2O_2 is not required and the purification steps are simplified, the capital investment and operating costs are expected to be lower than those for the AO process. This alternative is of great relevance for the chemical industry, especially for in situ production and integration with other processes, such as the HPPO process. The direct synthesis of H_2O_2 on site allows the costs and hazards associated with the transport and handling of concentrated hydrogen peroxide solutions to be considerably reduced or eliminated. Both academia and industry have investigated the direct synthesis particularly over the past 30 years, and a significant amount of patents are being issued continuously. However, there are still productivity and safety issues to be addressed and improved to render this process industrially applicable. Although the catalytic oxidation of hydrogen for the production of hydrogen peroxide has been known since 1914 (the first patent on the direct H_2O_2 synthesis was awarded to Henkel and Weber in 1914), little progress was made after that because of safety issues. The direct process

attracted renewed interest after 1980 due to the increased demand for H_2O_2 from the environmental perspectives. Several patents have been issued since (Pralus 1991, Chuang 1992, Van Weynbergh 1995, Germin 1996, Zhou 2001, Paparatto 2003, Hass 2004 and 2006, Parasher 2006, Rueter 2006), but no industrial application has been accomplished till date for the production of bulk H_2O_2, and this process has not yet been commercialized. If the process is developed and commercialized successfully, it would be a major breakthrough in the oxidation process technology.
The reaction:

$H_2 + O_2 \rightarrow H_2O_2$
(Eq. 1.1)
($\Delta H°298\ K$=-135.9 kJ mol^{-1}, $\Delta G°298\ K$ =-120.4 kJ mol^{-1})

is in principle the simplest method to form hydrogen peroxide but the reaction scheme is more complex because of thermodynamically favored side reactions (Figure 1.4):

a) formation of water

$H_2 + ½O_2 \rightarrow H_2O$
(Eq. 1.2)
($\Delta H°298\ K$=-241.6 kJ mol^{-1}, $\Delta G°298\ K$ =-237.2 kJ mol^{-1})

b) decomposition of hydrogen peroxide

$H_2O_2 \rightarrow H_2O + ½O_2$
(Eq. 1.3)
($\Delta H°298\ K$ = -105.8 kJ mol^{-1}, $\Delta G°298\ K$ =-116.8 kJmol^{-1})

c) reduction of hydrogen peroxide

$H_2O_2 + H_2 \rightarrow 2\ H_2O$
(Eq. 1.4)
($\Delta H°298\ K$ = -211.5 kJ mol^{-1}, $\Delta G°298\ K$ =-354.0 kJ mol^{-1})

Each of these reactions may be favored by the catalyst used, the additives in the reaction medium, and the operative conditions.

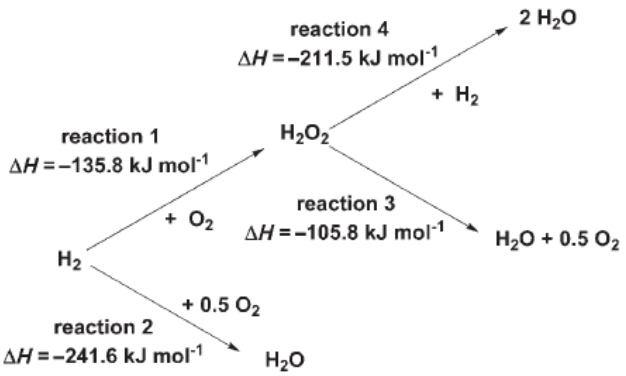

Figure 1.4. Reactions involved in the direct synthesis of H_2O_2.

The two major drawbacks in the direct synthesis of hydrogen peroxide are related to safety and selectivity. Hydrogen/oxygen mixtures are explosive for a wide range of concentrations (see Section 1.2.4.6), therefore the ratio of hydrogen to oxygen needs to be kept outside the explosive region, or an inert gas such as nitrogen or carbon dioxide must be added. This obviously reduces productivity. A way to avoid direct contact between O_2 and H_2 lies in the use of a membrane, circumventing the need of diluting with an inert gas . The other major problem resides in obtaining good selectivity for hydrogen peroxide, limiting side reactions, since normally the same catalyst that promotes H_2O_2 synthesis also induces decomposition to yield water. An appropriate solvent is also required to carry out the reaction, leading to a three-phase system (solid-catalyst, liquid-solvent, gas- H_2 and O_2) which is difficult to control and optimize.

These drawbacks, however, appear to be controllable, and a lot of attention from industry has been directed to research dealing with hydrogen peroxide direct synthesis.

1.2.4.1 Catalysts

The catalysts used in the direct synthesis of H_2O_2 are typically based on palladium. The most common supported Pd catalysts that have been used are Pd/C, Pd/SiO_2 and Pd/Al_2O_3 (Gosser 1988, 1989a, 1989b, 1992). A comprehensive list of supported Pd-based catalysts used in the direct synthesis of H_2O_2 is presented in Table 1.1.

Recently, other types of catalysts have been investigated in relation to the H_2O_2 direct synthesis, like a supported gold-containing catalyst which has proved to be effective for producing H_2O_2. In the literature there are numerous studies on the direct synthesis of H_2O_2 using gold (Au) as well as bimetallic Au–Pd alloys supported catalysts (Landon 2003). The Au catalysts supported on SiO_2, Al_2O_3, Fe_2O_3, TiO_2, H-ZSM-5 or H-Y zeolite, SiO_2–Al_2O_3, TS-1, activated carbon, MCM-

41, etc., have been used for the direct synthesis of H_2O_2. However, in most of the cases Au-only catalysts are found to be less selective and superior H_2O_2 selectivity is achieved only after the addition of a second metal to the Au catalysts. The best combination appears to be gold and palladium (with the best atomic ratio being 1:1), for which the rate of H_2O_2 production is higher than the sum of the individual monometallic systems rates. This is probably due to the isolation of the Pd atoms within the Au matrix, creating more active catalytic centers.

Considering a Pd based catalyst, the addition of a second metal, like Au, Pt, Ru or Rh can strongly affect the H_2O_2 decomposition activity of the catalyst. Rh and Ru show an increased H_2O_2 decomposition activity (Choudhary 2006a), whereas addition of a small amount of Pt efficiently increases the H_2O_2 formation selectivity.

Pd/C (Dalton 1982, 1983; Gosser 1985, 1987, 1989a; Brill 1987; Choudhary 2006, 2007)
Pd/SiO_2 (Pospelova 1961; Izumi 1976; Brill 1987; Liu 2006b; Samanta 2007c)
Pd/Al_2O_3 (Gosser 1988; Wanngangrd 1999; Burch 2003; Samanta 2007d)
Pd/TiO_2 (Kawakmi 1995)
Pd/Ga_2O_3 (Samanta 2007b)
Pd/ZrO_2 (Choudhary 2006)
Pd/CeO_2 (Samanta 2008)
Pd/ hydrophobic- hydrophilic support (fluorinated carbon) (Chuang 1992, 1993, 1998)
Pd, Pd–Pt/halogenated resin (Hiramatsu 1991)
Pd/sulfuric acid containing ZrO_2, Al_2O_3 or TiO_2 (Nagashima 1993)
Pd/H-moredenite and H-MFI zeolites (Nagashima 1993)
Pd/molybdenum oxide or tungsten oxide doped-zirconia (Nagashima 1993)
Pd/composite oxide with CeO_2 (TiO_2–CeO_2, ZrO_2–CeO_2, SiO_2–CeO_2) (Nagashima 1994)
Pd–Sn/SiO_2 (Tomita 1995)
Pd/activated carbon functionalized with sulfonic group (Paparatto 2001; Landon 2003)
Pd/zirconium phosphate viologen phosphate (Reis 1996; Thompson 1999)
Pd/hafnium phosphate viologen phosphonate (Thompson 1999; Krishnan 2000)
Pd/Hb absorbed with different organic compounds (Park 1999, 2000)
Pd and Pd–Pt/TS-1 (Meiers 1999; Danciu 2003)
Pd0, PdO/Al_2O_3 and halogenated Al_2O_3 (Gaikwad 2002; Samanta 2007d)
Pd0, PdO/fluoridated and sulphated ZrO_2, CeO_2 TiO_2, Y_2O_3 or Ga_2O_3 (Gaikwad 2002)
Pd0, PdO/ H-ZSM-5, H-GaAlMFI, Hb/HM zeolite (Choudhary 2002)
Pd, Pd–Pt/non-agglomerated uniform porous silica microspheres (Schwartz 1992, 1994)
Colloidal palladium (Dissanayake 2002, 2003)
Pd/F^-, Cl^- or Br^--doped ZrO_2 (Melada 2006)
Composite Pd-membrane (Kanada 1992; McIntyre 1996; Centi 2003)

Pd/sulphonic acid containing polystyrene resins (Brieva 2004)
Pd/functional cross-linked polymer (Burato 2006)
Pd–Pt/C, SiO_2 or Al_2O_3 (Gosser 1989b)
Pd–Au/ZrO_2 (Choudhary 2006a)
Pd–Au/a-Fe_2O_3 (Edwards 2005b)
Pd–Au/Al_2O_3 (Landon 2002, 2006; Edwards 2007)
Pd–Au/TiO_2 (Edwards 2005a)
Pd–Au/TS-1 (Landon 2003)

Table 1.1. Catalysts references

The catalysts described in the literature, which are based on noble metals, are supported on different substrates, such as silica, carbon, alumina or polymeric resins. To reduce the decomposition of hydrogen peroxide, which speeds up in alkaline conditions, acids are often added into the reaction medium (Pospelova 1961). Another alternative is the use of halides as catalyst poisons to limit water production and increase the selectivity for hydrogen peroxide (Choudhary 2006a). Phosphoric acid is often used as a hydrogen peroxide stabilizer and it also has the function of an acid. However, some disadvantages are that highly concentrated acid solutions require particular care to avoid corrosion, and the presence of acid solutions and halogen ions can cause catalyst deactivation.

For these reasons, acidic supports are often used to reduce the required concentration of inorganic acid in the medium. Examples include tungsten, molybdenum, or vanadium oxides on a zirconia substrate, supported sulfuric acid catalysts, and fluorinated alumina. However, the yield of hydrogen peroxide are quite low. In contrast, superior results have been reported with neutral solutions and heterogeneous catalysts consisting of sulfonic acid functionalized carbons or polystyrene resins (PS-SO_3H) (De Frutos 2003).

Pd based catalysts on PS-SO_3H ion-exchange resins (1.34–1.49%w/w Pd) have proved to be highly effective for the direct synthesis of hydrogen peroxide with methanol as the solvent. The high performance of these catalytic systems results from the ability of the sulfonic acid groups to stabilize the PdII ions, thus enhancing the selectivity for hydrogen peroxide.

The characteristics of the substrate are therefore of great importance for the optimization of the reaction. As such, hydrophobic substrates, like alumina, silica/alumina or zeolites coated with a polymeric layer, facilitate mass transport after hydrogen peroxide formation, limiting secondary reactions such as hydrogenation or decomposition to yield water. Fu et al. (Fu 1992) reported that Pd

deposited on hydrophilic supports is very efficient for H_2O_2 decomposition, but decomposition slowed down when Pd was supported on a hydrophobic substrate.
Another noticeable factor affecting H_2O_2 hydrogenation rate is the amount of catalyst, which has been found to proportionally increase the conversion into water. It has been demonstrated that the amount of H_2O_2 formed in the direct synthesis increased to a maximum and then gradually decreased with the catalyst amount.
Thus, catalytic H_2O_2 formation and decomposition under H_2/O_2 mixture is a very complicated process and it is extremely difficult to determine simultaneously the extent of all the reactions involved for a particular catalytic system, considering that the same catalyst that is active for H_2O_2 synthesis, is also active for its decomposition.

1.2.4.2 H_2/O_2 ratio

Since H_2O_2 is stable in presence of oxygen but unstable in presence of hydrogen towards its hydrogenation, H_2/O_2 ratio supposedly will have a significant effect on the direct synthesis of H_2O_2. Results in the literature regarding the effect of H_2/O_2 ratio on the direct H_2O_2 synthesis in commonly used solvents, though, are quite different leading to contrasting conclusions.
However, Lunsford et al. (Liu 2006b) have demonstrated that the net formation rate for H_2O_2 is first order with respect to H_2 and zero order with respect to O_2. At the larger H_2/O_2 ratios, the nonselective consumption of H_2 via the hydrogenation of H_2O_2 (formed in the reaction) becomes significant, leading to the increase in H_2 conversion and the decrease in H_2O_2 selectivity. The in situ activation of Pd catalysts towards H_2O_2 decomposition due to reductive H_2 pre-treatment also becomes significant at the larger ratios of H_2/O_2.
Interestingly, the influence of H_2/O_2 ratio on the H_2O_2 productivity and selectivity appears to be different when operating in a batch reactor with reactant gases continuously being depleted in the reaction and semi-batch or continuous mode with gases constantly entering and exiting the reactor. In a continuous trickle bed reactor, for example, or in a semi-batch reactor where H_2 and O_2 gases are continuously fed into the reactor, the ratio of H_2/O_2 in the gas-phase remains constant, while in the batch reactor the ratio of H_2/O_2 in the gas-phase of an enclosed system changes with the reaction time.

1.2.4.3 Solvents

Water provides a high level of safety, is nontoxic, nonflammable, and highly miscible with hydrogen peroxide. A major drawback though is the very low solubility of the reagent gases (H_2 and O_2) which is a great limitation in relation to hydrogen peroxide production. Some alternatives have been proposed such as, for example, a biphasic mixture of water and a fluorinated solvent, to increase the solubility of oxygen and hydrogen.

CO_2 is a more suitable solvent under both liquid and supercritical operating conditions. H_2 and O_2 are miscible with CO_2 in all proportions, and, even under subcritical conditions, the solubility of H_2 and O_2 in CO_2 is much higher than in organic solvents or water. Supercritical conditions anyway seem to overcome mass transport limitations between the gas and liquid phase. Furthermore, CO_2 is not reduced by hydrogen to form CO over a Pd catalyst at temperatures below 100°C. Noticeably, another advantage in using CO_2 is that the solubility of hydrogen peroxide in CO_2 is low, taking the product out of the solvent to form a biphasic system.

Another option is given by organic solvents, typically alcohols, that are more appropriate than water because of the greater solubility of H_2 and O_2 in them. The solubility of H_2 in alcohols is 4–5 times higher than in water while that of O_2 increases up to eightfold (H_2 in water=0.81mM; H_2 in methanol=3.96mM @25°C). Because of the higher solubility of H_2 and O_2, the mass transfer is expected to be increased proportionally in a non-aqueous solvent.

Indeed, the rate of H_2O_2 production in alcohol medium was found much higher than that in an aqueous medium (Krishnan 2000).

A systematic study on the effect of different solvents on a palladium catalyst was carried out. Methanol, ethanol, 2-propanol, dioxane, acetone, and water were compared, and differences in the rate of H_2O_2 formation were observed, with methanol being the most performant. Furthermore, organic solvents showed an enhanced H_2 conversion and H_2O_2 selectivity (Krishnan 2000). Interestingly, the rate of H_2O_2 conversion in the presence of hydrogen (secondary hydrogenation reaction to give water) in an aqueous medium was found much higher than that in methanol, even though the solubility of hydrogen is higher in methanol than in water (Melada 2006a).

To be also considered is that most oxidation processes, for which H_2O_2 can be used as the oxidizing species, are carried out in organic solvent. Thus producing H_2O_2 in methanol, for example, rather than water, would eliminate separation steps and related costs.

Also, anidrous organic media enable to measure the exact amount of water produced, allowing for accurate selectivity calculations.
Toluene and hexane have proved to be good solvents for that they increase the solubility of hydrogen and oxygen in the liquid phase, enhancing the reaction rate, but the selectivity for H_2O_2 is quite poor.
The principal role of the solvent is to increase the solubility of gases in the liquid phase, but it also has other effects. Solvents such as ethanol or acetonitrile tend to coordinate palladium and can therefore reduce side reactions that decompose H_2O_2 to form water.
All of these issues highlight the difficulty to find a suitable solvent with a good balance between several important factors, such as solubility of gases, selectivity for H_2O_2, reaction rate, catalyst activation etc. in order to accomplish a high performing process.

1.2.4.4 Thermodynamics and kinetics

The formation of H_2O_2 is favoured at low temperatures and short reaction times, while higher pressures will increase the overall rate of H_2O_2 formation (see Section 1.2.4).
A more detailed discussion on thermodynamic description and modeling for the system under investigation is presented in Appendix A.
In a chemical reaction, the rate of secondary reactions associated with the product becomes relevant with the progress of the reaction when the product starts accumulating. As concentration of H_2O_2 builds up, the decomposition and reduction of H_2O_2 become favourable. The catalyst also undergoes changes as the reaction proceeds, particularly its activity can vary. Thus, reaction duration and therefore contact times between gas, liquid and solid phases can strongly influence selectivity and productivity.
Pospelova et al. (Pospelova 1961) showed that H_2O_2 yield reached a maximum value with a short contact time and with the use of additives to prevent H_2O_2decomposition. Since a Pd catalyst also promotes H_2O_2 decomposition, high selectivity for H_2O_2 could be obtained only in a very short reaction period, under batch conditions, and reasonably with a short contact time for continuous operation.
Landon et al. (Landon 2003) showed that the extent of H_2 conversion, H_2O_2 selectivity and H_2O_2 yield strongly depends on the reaction time for their closed autoclave system, with a 0.6 wt.% Pd/sulfonated carbon catalyst. H_2 conversion increased with the reaction time, while the H_2O_2 yield increased initially and then

gradually decreased. On the other hand, H_2O_2 selectivity decreased exponentially with the reaction time.

1.2.4.5 Reactors

Typically hydrogen peroxide direct synthesis is carried out under batch or semi-batch conditions.

Recently, some new ideas are being put into practice. The use of catalytic membranes offer the potential of intrinsically safe operations, because a physical separation between H_2 and O_2 in the gas phase is established (Webb 1998; Abate 2006; Melada 2006a). Usually, the system is composed of an asymmetric tubular ceramic membrane (e.g., alumina) into which a catalyst (Pd, Pd/Au, Pd/Pt) is loaded in highly dispersed form in the porous surface layer. Hydrogen and oxygen are supplied separately on the opposite sides of the membrane, gaseous oxygen on one side and hydrogen dissolved in a solvent on the other side. This approach offers several advantages over conventional methods since it guarantees safe operation due to the separated supply of reactants, and also mass transfer limitations are reduced with an efficient contact of the gas phase with the catalyst surface. However, for H_2O_2 direct synthesis, the costs of membrane based systems are still higher than those of standard catalytic reactors, particularly in view of industrial implementation, but the benefits in terms of safety are attractive, especially for smaller scale applications.

Recently, a few studies also reported hydrogen peroxide synthesis by direct combination of H_2 and O_2 in a microreactor (Wang 2007). This is an interesting and promising new approach, but obviously it can't be scaled-up for massive productions.

Typically these microreactors are composed of a single channel coated with a supported palladium catalyst. A recent work from Voloshin et al. (Voloshin 2007) shows the first results on the role of reaction conditions. A maximum concentration of 1.3 wt% H_2O_2 was achieved.

With microreactors, direct H_2O_2 synthesis could be carried out safely even with a high concentration of hydrogen, which would be explosive in large-scale reactors, because the width of the channels is smaller than the quenching distance of hydrogen and oxygen radicals. Much higher temperatures and pressures are required to start an explosion in a microchannel than in a larger environment. With this set-up, direct synthesis is intrinsically safe for all H_2/O_2 ratios and all process conditions. Furthermore, since a big plant is not required, small productions can be implemented on site, reducing transportation costs and associated risks.

1.2.4.6 Safety

A significant problem associated with the direct route is the inherent hazard associated with mixing H_2 and O_2 over a supported metallic oxidation catalyst. H_2/O_2 mixtures are explosive over a wide range of concentrations. When the concentration of H_2 in air and oxygen is in the range of 15-90% vol. and 4–94% vol. respectively, at 1.0 atm pressure and 25°C, the resulting gas mixture is flammable/explosive, if ignited (Lewis 1961). The flammability/explosive range is further widened with increasing pressure. Hence for safe working practice H_2 concentrations below 4% should be employed, and this can result in lower yields of H_2O_2. For these reasons there is at present no commercialized direct H_2O_2 synthesis process, although plans have been announced by Degussa–Headwaters for such a plant, there are no announcements concerning active commercialization and all new plants are still based on the indirect process (AQ oxidation).

Since it is important to try to achieve the highest rate of product formation, most of the earlier studies used H_2/O_2 mixtures in the explosive region, and solutions of over 35 wt% H_2O_2 have been made by allowing H_2 and O_2 to react over palladium catalysts at elevated pressures. However, the commercial operation of such a process in the explosive region would be extremely dangerous, and after the explosion of a pilot-scale reactor at DuPont, the research on the direct oxidation of H_2 to H_2O_2 declined. In the last decade, due both to new catalysts and reactor solutions, the industrial interest and academic research started again.

Studies recently have concentrated on carrying out the reaction with dilute H_2/O_2 mixtures well below from the explosive regime. Alternatively, a catalytic membrane can be employed to prevent the contact of hydrogen and oxygen during the reaction, and in this case pure gases can be used thus obtaining higher yields of H_2O_2.

During the last decade, most of the patents report results outside the explosive region (ENI –Paparatto 2003, HTI-Zhou 2001, Degussa-Hass 2006), while some companies (BASF-Fisher 2002) operate inside the explosive region, but with a particular reactor design and diluting H_2 along the catalytic bed. However, operating inside the explosion limits is potentially hazardous, particularly for large reactors.

The issue of safety has been addressed in all the recent patents regarding the direct catalytic synthesis of H_2O_2 and even if some patents, as said, still report working conditions inside the explosive region, in most cases operation is conducted below the lower limit. However, there are still some safety concerns, because in the mixing region or if a dead zone forms in the reactor, local hazardous concentrations may originate.

A solution that has recently been proposed is the use of microreactors, where the high surface to volume ratio allows an effective quenching of radical side reactions,

thus allowing to operate safely with H_2 concentrations higher than 5%. This solution is obviously suited for small-scale applications owing to its inherent low productivity.

1.3 Definitions

In the following chapters experimental results and considerations are usually presented in terms of production rate and selectivity for hydrogen peroxide. It's worth defining those quantities before proceeding with the discussion.
The concentration of hydrogen peroxide is determined by iodometric titration, while the water content is measured via Karl-Fisher titration method.

Production rate is defined as follows:
Production rate=mol of H_2O_2 produced/min

Productivity is defined as follows:
Productivity=grams of H_2O_2 produced/grams Pd per hour

Selectivity is defined as follows:
Selectivity=$[H_2O_2]/[H_2O_2]+[H_2O]x100$
which corresponds to the moles of hydrogen peroxide produced, divided by the moles of hydrogen consumed, %

1.4 Aim of the work

The aim of the work is to study hydrogen peroxide direct synthesis from an engineering point of view, taking into account a possible implementation of the process on an industrial scale. Particularly, continuous operation is regarded as an important feature for such a process to be attractive and applicable for industry. Thus a trickle bed reactor is developed to allow for catalyst loading and continuous reagents feed and H_2O_2 production. Operative conditions are extensively investigated, with particular attention to gas and liquid flow rates. Pressure effect and different concentrations of reagents in the gas feed are also considered.
Since H_2O_2 direct synthesis process requires an active catalyst to be performed, various catalytic systems are examined. Typically, the active metal of choice is palladium, but bi-metallic (palladium-gold) catalysts are also investigated, with the purpose of enhancing the process performance. Metal clusters are incorporated on either organic or inorganic support substrates, which play a significant role themselves as demonstrated in this study.

All of these issues are explored and correlated, in order to optimize conditions and maximize hydrogen peroxide direct synthesis performance.
A batch reactor is also developed to carry out kinetic studies to measure reaction rates and to provide a kinetic model to unravel the complex reaction network which include H_2O_2 synthesis.
The first chapter presents an introductory overview on green chemistry and hydrogen peroxide, from its production to its use, and why there is a great interest in its direct synthesis from an industrial point of view.
Chapter 2 deals with the development of the reactors used for this work: a continuous, trickle bed reactor and a batch reactor.
Chapter 3 presents kinetic studies performed in the batch reactor, which result in a novel kinetic model for hydrogen peroxide direct synthesis and other secondary reactions involved.
In Chapter 4 a thorough study investigating the reaction pathway and operative conditions is reported, performed in the trickle bed reactor with a palladium on sulfated ceria catalyst.
An extensive study on the effect of gas and liquid flow rates is presented in Chapter 5, where four different catalysts are compared.
In Chapter 6 is discussed how varying flow rate conditions and reagents concentration affects the reaction course, with a particular emphasis on the comparison between mono-metallic and bi-metallic catalytic systems.
Conclusions and future perspectives are reported in Chapter 7.
At the end, the description of a thermodynamic model for determining vapor-liquid equilibrium for the quaternary system of interest (CO_2, H_2, O_2, MeOH) is presented (Appendix A).

Chapter 2

Experimental Reactors and preliminary data

2.1. Introduction

In this chapter the development of our different reactor set-up used for experiments on the hydrogen peroxide direct synthesis is presented. A 100 ml batch reactor for preliminary studies was developed in Padua, for preliminary studies; a second larger one (600ml) was developed at Abo Akademi, Finland, where also a continuous, trickle bed reactor was set up.
Each one will be illustrated in this chapter, together with their development, throubleshooting and preliminary data.

2.2. Batch reactor development

The first experimental set-up developed at DIPIC is schematically summarized in Figure 2.1. The reactor (12) is an autoclave with an internal volume of 100 ml (Autoclave Engineers), made of Hastelloy C steel. Stirring is realized with a magnetically coupled electric engine (MagneDrive, Autoclave Engineers) and a radial turbine. The reactor is fitted with a thermocouple connected to a computer that allows to register temperature values for the duration of experiments.

Gases are loaded in the reactor directly from the gas cylinders: H_2, O_2, CO_2, and N_2 (1, 2, 3 and 15in the scheme, respectively). Three on/off valves are located between the gas cylinders and the batch reactor to allow for separation and control (4). Regulation valves are used to carefully dose gas amount from the cylinders (5), and also for liquid (7) and gas sampling (6). Two one-way valves (10 and 11) are used to ensure no backmixing from the reactor environment to the pipelines. A safety valve is added to guarantee safe operation in case of uncontrolled pressure increase (23). Pressure is constantly monitored through a pressure transducer (9), the values are

then registered by the computer. A mechanical pressure gauge is used to control pressure conditions (8). A back pressure controller (18) is inserted to dose the gases from the reactor to the MicroGC allowing not more that 2bars in its inlet. A three way valve is located close to the back pressure controller (14), with one end connected to the nitrogen cylinder (15), one to the reactor and the last one to the back pressure controller (18).

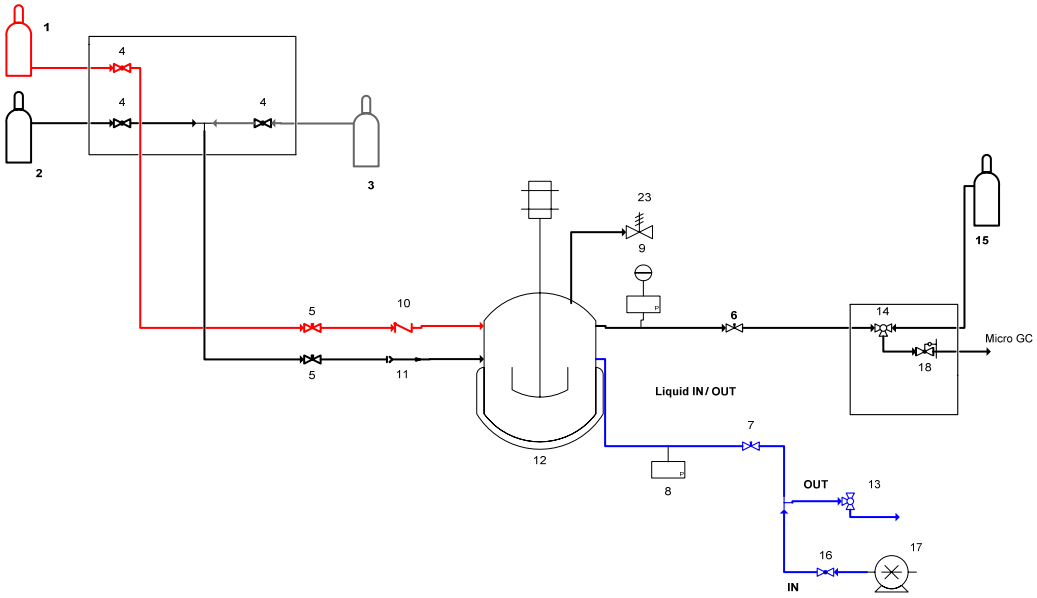

Figure 2.1. Schematic of the initial batch reactor set-up.

A three way valve (13) is used for liquid sampling. An HP (high pressure) pump (17) is employed to (re)fill the liquid inside the reactor at the beginning and during the experiments. An on/off valve (16) is needed before the HP pump for operating reasons as specified in the pump manual. All components are connected through 1/16" stainless steel pipes. To control the temperature and maintain it constant during the experiments a refrigerator coupled with a Peltier system is implemented.
The reactor was tested for several days at high pressure to check for leaks.
A custom control panel was built to control and register the parameters during the reaction. These include temperature, pressure, stirring rate and the strain of the stirrer due to liquid phase viscosity in the reactor. The controlled parameters are stirring rate and temperature, which can be programmed in time to follow any kind of policy. The control panel is recalibrated periodically to ensure its precision, and particulary transducers stability, which may decline with use. The time needed for a good calibration is quite long, because the precision required for the experiments in terms of pressure and temperature is high.

Initial experiments were carried out to develop an appropriate procedure to load the desired composition of reagents to carry out the reaction batchwise. Initially, the pressure method was used, apparently applied by Others working with batch reactors. It is based on additions of given amount of gas as determined by the increase of pressure. The procedure was as follows:

1) we loaded 50 ml of methanol in the reactor, and then a mixture of carbon dioxide and oxygen at 25 °C and 20 bar. After that, the stirrer was started;
2) then CO_2 and O_2 are fed to the reactor; a peak of pressure could be observed, which decreased to finally reach equilibrium conditions after some time;
3) when equilibrium with the previous mixture was achieved, the H_2 was loaded, and again a peak of pressure could be observed, followed by a sharp decrease and a slow stabilization to equilibrium conditions; stirring was noticed to accelerate the process of reaching equilibrium.

Following this procedure, we realized that the right amount of gases loaded in the reactor cannot be accurately estimated, because of the solubilization processes into the solvent (methanol). Measuring the peak of pressure cannot be used to determine the right amount of gases. Indeed, if the reactor free volume and the peak of pressure of the gases are considered, the amount of gas loaded calculated from these data will be less compared to the real amount, because of the solubilization takes place in parallel to the feeding, thus decreasing the maximum theoretical overpressure due to the filling of the reactor atmosphere by the entering gas.
In addition, the ideal gas model does not fit the case of CO_2 at our working pressure. Thus, a suitable thermodynamic model for equilibrium calculations is required (Appendix).

Gas phase composition inside the reactor was measured by gas chromatography analysis. The use of a back pressure regulator is needed to feed the gas mixture to be analyzed to the microGC. The microGC cannot operate at high pressure, which must therefore be reduced before the analysis.
The procedure was as follows: first the line from the reactor to the microGC was purged, because some gases could be already present in the pipes, with a different composition than the reactor, due to backmixing phenomena and other reasons. The back pressure controller was then opened to send a sample of the gas phase to the microGC, at 2 bar. However, a drawback of this procedure is that a subsequent sampling from a small volume reactor causes a pressure decrease in the reactor of 1-

2 bar over time, which leads to a change in gas phase composition even if no reaction occurs inside the reactor. A change in pressure causes a new vapor-liquid equilibrium (VLE) to develop, with a different gas phase composition. In fact a new gas analysis of a second sample was performed, and a different composition of the gas phase was measured.
Thermodynamic calculations are needed to predict the VLE and both the gas and liquid phase composition, but the total amount of gas loaded is necessary to calculate the VLE. However, this is not straightforward, as time and velocity to charge the gases influence the final amount, given that solubilization kinetics depend on the concentration of the given gas in the reactor atmosphere. For example, if a gas is loaded quickly, then solubilization progress is small, and a higher pressure is achieved, in comparison to slow gas loading.

To try to overcome those problems, reagents loading strategy was changed. It was decided to load the gases first, and then the given amount of liquid solvent with an HP pump. This procedure is much more reliable than the previous one, and importantly, calculating the amount of gas is easier since no liquid phase is present at the moment when the gas is loaded. Still it is quite difficult to dose exactly the same amount of gas for each experiment, if it is taken directly from the cylinders.
This new procedure allows to charge the gases in a more precise way, and after loading the methanol the pressure finally reached is always about the same. In this way it is possible to calculate the amount of gases loaded and the amount of gases solubilized in the liquid phase. The only problem now is the loading of the limiting reagent (hydrogen) that has to be loaded after all the other reagents.
Hydrogen has great affinity for methanol, especially for methanol expanded with carbon dioxide. That means that when the gas is charged directly from the cylinder it will be solubilized very rapidly inside the liquid phase, leading to difficulties in quantifying its exact amount.
Gas analysis was tried again but the previous problems were encountered yet again, with very fluctuating measurements.
Therefore, summarizing, the main issues with the set-up presented in Figure 2.1 are:

1) non reproducibility in the amount of gas loaded
2) pressure drop connected to gas analysis
3) H_2 quantification in the reactor
4) difficulty in liquid sampling

Some modifications were thus implemented on the previous batch reactor set-up, until the final version: The new scheme is shown in Figure 2.2 and the actual appearance in Figure 2.3.

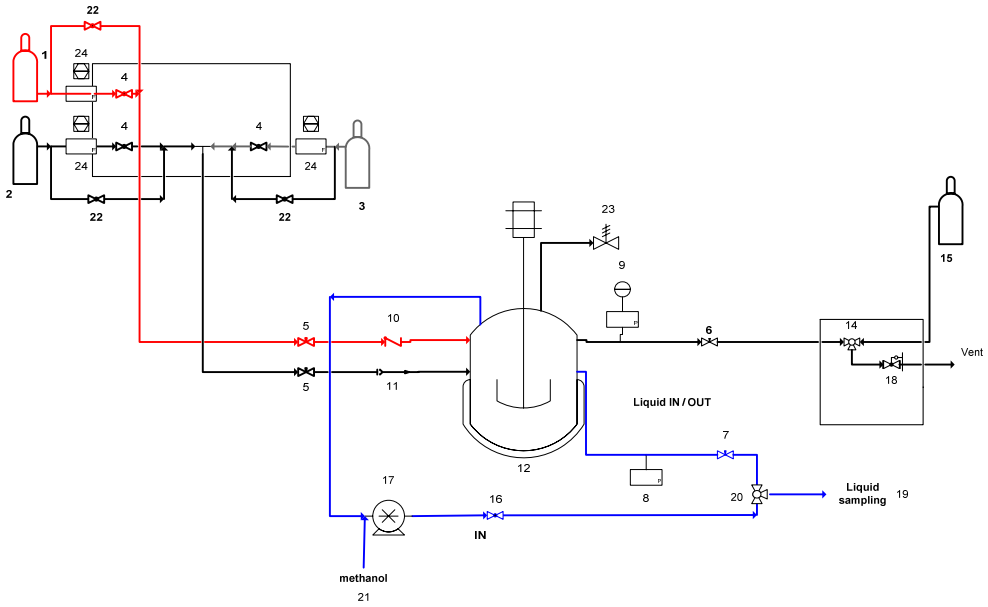

Figure 2.2. Schematic of the final batch reactor set-up.

Figure 2.3. Final batch reactor set-up.

Gas analysis was suppressed, and the MicroGC was replaced with a vent. Recirculation of the liquid phase was also included, through the HP pump (17)

coupled with a six-way valve (20). Before the HP pump, a tank with fresh methanol (21) was also added. The reasons behind that were: i) precise liquid sampling in terms of quantity and time; ii) GC analysis of the liquid phase thanks to the six-way valve connected to the GC. However, GC analysis of the liquid phase were not performed, because some difficulties still existed: the liquid phase could contain some by-products from the direct synthesis reaction (e.g. O_2), and the heater before the GC, used to gasify the liquid, could decompose H_2O_2. Thus quantifying H_2O_2, O_2, H_2, CO_2, CH_3OH and water with a GC analysis on the liquid phase is not straightforward. Iodometric titration and Karl Fischer analysis were then chosen as the methods to determine product concentrations in the liquid phase.

Another significant improvement from the initial set-up was the addition of three mass flow controllers (MFC) (24) after the gas cylinders, which allow for precise gas loading. All the species could then be exactly measured before the reaction started. The MFC were also equipped with a by-pass valve (22) to allow for direct gas loading from the cylinders, if required.
Finally, with thermodynamic predictions, quantification of the amount of reactants in the liquid phase can be obtained (see Appendix).
The implemented modifications lead to a more versatile and precise set-up for batch operations.

These improvements coupled with the backpressure controller (18) after the reactor, allow for semi-batch operation, i.e. continuous bubbling of the gas in the batch liquid phase, at high pressure. Because the gas phase is well mixed, thanks to bubbling and stirring, it can be regarded as a CSTR (G-CSTR)

Karl Fisher analysis was carried out to evaluate the water content in the liquid phase. Water is an unwanted product, deriving from parallel and series reactions that are part of the reaction network in which H_2O_2 also forms (see Section 1.2.4).
Using methanol as the reaction medium causes and additional difficulty of its highly hygroscopic behaviour. Indeed during liquid sampling atmospheric water can be absorbed leading to significantly different results. After numerous attempts, a standard procedure was defined to carefully and consistently analyze water content by Karl Fischer titration:

1) liquid sampling duration has to be the same every time;
2) liquid sample has to be closed immediately after sampling, to avoid interferences with room humidity, and then analyzed after the same time for all the samples;

3) the sample has to be weighed before and after the analysis to calculate its density and the percentage w/w of the product formed;
4) a six-way valve is required for sampling the same volume for each sample.

2.2.1 Preliminary studies

When the final batch reactor set-up was defined, preliminary studies on hydrogen peroxide decomposition were carried out.
At the beginning, it was important to determine whether the steel reactor surfaces were able itself to decompose H_2O_2 in the absence of a catalyst.
As a comparison, a solution of 2.2 wt.% H_2O_2 in methanol was put inside a glass becker at room pressure and temperature. Similarly, 50 ml of the same solution was loaded inside the reactor. The reactor temperature was 25°C and the pressure 1 Bar without stirring. Every 30 minutes hydrogen peroxide concentration was measured by iodometric titration. The results obtained (Figure 2.4) indicate that no hydrogen peroxide decomposed in both the glass and steel containers.
The same solution was also tested at -10°C (the chosen reaction temperature), with hydrogen peroxide decomposition again resulting negligible (data not shown).

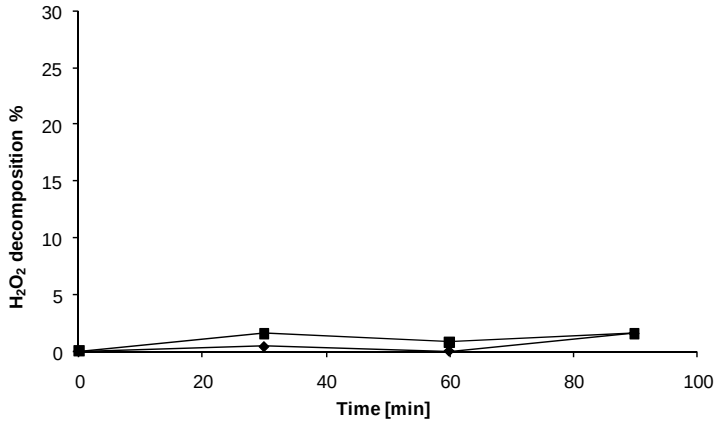

Figure 2.4. Decomposition of a 2.2 wt.% H_2O_2 in methanol solution at 1 bar and 20°C in a glass becker (diamonds) and in the batch reactor (squares).

The same experiments were repeated for a 0.5 wt. % of H_2O_2 in methanol solution, again in a glass becker and in the Hastelloy C steel reactor. Results are reported in Figure 2.5. The error was larger in this case because of the low H_2O_2 concentration, but decomposition was again negligible. Therefore it was possible to assume that

hydrogen peroxide was not decomposed by the reactor system. No passivation treatment is necessary for this reactor, since hydrogen peroxide was proved to be stable at various conditions.

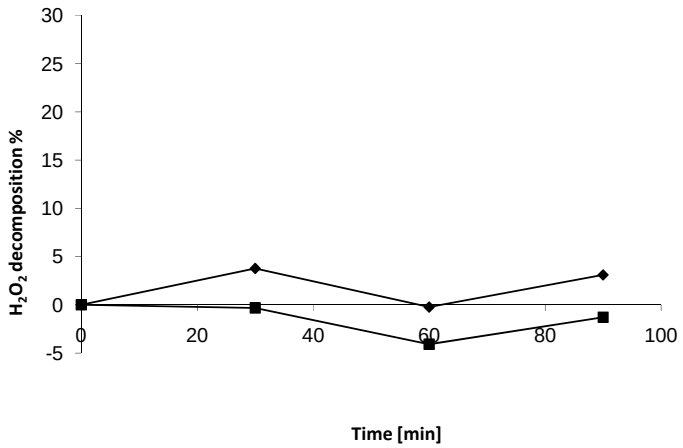

Figure 2.5. Decomposition of a 0.5 wt.% H_2O_2 in methanol solution at 1 bar and 20°C in a glass becker (diamonds) and in the batch reactor (squares).

The situation changed when the catalyst was present and the stirrer turned on. 0.4 grams of Pd-K2621 catalyst were used, and two different temperature conditions (20°C and -10°C) were examined, with a stirring rate of 1000 rpm. Results are reported in Figure 2.6.

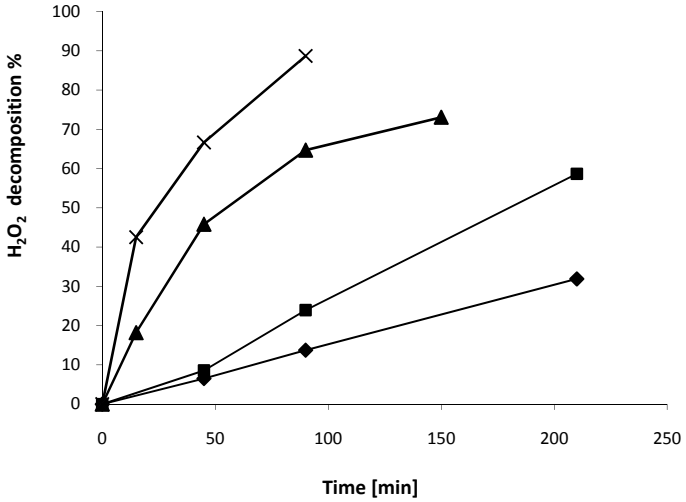

Figure 2.6. Decomposition of a 0.5 wt.% H_2O_2 solution with 0.4 grams of catalyst. T=-10°C without stirring (diamonds),T=-10°C, stirring rate 1000 rpm (squares), T=20°C without stirring (triangles), T=20 °C, stirring rate 1000 rpm (X-shaped).

The results show that the the same catalyst used for hydrogen peroxide direct synthesis also promotes its decomposition. It is worth noticing that a big difference exists in terms of decomposition for experiments carried out at 20°C and -10°C. For a prolonged time, hydrogen peroxide decomposition at 20°C is six-fold higher than that at -10°C. This was the main reason why it was decided to carry out subsequent experiments on H_2O_2 direct synthesis at the lower temperature. Another important observation that can be deduced from these results is that the stirring rate also significantly impact on the results by accelerating the decomposition process. Furthermore, if the catalyst is in the form of pellets, it is partly eroded by the rotating helix, with loss of catalyst structure and waste of active metal.
A batch reactor is undoubtedly an essential tool for laboratory research and catalytic tests, but it is unsuitable for implementation on an industrial scale.

Some preliminary direct synthesis experiments were also carried out in the batch reactor with the configuration shown in Figure 2.2. 0.4 grams of the of Pd-K2621 catalyst were loaded in the reactor. The reactor was flushed with nitrogen four times to ensure complete water removal and to have an inert environment. Carbon dioxide (30 bar) and oxygen (8 bar) were loaded in the reactor directly from the cylinders at 25°C, then 50 ml of methanol were loaded with the HP pump. The stirrer was then started and the reactor cooled down to -10°C. After achieving stable pressure conditions, the stirrer was turned off and H_2 (1 bar) was loaded in the reactor (t=0, beginning of the reaction). Than the stirrer was turned on again at 1000 rpm.

Experiments with three different durations were performed: 30, 90 and 150 minutes. At the end of each experiment, H_2O_2 concentration was immediately measured by iodometric titration. The same experiments were repeated, but in this case initial hydrogen pressure was restored at a certain stage, by topping up H_2 in the reactor.

Figure 2.7 illustrates the results in terms of H_2O_2 production after 30, 90 and 150 minutes. As clearly visible, H_2 top-up enhanced hydrogen peroxide production. This can be explained considering the reaction network of hydrogen peroxide direct synthesis. When the amount of hydrogen is too little the reaction that prevails is H_2O_2 decomposition, but if hydrogen is refilled regularly hydrogen peroxide synthesis can go further. At the beginning, direct synthesis reaction proceeds faster, but when hydrogen is increasingly consumed the reaction rate decreases and decomposition overcomes it. When hydrogen is topped up, a new supply of this reagent helps maintaining H_2O_2 synthesis reaction rate significantly high to have good selectivity.

This fact reveals that in order to enhance hydrogen peroxide direct synthesis, not only the catalyst has to be optimized, but reactor conditions and operation may contribute to raise the performances in terms of conversion and selectivity.

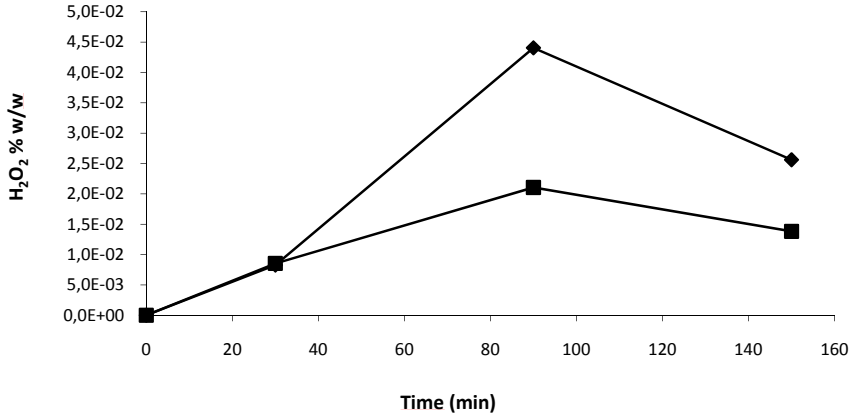

Figure 2.7. Production of hydrogen peroxide under batch conditions (squares), and with hydrogen refill (diamonds).

Another aspect that was examined, was how the amount of catalyst affects the outcome. Important preliminary result are shown in Figure 2.8, with different amounts of catalyst being tested at the same conditions. The first experiment was conducted with 0.4 grams of catalyst, the second one with 0.2 grams and the third one with 0.1 grams of catalyst. The results were quite surprising. With the smallest amount of catalyst, i.e. 0.1 grams, the highest hydrogen peroxide production was obtained. This finding is in contrast with what typically happens in a standard catalytic reaction, with more catalyst leading to a faster reaction. The reason can be searched in the reaction mechanism, as other parallel and series reaction are also catalyzed by the same catalyst (see Section 1.2.4).

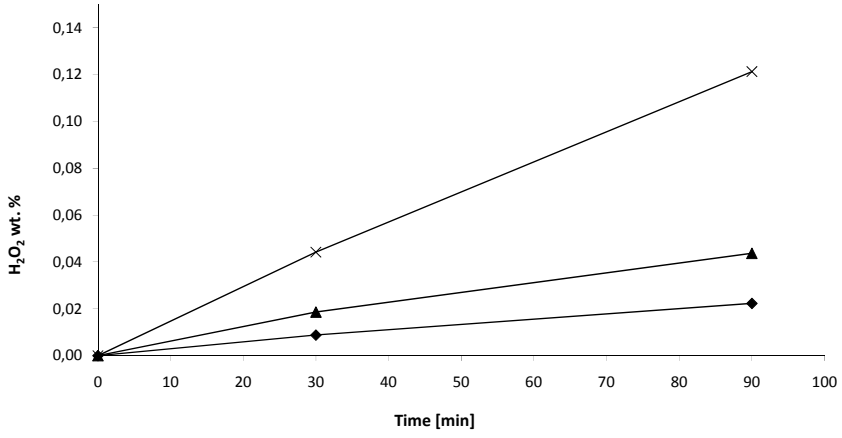

Figure 2.8. H_2O_2 production with different amounts of catalyst: 0.1 g (X-shaped), 0.2 grams (triangles), 0.4 grams (diamonds).

2.3 Trickle Bed Reactor (TBR) development

A TBR was developed for continuous hydrogen peroxide direct synthesis process. Motivations are threefolds: i) industrially, it would be the only feasible arrangement ii) operating under flow allows to control phases contact time, in case, operate also with very short residence time, iii) analysis of products is easier, being a stationary stream.

The trickle-bed reactor set-up is shown schematically in Figure 2.9.

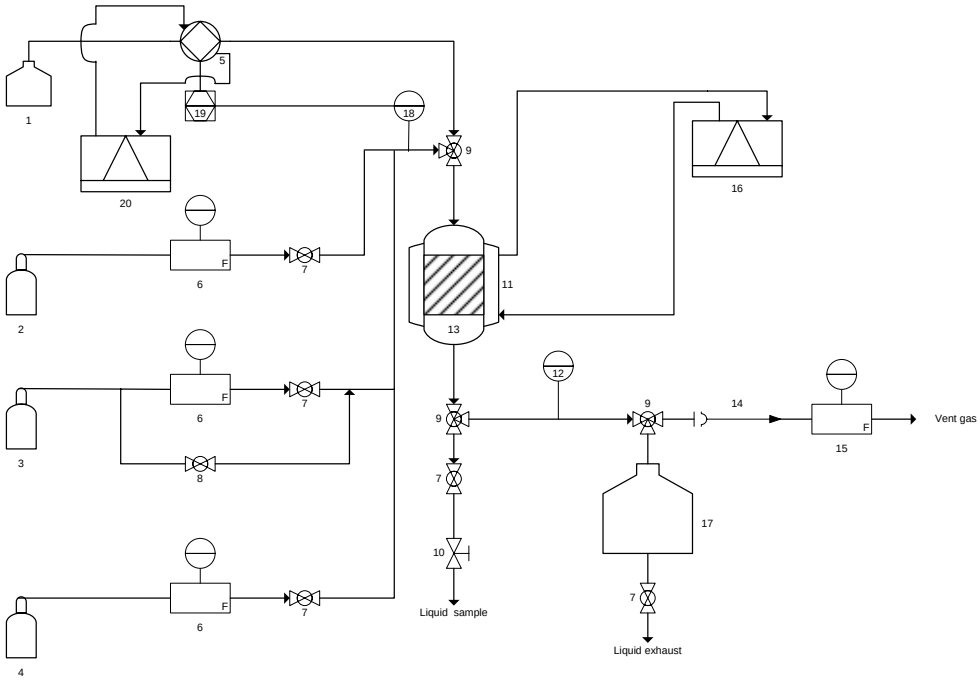

Figure 2.9. Schematic of the TBR set-up for H2O2 direct synthesis.

The reactor (13) is made of AISI 316 stainless steel, 30 cm in overall length, 1.5 cm I.D., internally lined with Teflon (1.15 cm final I.D.) to prevent H2O2 decomposition due to accessible Fe3+ ions from steel. The reactor can accommodate a catalyst bed up to 20 cm long. An external cooling system (11) based on a chiller (GRANT LT D6G) (16) allows for working temperatures between -20°C and 60°C. Three mass flow controllers (MFC) (Brooks 5850 series) (6) are used to feed the gases into the reactor. Every MFC is connected to a gas cylinder: N_2, CO_2/ H_2 97.5/2.5%, and O_2 (AGA gas). The pressure inside the reactor is controlled and regulated with a back pressure controller (BPC) (Brooks 5866 series) (15). A rupture disc is located before the BPC for safety reasons (14). A bypass is used to achieve the desired pressure inside the reactor more rapidly (8). After every MFC an on/off

valve (7) is inserted to exclude the MFC when not in use. The liquid phase is fed in through a syringe pump (TELEDYNE ISCO MODEL 500D syringe pump, TELEDYNE ISCO D-SERIES pump controller) (5). The syringe pump is then connected to a pressure transducer (18) to pump the liquid phase in the reactor at a certain pressure, and it is controlled by a computer (19). The syringe pump can be cooled/heated by a chiller (20), and a tank (1) provides fresh liquid solvent supply.
A T-connection allows to feed the liquid and the gas phase into the reactor (9). A regulation valve (10) is used to sample the instantaneous liquid phase, while a 1.5 L tank provides gas-liquid separation (17), cumulating all the liquid product. A pressure gauge (12) is used to control the pressure in the reactor/tank system. All the connections are realized with 1/8" stainless steel pipelines.

The catalyst bed is normally placed between two quartz wool plugs. Above the upstream quartz wool plug, quartz sand is used to improve gas-liquid mixing. Temperature inside the reactor is measured with a thermocouple (Type: K) before the catalyst bed.
The system is located in a fume hood, which is equipped with a sensor for hydrogen, and if it detects dangerous levels in the environment the computer disconnects hydrogen feeding to the reactor by blocking the alimentation of hydrogen to the MFC.

2.3.1 Preliminary studies

At the very beginning, decomposition tests were carried out in order to verify that the reactor itself was not able to decompose hydrogen peroxide. Commercially available H_2O_2 (Merck, 30% w/w, pro analysis) was used. Methanol is the common solvent for direct synthesis because it improves hydrogen solubility and allows operating at lower temperature than just with water. Initially, a 0.5 wt.% H_2O_2 solution in methanol (with approx 1.1% water) was tested. Temperature was set at 20°C. Decomposition was assessed inside tank (1), which provides the liquid phase to the syringe pump, and no decomposition was detected. This is important because when decomposition kinetic studies (see Chapter 4) are carried out, H_2O_2 is loaded in tank (1) before being fed into the reactor.
The syringe pump was also loaded with the H_2O_2 solution, and after four hours no hydrogen peroxide was decomposed. Subsequently, decomposition in the pipes connecting the syringe pump with the reactor was checked, and again no decomposition was noticeable.

Decomposition was eventually measured inside the reactor, with a liquid flow rate of 1ml/min. The reactor was loaded with quartz wool (hydrogen peroxide decomposition on the quartz wool alone was previously checked, with the result that the quartz wool doesn't decompose it), and at the end of the experiment the solution exiting the reactor contained no hydrogen peroxide left.

Therefore it was decided to proceed with a passivation treatment of the reactor. Passivation was made with a 50 wt.% nitric acid solution at 40°C for four hours. After this treatment, H_2O_2 decomposition was about zero in the beginning, but then after a few hours it increased until all H_2O_2 was consumed. Thus two four-hour cycles with nitric acid were repeated to improve the passivation treatment. As a results, H_2O_2 decomposition increased more slowly compared to the previous case, however after a few hours decomposition was again total. Even with three or four passivation cycles no significant improvement was achieved.

Some welding material was found to be present inside the reactor, and this was thought to be the primary cause of hydrogen peroxide decomposition even after a severe passivation treatment.

Since this procedure proved to be unsatisfactory, a Teflon pipe was put inside the reactor to ensure complete hydrogen peroxide stability. Indeed after 6 hours of experiments no H_2O_2 decomposition was detected.

Those preliminary experiments were carried out in order to investigate stability conditions within the reactor, primarily to check that exposed metal surfaces did not catalyze any H_2O_2 decomposition. Subsequently, H_2O_2 stability was measured as a function of the amount of catalyst, its dispersion along the bed, and contact time.

The catalyst bed was made of 8 g of resin, spanning 8.6 cm in the reactor, between the quartz wool plugs and after approx 14 cm of quartz sand to improve uniformity in gas and liquid mixing. Between the two quartz wool plugs, four different arrangements were examined (Table 2.1): A) 8 g of K2621 (unloaded resin), B) 8 g of Pd/K2621, C) 2 g of Pd/K2621 uniformly dispersed in 6 g of K2621, D) a layered bed with, from the bottom, resin support (2.7 g K2621, 2.9 cm long), active catalyst (0.3 g of Pd/K2621, 0.3 cm long) and resin support (5 g K2621, 5.4 cm long).

Arrangement	**K2621**	**Pd/K2621**
A	8 g	-
B	-	8 g
C	6 g	2 g
D	2.7+5 g	0.3 g

Table 2.1. Different catalytic bed arrangements tested.

The liquid phase flow rates investigated were 0.5, 1, 2, 4, 10 and 20 ml/min.
As expected, no hydrogen peroxide decomposition was detected at any flow rate when the reactor was loaded with inert resin only (bed arrangement A).
Hydrogen peroxide decomposition was assessed at room pressure in the presence of the catalyst (bead arrangement B), with different liquid flow rates of a 0.5 wt.% H_2O_2 solution in methanol, and various temperature conditions (Figure 2.10). The lower the temperature, the smaller the amount of hydrogen peroxide decomposed.

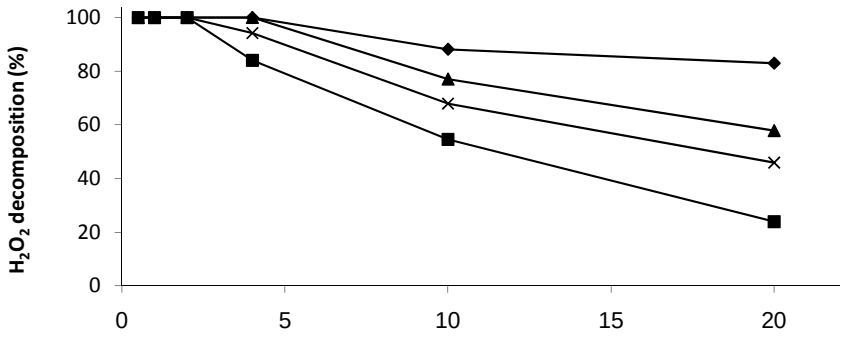

Figure 2.10. Decomposition of H_2O_2 at 1 bar varying liquid flow rate and temperature: -10°C (squares), 0°C (X-shaped), 10°C (triangles), 25°C (diamonds).

The trickle bed reactor, after loading the catalyst and before the experiments, was flushed with N2 for 30 minutes, than pressurized with carbon dioxide and hydrogen mixture, and finally liquid flow was started. The reactor was cooled down to the desired temperature, and decomposition tests could therefore be performed at pressures different from 1 bar.
With bed arrangement C (Figure 2.11), hydrogen peroxide decomposition evidently decreased compared to the previous case, i.e. when only one fourth of the active catalyst was loaded, but it was still relevant at 263 K and low flow rates (e.g. about 50 % with 4 ml/min liquid flow rate). Addition of hydrogen caused decomposition to increase, even at high pressure conditions, which should shift the equilibrium of the decomposition reaction (Eq. 1.3, Section 1.2.4) back towards H_2O_2 formation. However, H_2O_2 reduction reaction (Eq. 1.4, Section 1.2.4) might be the cause of a larger decomposition when H_2 is co-fed with the liquid, as also confirmed by the larger decomposition observed with greater H_2 partial pressure (case 3 vs. 5 in Figure 2.11). Interestingly, the amount of gas fed in this test appeared not to be sufficient to reduce catalyst wetting at a point where its activity (decomposition, in this case) could be affected.

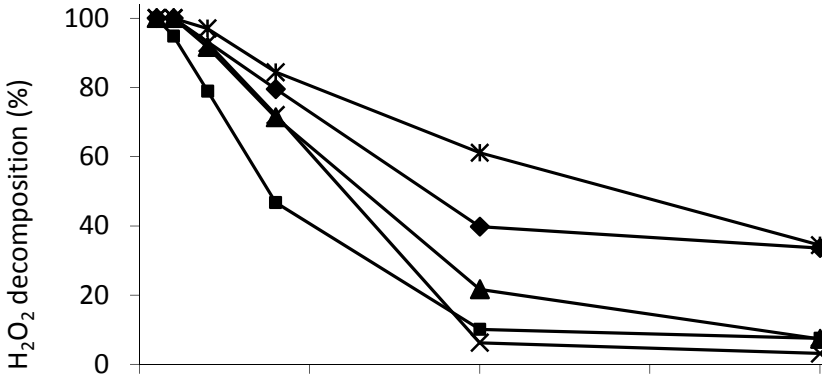

Figure 2.11. H2O2 decomposition, bed composition: 25% Pd/K2621- 75% K2621. Total weight= 8g. T=263K . 1) 1 bar; 2) 15 bar, 1 ml/min H2. 3) 15 bar, 4 ml/min H2. 4) 15 bar 1 ml/min 97.5 % CO2 and 2.5% H2. 5) 15 bar 4 ml/min 97.5 % CO2 and 2.5% H2.

CO_2 and H_2 were used for these experiments as the gas phase, and from the results in Figure 2.11 it is noticeable how they affected decomposition in opposite ways: H_2 promoted H_2O_2 consumption, particularly through its reduction, as already recalled, while CO_2 improved hydrogen peroxide stability by increasing the acidity of the medium. It is known that H_2O_2 is stable within a pH range between 3 to 5.

In general, it was proved how gases can modify the decomposition pathway, but also it was confirmed that the amount of catalyst used plays a very relevant role in this process characterized by a complex reaction network, with unpredictable conclusions since, against the good sense, a lower catalyst amount leads to better results.

Accordingly, the catalyst loading in the bed was further reduced (arrangement D) down to 3.75%, as a thin layer (3 mm) between two inert resin layers. Results are shown in Figure 2.12, and clearly confirm that, with a little amount of catalyst, depending on temperature conditions and space velocities, decomposition can be limited to low values, even at fairly small flow rates.

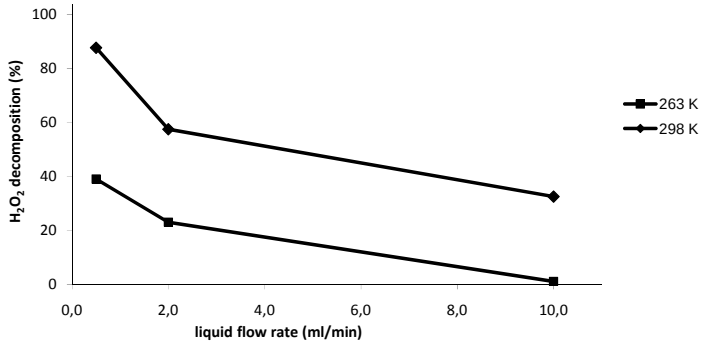

Figure 2.12. H2O2 decomposition, catalyst bed: 3.75% of active catalyst in 8g total. P=1bar

However, with the set up described above and illustrated in Figure 2.9, it was not possible to analyze the gas phase composition, thus an upgrade was implemented in order to make this type of analysis feasible. A schematic diagram is presented in Figure 2.13.
The aim was to be able to measure selectivity based on hydrogen conversion.
A mass spectrometer (21) (MS, Blazer, Omnistar) was placed after the back pressure controller (15). Instrument stability was checked over a 24 hour period, and the calibration for the gases of interest (H_2, O_2, CO_2, N_2) was conducted.
However, a few problems were encountered, as part of the gas was solubilized in the liquid in the tank (17), and the large volume of it prevented a quick measure of the actual gas composition at the exit of the reactor. Another problem was that the amount of liquid phase in the system was increasing during the experiments, and as a consequence, gas solubility inside the tank was changing.
Hence it was decided to replace the 1.5 L tank (17) for gas-liquid separation with a smaller one of 0.3 L. Unfortunately, the problem was still present and moreover experiments longer than 6 hours couldn't be carried out due to the limited capacity of the tank, which was filled with the liquid phase after a few hours.
Another attempt was made (Figure 2.14) by placing a flash (22) right after the trickle bed reactor in order to separate small amount of gas and liquid, and it was connected to the mass spectrometer (21) to perform gas analysis.
However the flash was too little and the gases were carrying some methanol from the liquid phase with problems in gas analysis as the consequence.
Since gas analysis carried some intrinsic problems that couldn't be solved, it was decided to avoid gas analysis and measure selectivity and production values directly on the liquid phase, through iodometric and Karl Fisher titration. A picture of the reactor set-up that was used for all the experiments reported in the following chapter is shown in Figure 2.15.

The set up to measure water content in methanol was not straightforward. First we made experiments using a liquid flow rate of pure methanol and only nitrogen as carrier gas. We measured the amount of water in the liquid phase. first we prepared all the things for the experiments. we put in the line with bybass in figure 2.4 the cylinder of nitrogen. Then we flushed the reactor for 30 minutes with hydrogen. than we pressurized the reactor with nitrogen and putting a gas flow rate of 3 ml/min to ensure pressure stabilization (30 minutes). After that the syringe pump was turned on with a liquid flow rate of 1 ml/min and the system was cooled down to -10°C (1 hour). after that we decreased the gas flow rate to ensure a completely wetting of the

catalyst (1 ml/min of nitrogen at 10 bar for 30 minutes) and then we started to take liquid samples of methanol every 15 minutes.

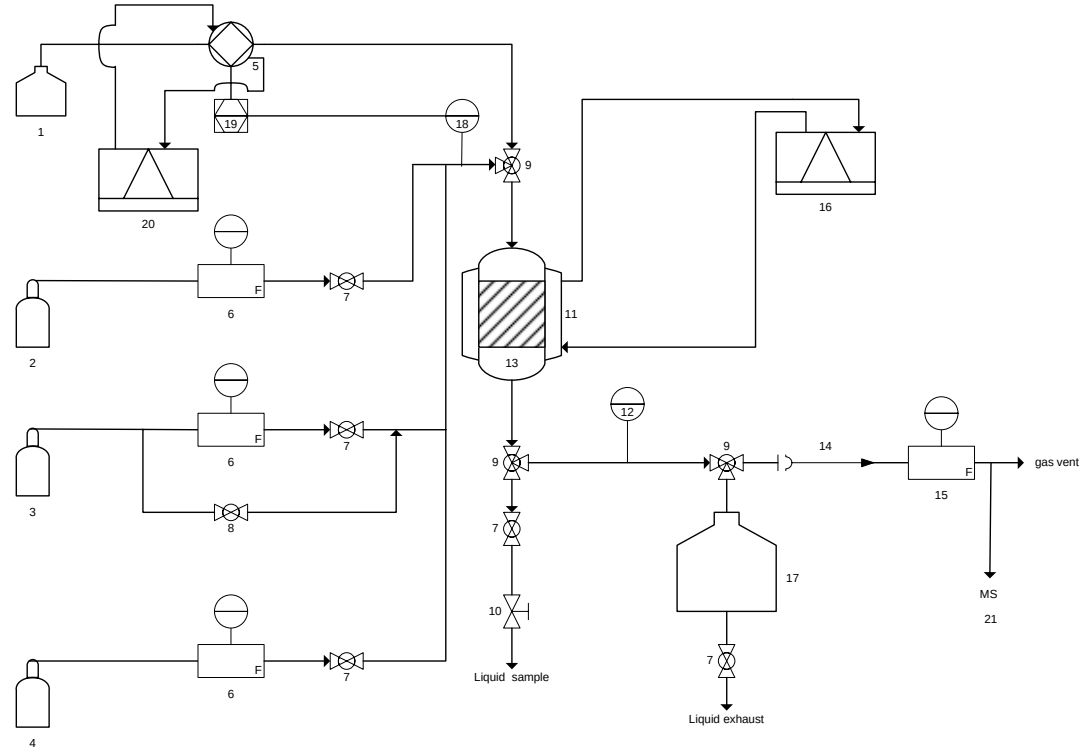

Figure 2.13. First TBR set-up upgraded with gas analysis.

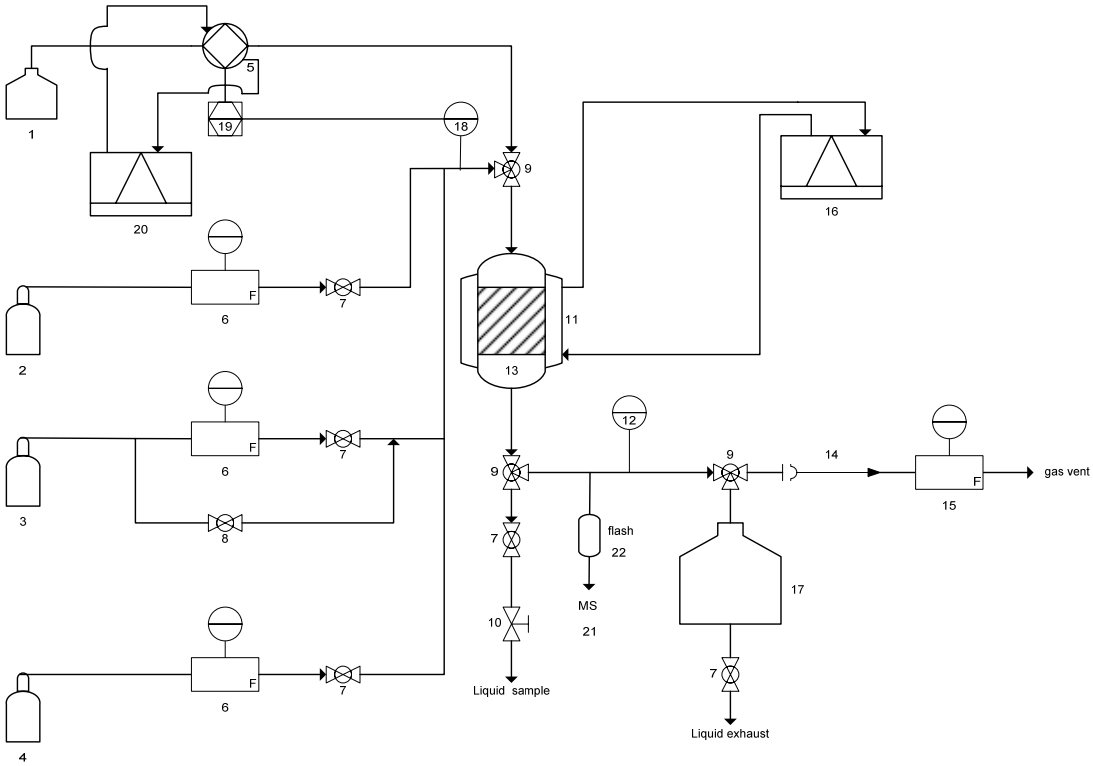

Figure 2.14. Second TBR set-up upgraded with gas analysis.

Figure 2.15. Representation of the TBR set-up.

The amount of water found was varying during these sampling. Only after one hour and a half from the beginning of the sampling the water measured was stable. This result is to be ascribed to the presence of water in the reactor environment and only after one hour and a half this water is taken away from the reactor. The presence of some trace of water after that is to be ascribed to the water in the methanol and to the traces of water in the gas cylinders.

After these experiments we defined the final procedure to make before every experiment to have stable analysis.

The Trickle bed reactor after the loading of the catalyst and before the experiments is flushed with N_2 for 30 minutes, than it is pressurized with the mixture of carbon dioxide and hydrogen, than the gas flow rate is chosen (30 minutes). After that the liquid flow rate is turned on and reactor is cooled down to the desire temperature (1 hour). after reaching the desired temperature the gas flow rate of hydrogen and carbon dioxide is decreased (30 minutes) and then increased again (30 minutes). after that mass flow controller of oxygen (30 minutes for stability) is turned on and the reaction is ready to start. only after these operations the analysis of water and hydrogen peroxide are stable. The time for the start up of the reactor is about four hours before every experiment.

These preliminary results were made to study the operative conditions to use in the future experiments.

These results were made with a catalyst easy to prepare and based on an inorganic support. After that we changed the support with an inorganic one. To improve our reaction we decided to use the same catalyst but also catalysts on inorganic support with the same diameter of the catalyst based on resins balls. we decided so to use a mixture between the catalyst and a inert support without catalyst (SiO_2). We took the powder of the catalysts with inorganic support, we made the pellets crushed them and sieved with dimensions between 0.5 and 1 mm. The same was made for silica powder as inert to mix with the catalysts. we put the mixture of catalyst and inert in a plug of two pieces of quartz wool and then quartz sand to improve mass transfer between liquid and gases. The results are discussed in Chapters 4, 5 and 6.

At the end the temperature chosen for the direct synthesis reaction was -10°C for two reasons. The first one is that is the same temperature that we used in batch reactor and the second one is that with our composition and with no stabilizers the decomposition is almost suppressed. The pressure decided to be used in the TBR was 10 bar for safety reasons and to try to complicate to much the further calculations on gas solubilities.

2.4 Development of a larger batch/semi-batch reactor for kinetics studies

Thanks to the experience acquired by setting up the previous reactors, the development of a larger semi-batch reactor used for kinetics studies was quite simple and fast.

In this case, the reactor volume chosen was larger (600 ml). The final set-up is shown schematically in Figure 2.16.

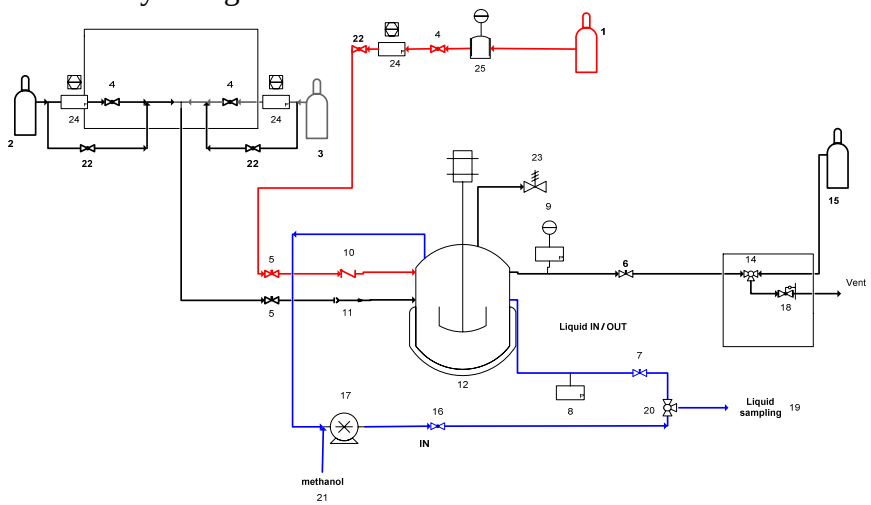

Figure 2.16. Schematic of the 600ml batch reactor set-up for kinetics studies.

The batch reactor (12) is an autoclave stainless steel reactor (Parr) with a volume of 600 ml and a maximum working pressure of 200 bar. Mixing is carried out with a Heidolph RZR 2021 rotor operating at 1000 rpm. The reactor is fitted with a thermocouple connected to a computer that permits to register the temperature during the experiments. Gas can be loaded in the reactor directly from gas cylinders: O_2, CO_2 and N_2 (2,3 and 15 in the scheme, respectively). Three on/off valves (4) are inserted after the gas cylinders to ensure separation between cylinders and reactor. Regulations valve are used to dose the gas from the cylinders (5) and for liquid (7) and gas (6) sampling. Two one-way valves (10 and 11) are used to avoid backmixing from the reactor environment to the pipelines. A safety valve (23) ensures overpressure control. Pressure is constantly monitored through a pressure transducer (9), values are then registered by a computer. A mechanical pressure gauge is used to control pressure conditions (8). A three-way valve (14) is included after the back pressure controller: one pipe is connected to the nitrogen cylinder (15), one to the reactor and the last one to the back pressure controller (18) that goes to the vent.

A six-way valve (20) is used for liquid sampling. An HP (high pressure) pump (17) ensures liquid recirculation and doses the solvent inside the reactor before and during the experiments. An on/off valve (16) is necessary before the HP pump as specified in the pump manual. The HP pump is connected with 1/16” stainless steel pipes, while the gas cylinders are connected to the reactor with 1/8” stainless steel pipes. To control the temperature and maintain it constant during the experiments a refrigerator is included.

Three mass flow controllers (MFC) (24) are inserted after the gas cylinders for precise quantification of gas loading. A by-pass valve (22) also allows for direct quick gas loading from the cylinders. A 35 ml vessel (25) coupled with a pressure transducer and a heating jacket is placed before the MFC for hydrogen. This is used to precisely calculate the amount of hydrogen fed into the reactor.

The reactor was tested for several days at high pressure to check for leaks.

Before the experiments, a 5 hour passivation treatment was performed on the reactor, using 40% wt. nitric acid at 40°C. After that a solution of 0.5 wt.% H_2O_2 in methanol was loaded inside the reactor. No H_2O_2 decomposition was detected after 4 hour at 1 bar and 25°C. another similar experiment was made in this way: a solution of 0.5 wt.% H_2O_2 in methanol was loaded inside the reactor the stirrer was turned on around 1000 rpm. H_2O_2 decomposition was detected after 4 hour at 1 bar and 25°C: it was around 10%.

A picture of the experimental set-up is in shown Figure 2.17.

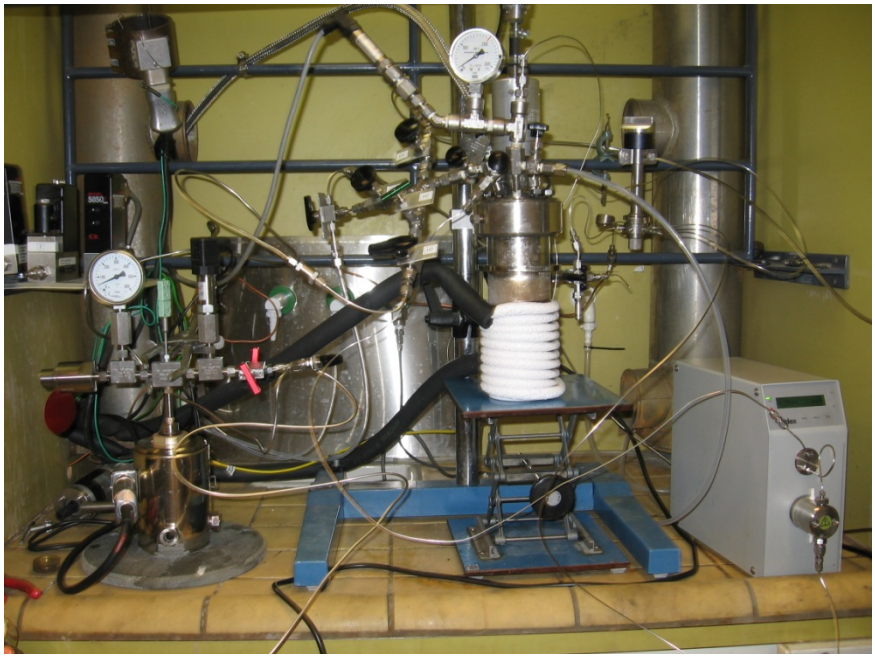

Figure 2.17. Representation of the batch reactor set-up for kinetics studies.

The protocol developed for experiment is the following: 0.15 grams of a 5% Pd/C catalyst are loaded in the reactor. The reactor is then flushed with nitrogen four times to remove all the water present in the reactor and leaving an inert environment. Carbon dioxide (30 bar) and oxygen (8 bar) are loaded in the reactor directly from the cylinders at 25°C, than 50 ml of methanol are injected with the HP pump. The stirrer is then turned on and the reactor cooled down to the desired temperature (-10°C, 0°C and 10°C). After stable pressure conditions are achieved, the stirrer is turned off. Vessel (25) before the MFC controller is loaded with pure hydrogen (100 bar) and pipes are purged three times with hydrogen. The desired amount of H_2 is then fed into the reactor through the MFC, and it can be measured with precision in two ways: 1) considering the time and the flow rate through the mass flow controller and 2) from the pressure decrease in the vessel, considering also the temperature and the volume of vessel and pipeline. At t=0, beginning of the reaction. hydrogen is charged and then the stirrer is turned on at 1000 rpm.

Iodometric and Karl Fisher titrations were implemented as the methods for assessing hydrogen peroxide and water content. Karl Fisher standard reference was obtained by measuring the water content before loading hydrogen, i.e. on methanol with oxygen and CO_2, after contact with the reaction environment.

2.5 Conclusions

Different reactor set-ups were successfully developed, starting with a batch reactor for preliminary tests. Then a novel trickle bed reactor for continuous operation was developed, with the aim of optimizing design and operative conditions to make H_2O_2 direct synthesis a viable process and applicable on an industrial scale, where continuous production is required.
Finally, a batch reactor set-up was developed and optimized for performing kinetics studies, with the aim of shedding some light on the complex reaction network involving H_2O_2 direct synthesis.

Chapter 3

Batch and semi-batch reactors data and modelling

3.1. Introduction

The direct synthesis of hydrogen peroxide from molecular hydrogen and oxygen over a supported palladium catalyst is studied in a laboratory-scale semi-batch reactor.
Much has been published recently on catalyst development; the most promising heterogeneous catalysts for the direct synthesis being Pd and Pd-Au catalysts (London et al. 2002, Edwards et al 2005). However, catalyst development alone does not bring us to a success in the development of a hydrogen peroxide process based on the direct synthesis. Early attempts to apply direct synthesis failed because of poor reaction rates and selectivities – the catalyst supports water formation and hydrogen peroxide decomposition, too. Thus the study of direct synthesis should always be combined to investigation on the hydrogen peroxide decomposition. The introduction of methanol as a solvent and the presence of carbon dioxide in the reaction environment introduced a breakthroughs in the process development. In this way, the solubilities of the reacting gases can be dramatically improved and the reaction enhanced.
In spite the huge interest on the direct synthesis, only few detailed kinetic studies are available for the reaction. In this chapter we illustrate an experimental campaign in a semi-batch reactor supporting a modeling effort to determine the kinetics of hydrogen peroxide synthesis and decomposition. Experiments at different temperatures and partial pressures have be performed. The final goal of this work is to develop an understanding of the kinetics of direct synthesis on a standard, commercial catalyst. The method can further be used to study the kinetics of other catalysts and as part of more complex reactor models.

3.2. Experimental

We used a commercial catalyst, in a semi-batch reactor, collecting measurements of concentration of H_2O_2 and H_2O in time, at different temperatures. Details are as follows.

3.2.1 Catalyst and catalyst characterization methods

The catalyst used is a 5% Pd on Carbon commercial catalyst from Degussa (Evonik).
Surface area and pore size distributions were obtained from N_2 adsorption/desorption isotherms at 77 K (using a Carlo Erba Sorptomatic 1900). Samples (300 mg) were pretreated at 573 K for 2 h under vacuum conditions. Surface area was calculated from the N_2 adsorption isotherm by the BET equation, and pore size distribution was determined by the BJH method. Total pore volume was taken at $p/p^0 = 0.99$.
CO chemisorption measurements were performed at 298 K using a Micromeritics pulse flow system. Prior to measurements, samples were subjected to a pretreatment involving exposure to hydrogen flow for 1 h at 298 K, followed by He purge for 2 h at the same temperature of reduction. A Perkin-Elmer 5400 ESCA spectrometer was used with monochromatized Al Kα radiation (photon energy 1486.6 eV) and a pass energy value of 35 eV. Samples were transferred to the XPS system in an ethanol solvent to protect them from oxidation in ambient air. A low energy electron gun (flood gun) was used to stabilize the charging that arises from loss of photoelectrons during X-ray bombardment. To calibrate the binding energy (BE) axis accurately, carbon 1s line at 284.6 eV was used as BE reference (Moulder 1992). In the line fitting procedure, intensity ratios of Pd 3d5/2:3d3/2 lines were kept fixed at their theoretical values (3:2) and a Doniach-Šunjić line shape (Doniach-Šunjić 1970) was used. Sensitivity factors used in determining atomic concentration ratios for Pd 3d, C 1s, Cl 2p and O 1s were 4.642, 0.296, 0.770 and 0.711, respectively (Moulder 1992). FitXPS software by D. Adams, University of Aarhus, was used in the line fitting procedure. Pd 3d lines were found on a non-linear background and parabolic background was used in the line fitting.
BET results show that the surface area is 792.8 m^2/g and the Pore specific volume is 0.887 cm^3/g. chemisorptions reveals that the average particle size is 2.62 nm and the dispersion 42.8%.
Generally, the Pd peaks for the Pd(3d5/2) and Pd(3d3/2) spin-orbit doublet reported for bulk Pd occur at about 334.9 and 340.1 eV, respectively. PdO peaks occur at about

336.5 and 341 eV. In our samples, however, the binding energies of the Pd(3d) peaks for Pd nanoparticles on C are about 1 eV higher, and are located at 337.6 and 342.3 eV, respectively (Tab 3.1) . The larger binding energies of supported Pd have been previously reported. Our result, in fact, are very close to those reported by Campbell et al. (Penner 2006), who obtained the XPS of small Pd particles (2–10 nm) on an a-Al_2O_3 (0001) single crystal under different conditions. Also Liu et al. (Liu 2009) reported a shift of 1 eV for palladium nanoparticles on silica. They also found that the binding energies of the Pd(3d) peaks increased about 1 eV compared to bulk palladium, and suggested that the shift to higher BE's for Pd nanoparticles compared to bulk Pd metal is mainly a result of final-state screening by conduction electrons. The catalyst presents an oxidized surface as explained. No changes occur to the catalyst after a 4 h reaction (Table 3.1).

Table 3.1. XPS results for the catalyst Pd/C.

Catalyst	C 1s (eV)	Pd $3d_{5/2}$ (eV)	O 1s (eV)	Cl 2p (eV)
Fresh	284.60	337.6	531.2 (34 %) 533.3 (26 %) 534.9 (28 %) 537.0 (11 %)	198.6
Used	284.60	337.6	531.5 (45 %) 533.2 (21 %) 534.7 (23 %) 536.5 (11 %)	198.6

3.2.2 Chemical analysis

During catalytic tests small aliquots of the liquid phase were sampled through a five way valve and used for water and hydrogen peroxide determination. H_2O_2 concentration was measured by iodometric titration, whereas water was determined by volumetric Karl–Fischer method. The water content in the reaction medium before catalyst addition was determined prior to each catalytic experiment.

3.2.3 Reactor system

The reactor system is a batch reactor described in details in Section 2.4.

3.2.4 Experimental procedure

The procedure and the tests carried out for H_2O_2 decomposition are described in Section 2.4. A cylinder with 25% O_2 and 75% CO_2 (mol/mol) is used. The reactor is loaded until the pressure of 22, 23 and 24 bar is reached. 400 ml of methanol are charged by the HP pump. The chiller is turned on to achieve the desired temperature. The equilibrium is reached at about 15 bar. Karl Fischer analysis is performed before introducing hydrogen. Hydrogen is loaded through a mass flow controller. The reaction starts and liquid sampling is conducted after 1, 10, 20, 30, 60, 90, 120, 150, 180, 210, 240, 300 and 360 minutes.

3.3. Qualitative observations

Kinetics experiments on hydrogen peroxide direct synthesis are carried out by varying temperature. The H_2/O_2 ratio is 1:6. In Figure 3.1 production of hydrogen peroxide and water are reported for a test at P=15bars and T= 0°C. Water production prevails and increases up to complete H_2 consumption. Hydrogen peroxide production increases more rapidly in the first hour passing through a maximum and then its concentration in the products gradually decreases.

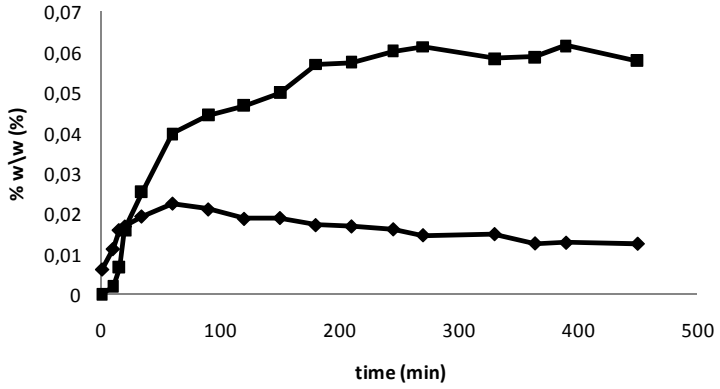

Figure 3.1. Batch synthesis of hydrogen peroxide. P=15 bar, T=0°C. H_2O_2 wt. % (diamonds), H_2O wt. % (squares).

From these results some considerations can be made. The first one is that at the beginning the reaction rate of the hydrogen peroxide direct synthesis is faster than the reactions of water formation, decomposition and hydrogenation. After thirty minutes,

the reaction rate of hydrogen peroxide begins to decrease while other reactions prevail on the direct synthesis. After one hour H_2O_2 concentration begins to decrease while water keeps increasing. The reactions of hydrogenation, decomposition and water formation are obviously faster than H_2O_2 synthesis.

Probably due to these reasons, at a certain stage molecular hydrogen decreases so the reaction of hydrogen peroxide slows down with a decreased production as a result. Moreover, hydrogen peroxide decomposition and hydrogenation accelerate owing to the increase in H_2O_2 concentration. After one hour experiment, the combination of the facts cited above leads to the evolution reported in Figure 3.1. Similar results are obtained for the evolution at different temperatures (Figures 3.2-3.3).

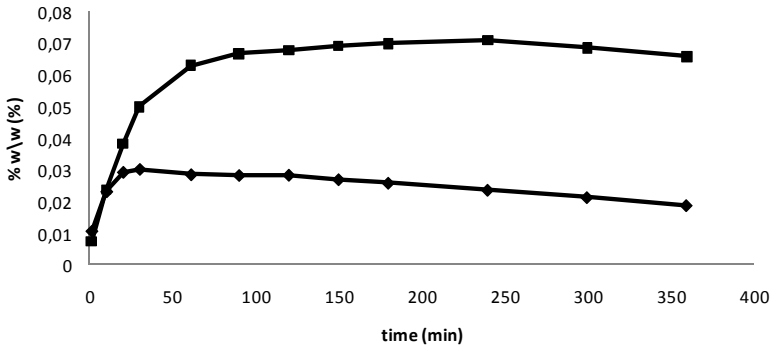

Figure 3.2. Batch synthesis of hydrogen peroxide. P=15 bar, T=10°C. H_2O_2 wt. % (diamonds), H_2O wt. % (squares).

The trend is the same for the three cases, the only difference is in the amount of water and hydrogen peroxide formed. At 0°C, Figure 3.1, the maximum H_2O_2 concentration is 0.02 wt. % at 60 minutes, and the maximum concentration of water is 0.06 wt. % at approx 300 minutes. At 10°C, Figure 3.2, the maximum H_2O_2 concentration is 0.03% wt. at 40 minutes, and for water it is 0.07 wt. % close to 300 minutes.

At -5°C, Figure 3.3 the maximum hydrogen peroxide production is about 0.03 wt.% at 70 minutes, and the maximum water production is 0.05 wt. % after 300 minutes.

The hydrogen peroxide production changes with temperature, with the maximum value being reached at 10°C after 40 minutes, at 0°C after 60 minutes and at -5°C after 70 minutes. The maximum H_2O_2 production value in wt. % is 0.03 wt.% at 10°C, 0.02 wt.% at 0°C, and 0.03 wt. % at -5°C. Probably the high production of hydrogen peroxide is due to the higher solubility of hydrogen in the liquid phase at higher temperature, meaning that there is more hydrogen in the liquid phase available for the reaction. The high production of hydrogen peroxide at -5°C is to be ascribed to the low

temperature that depress the reaction of decomposition and hydrogenation. Two different temperature conditions (10 and -5 °C) can lead to the same results in terms of maximum H_2O_2 production, as reported here (Figure 3.4).

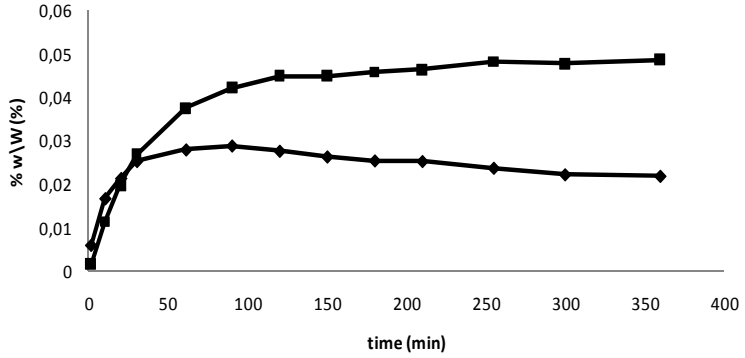

Figure 3.3. Batch synthesis of hydrogen peroxide. P=15 bar, T= -5°C. H_2O_2 wt. % (diamonds), H_2O wt. % (squares).

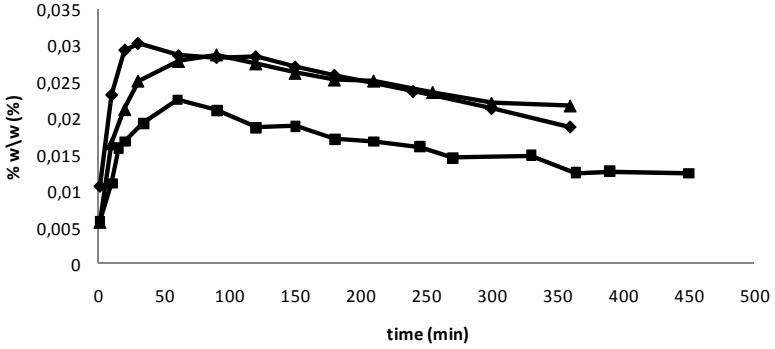

Figure 3.4. Batch synthesis of hydrogen peroxide. Production of hydrogen peroxide. 10°C (diamonds), 0°C (squares) and -5°C (triangles).

As shown in Figure 3.5, the amount of water that forms in the reactor gradually increases with time, reaching a plateau after an average of two hours, but this depends on the temperature conditions.

Selectivity data at different temperatures (Figure 3.6) are of major importance. The selectivity for all the three experiments is highest at the beginning and then it decreases sharply in the first hour, after that it remains constant for values around 10-20%. Taking into account the results of both H_2O_2 production and selectivity it is reasonable to say

that: 1) the reaction of hydrogen peroxide direct synthesis is very fast at the beginning with high selectivity; 2) hydrogenation and decomposition increase when hydrogen peroxide is produced; 3) H_2O_2 production decreases and water formation is favored when hydrogen concentration in the liquid phase decreases.

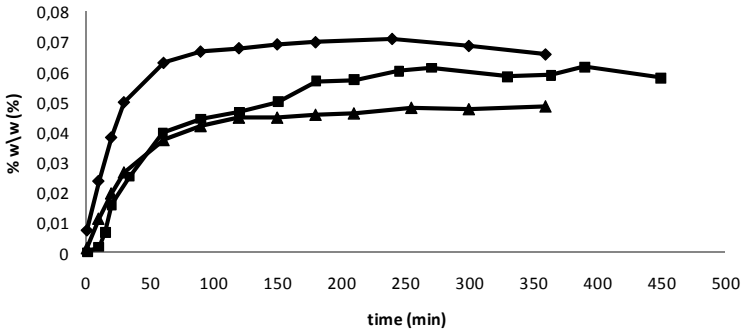

Figure 3.5. Batch synthesis of hydrogen peroxide. Production of water. 10°C (diamonds), 0°C (squares) and -5°C (triangles).

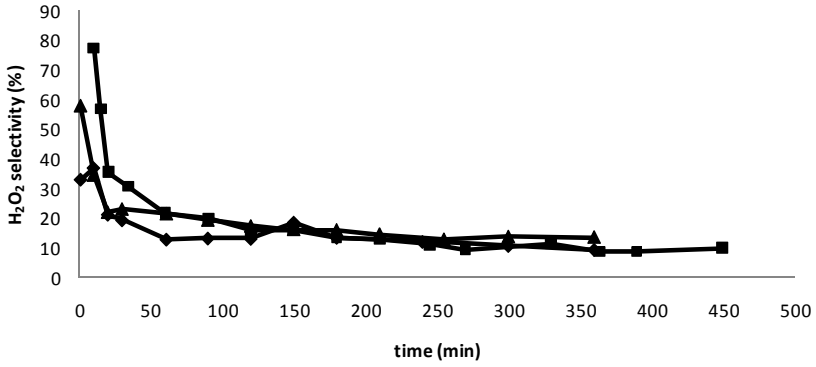

Figure 3.6. Batch synthesis of hydrogen peroxide. Selectivity to hydrogen peroxide. 10°C (diamonds), 0°C (squares) and -5°C (triangles).

The maximum selectivity is about 80% at 0°C, then 60% at -5°C, and 40% at 10 °C. That means that without stabilizers the temperature and reaction time play an important role on the selectivity. Further, a short contact time is necessary to achieve high selectivity, but the highest selectivity corresponds to very low productivity.

3.4. Quantitative speculations

In the following we attempt to speculate quatitatively on the data collected so far in the batch reactor, shown in Figures 3.1-3.4. The effort aims at shaping a first modeling framework to further analyses of experimental data and simulation of more complex reactor configurations.

3.4.1 Mass balances for batch and semi-batch operation

The derivations of the mass balances of the components in the batch reactor is based on the assumption that the reactor is completely backmixed and thus the interfacial gas-liquid mass transfer resistance is negligible. The system can either be completely under batch conditions, or alternatively, gas mixtures (H_2/CO_2 and O_2/CO_2) are continuously added in such a way that the total pressure is maintained constant. This kind of addition policy implies that the gas and liquid phases are gradually enriched with respect to CO_2, since it is continuously fed into the system but not consumed in any reaction.
The mass balances for H_2, O_2 and CO_2 (i) in the gas phase can be written as:

$$dn_{i,G} / dt = n'_{0,i} - N_i A \qquad \text{(Eq. 3.1)}$$

where n'_0 and N denote the added flow and the interfacial flux, respectively (see Notation).
For the same species in the liquid phase we write similarly

$$dn_{i,L} / dt = \rho_B r_i V_L + N_i A \qquad \text{(Eq. 3.2)}$$

Assuming that

1. reaction (r_i) takes place in the liquid only
2. mass flux is positive if entering the liquid from the gas phase
3. no liquid is fed into the system during the experiment
4. no reactions proceed in the liquid film
5. the interfacial mass transfer is rapid.

Total *i-th* amount balance is given by the addition of the balances for gas and liquid phases:

$$dn_{i,G} / dt + dn_{i,L} / dt = \rho_B r_i V_L + n'_{0i} \qquad \text{(Eq. 3.3)}$$

The amounts (moles) of substance can be related to molar concentrations as:

$$n_{iG} = c_{iG} V_G \qquad \text{(Eq. 3.4)}$$

$$n_{iL} = c_{iL} V_L \qquad \text{(Eq. 3.5)}$$

Gas-liquid equilibrium is assumed for the case of a rapid mass transfer. Accordingly, concentrations of the same species in gas and liquid is constrained by the equilibrium:

$$c_{iG} = K_i c_{iL} \qquad \text{(Eq. 3.6)}$$

where K_i is the equilibrium ratio, which in its general form depends on the composition, total pressure and temperature. The values of K_i can estimated from a VLE model (see Appendix).

With the equations above we can rewrite the variation of total moles of species *i* in terms of the sole concentration in one phase, say the liquid one, where reaction occurs:

$$dn_{i,G} / dt + dn_{i,L} / dt = (K_i V_G + V_L) dc_{iL} / dt \qquad \text{(Eq. 3.7)}$$

The mass balance can now be reformulated as:

$$(K_i \alpha + 1) V_L dc_{iL} / dt = \rho_B r_i V_L + c_{0iG} V'_{0G} \qquad \text{(Eq. 3.8)}$$

or explicitly as:

$$dc_{iL} / dt = (K_i \alpha + 1)^{-1} (\rho_B r_i + c_{0iG} V'_{0G} / V_L) \qquad \text{(Eq. 3.9)}$$

The mass balance of species *i* can be formulated in term of gas-phase concentrations ($c_{iG}=K_i c_{Li}$) as well:

$$dc_{iG} / dt = K_i (K_i \alpha + 1)^{-1} (\rho_B r_i + c_{0iG} V'_{0G} / V_L) \qquad \text{(Eq. 3.10)}$$

The total pressure of the system is controlled and kept constant by further additions of gas, $P=P_0$. If we assume for simplicity that the gas phase behaves as an ideal gas mixture, and the only species in this phase are H_2, O_2, and CO_2 (we neglect vapor pressure of methanol and water) then $P=c_G RT$. At constant T, isobaric conditions requires $dc_G/dt=0$, which implies in practice that:

$$dc_{H2G} / dt + dc_{O2G} / dt + dc_{CO2G} / dt = 0 \qquad \text{(Eq. 3.11)}$$

or $c_G = cost = c_{0G} = c_{0\,H2\,G} + c_{0\,O2\,G} + c_{0\,CO2\,G}$.

After inserting the mass balances (Eq. 3.10) into Eq. 3.11 it results:

$$K_{H2}(\alpha K_{H2}+1)^{-1}\rho_B r_{H2} + K_{O2}(\alpha K_{O2}+1)^{-1}\rho_B r_{O2} + K_{H2}(\alpha K_{H2}+1)^{-1} c_{0H2G} V'_{0G}/V_L + K_{O2}(\alpha K_{o2}+1)^{-1} c_{0O2G} V'_{0G}/V_L + K_{CO2}(\alpha K_{CO2}+1)^{-1} c_{0CO2G} V'_{0G}/V_L = 0$$

(Eq. 3.12)

From the above expression, the total molar flow added-to-liquid volume can be solved explicitly:

$$c_{0G} V'_{0G}/V_L = \frac{-(K_{H2}(\alpha K_{H2}+1)^{-1}\rho_B r_{H2} + K_{O2}(\alpha K_{O2}+1)^{-1}\rho_B r_{O2})}{K_{H2} x_{0H2}(\alpha K_{H2}+1)^{-1} + K_{O2} x_{0O2}(\alpha K_{O2}+1)^{-1} + K_{CO2} x_{0CO2}(\alpha K_{CO2}+1)^{-1}} = \beta$$

(Eq. 3.13)

It should be noticed that factor β has the unit mol/(dm^3 min), i.e. the same unit as the reaction rate and it vanishes in the absence of any addition.
The balance equation can now be written in a compact form:

$$dc_{iL}/dt = (K_i\alpha + 1)^{-1}(\rho_B r_i + x_{0iG}\beta) \qquad \text{(Eq. 3.14)}$$

where:

$$\beta = \frac{-(K_{H2}(\alpha K_{H2}+1)^{-1} r_{H2} + K_{O2}(\alpha K_{O2}+1)^{-1} r_{O2})\rho_B}{\sum K_j x_{0j}(\alpha K_j + 1)^{-1}} \qquad \text{(Eq. 3.15)}$$

3.4.2 Overall thermodynamics and gas-liquid equilibrium

The overall thermodynamics, i.e. the reaction enthalpies and Gibbs free energies are given in Section 1.2.4. For the calculation of the vapor-liquid equilibrium, the Peng-Robinson equation of state, suitably corrected and adjusted, is used. From these calculations, vapor-liquid equilibrium ratios needed in the reactor model are obtained for hydrogen, oxygen and carbon dioxide. The densities of the reaction mixtures are also estimated.

3.4.3 Reaction mechanism and rate equations

The following overall reactions are considered to explain the hydrogen peroxide formation and decomposition: the reactions between hydrogen and oxygen yielding

hydrogen peroxide and water as well as the spontaneous and hydrogen-assisted decomposition of hydrogen peroxide to water and oxygen. The overall reactions can be summarized as follows,

$$H_2+O_2=H_2O_2 \quad \text{(Eq. 1.1)}$$

$$H_2+½O_2 = H_2O \quad \text{(Eq. 1.2)}$$

$$H_2O_2=H_2O +½O_2 \quad \text{(Eq. 1.3)}$$

$$H_2O_2+H_2=2H_2O \quad \text{(Eq. 1.4)}$$

All these reactions are highly exothermic and thermodynamically favored, as discussed in Section 1.2.4.

Several surface mechanisms on palladium can give the overall process described by equations (Eqs. 1.1-1.4). Voloshin et al. (2007) screened some mechanisms to describe kinetic data obtained from microstructured reactors and concluded that a Langmuir-Hinshelwood-type mechanism with the surface reaction steps as the rate determining ones gave the best agreement with experimental data. Some mechanistic studies have given information about the reaction mechanism. For instance, Dissanyake and Lunsford (2003) proposed that the O-O bond does not dissociate during the H_2O_2 synthesis process and Sivadinarayana et al. (2004) confirmed the presence of HO_2- species on a gold catalyst surface. However, it is clear that water formation requires the rupture of the O-O bond on the catalyst surface. Oxygen is known to adsorb both dissociatively and non-dissociatively on Pd surfaces.

Some basic assumptions are used here to describe the rate equations for the overall reactions reported in Eqs. 1.1-1.4 in a manner as simple as possible, yet mechanistic. Hydrogen and oxygen are assumed to adsorb dissociatively on the metal surface, surface hydroxyl groups are formed and they play a key role in the formation of both hydrogen peroxide and water; hydrogen peroxide and water adsorb on the metal surface. The decomposition of hydrogen peroxide in the absence of the catalyst is neglected, since it does not play any role under the current experimental conditions. Based on these assumptions, the reaction mechanism – the adsorption, desorption and surface reaction steps along with the stoichiometric numbers (ν) – can be summarized in Table 3.2. By combining the reaction steps with the corresponding stoichiometric number along the reaction routes, the four overall reactions are obtained (Eqs. 1.1-1.4).

Table 3.2. Surface reaction steps, and stoichiometric numbers.

	Step #	ν_{P1}	ν_{P2}	ν_{P3}	ν_{P4}
$H_2 + 2* = 2H*$	I	1	1	0	1
$O_2 + 2* = 2O*$	II	1	½	½	0
$O* + H* = OH* + *$	III	2	1	0	0
$OH* + OH* = HOOH* + *$	IV	1	0	0	0
$OH* + H* = H_2O* + *$	V	0	1	0	1
$HOOH* + * = H_2O* + O*$	VI	0	0	1	0
$HOOH* + H* = OH* + H_2O*$	VII	0	0	0	1
$HOOH* = H_2O_2 + *$	VIII	1	0	-1	-1
$H_2O* = H_2O + *$	IX	0	1	1	2

The adsorption and desorption steps are assumed to be rapid enough to reach quasi-equilibria, while the surface reaction steps are assumed to limit the rates. For hydrogen and oxygen, the quasi-equilibrium hypothesis yields:

$$K_H = \frac{c_H{}^{*2}}{c_{H2}\, c\, {}^{*2}} \qquad \text{(Eq. 3.16)}$$

$$K_O = \frac{c_O{}^{*2}}{c_{O2}\, c\, {}^{*2}} \qquad \text{(Eq. 3.17)}$$

from which the concentrations of the adsorbed species can be expressed as function of the gas-phase concentrations:

$$c_{H*} = (K_H\ c_{H2})^{1/2} c_* \qquad \text{(Eq. 3.18)}$$

$$c_{O*} = (K_O\ c_{O2})^{1/2} c_* \qquad \text{(Eq. 3.19)}$$

Application of the quasi-equilibrium hypothesis on the surface hydroxyls gives:

$$K_3 = \frac{c_{OH*} c_*}{c_{O*}\ c_{H*}} \qquad \text{(Eq. 3.20)}$$

which combined with the quasi-equilibria for adsorbed hydrogen and oxygen gives:

$$c_{OH*} = K_3 (K_H\ c_{H2})^{1/2} (K_O\ c_{O2})^{1/2} c_* \qquad \text{(Eq. 3.21)}$$

Analogously, the adsorption equilibria of hydrogen peroxide and water give the corresponding surface concentrations as described below:

$$c_{HOOH*} = K_{H2O2}\ c_{H2O2} c_* \qquad \text{(Eq. 3.22)}$$

$$c_{H2O*} = K_{H2O}\ c_{H2O} c_* \qquad \text{(Eq. 3.23)}$$

The total site balance comprises all the adsorbed species and the vacant sites:

$$c_* + c_{H*} + c_{O*} + c_{OH*} + c_{HOOH*} + c_{H2O*} = c_O \qquad \text{(Eq. 3.24)}$$

where c_0 denotes the total number of surface sites. After inserting the quasi-equilibrium expressions (Eqs. 3.18-3.19) and Eqs. 3.21-3.23 into the balance equation, the fraction of vacant sites can be calculated:

$$((K_H\ c_{H2})^{1/2} + (K_O\ c_{O2})^{1/2} + K_3 (K_H\ c_{H2})^{1/2} (K_O\ c_{O2})^{1/2} + K_{H2O}\ c_{H2O} + K_{H2O2}\ c_{H2O2} + 1) c_* = c_0 \qquad \text{(Eq. 3.25)}$$

$$c_* / c_0 = ((K_H\ c_{H2})^{1/2} + (K_O\ c_{O2})^{1/2} + K_3 (K_H\ c_{H2})^{1/2} (K_O\ c_{O2})^{1/2} + K_{H2O}\ c_{H2O} + K_{H2O2}\ c_{H2O2} + 1)^{-1} = D^{-1} \qquad \text{(Eq. 3.26)}$$

The rates of the rate-limiting steps can now be written as:

$$r_4 = k_4 (c_{OH*}{}^2 - c_{HOOH*} c_* / K_4) \qquad \text{(Eq. 3.27)}$$

$$r_5 = k_5 (c_{OH*} c_{H*} - c_{H2O*} c_* / K_5) \qquad \text{(Eq. 3.28)}$$

$$r_6 = k_6 (c_{HOOH*} c_* - c_{H2O*} c_{O*} / K_6) \qquad \text{(Eq. 3.29)}$$

$$r_7 = k_7 (c_{HOOH*} c_{H*} - c_{OH*} c_{H2O*} / K_7) \qquad \text{(Eq. 3.30)}$$

The concentrations of the surface species are expressed with the quasi-equilibria and the fraction of vacant sites. After inserting all these expressions, the rate equations can be rearranged. The constants can be merged, so that just a forward rate constant and an equilibrium constant is used for each step (see Notation for the merged constants):

$$r_4 = k'_4 (c_{H2} c_{O2} - c_{H2O2} / K'_4) / D^2 \qquad \text{(Eq. 3.31)}$$

$$r_5 = k'_5 (c_{H2} c_{O2}{}^{1/2} - c_{H2O} / K'_5) / D^2 \qquad \text{(Eq. 3.32)}$$

$$r_6 = k'_6 (c_{H2O2} - c_{H2O} c_{O2}{}^{1/2} / K'_6) / D^2 \qquad \text{(Eq. 3.33)}$$

$$r_7 = k'_7 c_{H2}{}^{1/2} (c_{H2O2} - c_{O2}{}^{1/2} c_{H2O} / K'_7) / D^2 \qquad \text{(Eq. 3.34)}$$

A comparison of r_6 and r_7 is interesting; at equilibrium, both rates are zero, which also implies that $K'_6 = K'_7$, i.e. the reactions have the same equilibrium constant because of the thermodynamic constraints.

If all steps are irreversible, the simple rate expressions are obtained, as summarized below:

$$r_4 = k'_4 c_{H2} c_{O2} / D^2 \quad \text{(Eq. 3.35)}$$

$$r_5 = k'_5 c_{H2} c_{O2}^{1/2} / D^2 \quad \text{(Eq. 3.36)}$$

$$r_6 = k'_6 c_{H2O2} / D^2 \quad \text{(Eq. 3.37)}$$

$$r_7 = k'_7 c_{H2}^{1/2} c_{H2O2} / D^2 \quad \text{(Eq. 3.38)}$$

It should be noticed that the adsorption of methanol and carbon dioxide is not considered so far. If the adsorption is assumed to be molecular, i.e. A + *= A* (A=CO_2 or A=CH_3OH), the denominator (D) is completed by adding the terms $K_i c_i$ for i=CO_2, CH3OH also.

Based on the irreversible reaction rates (Eqs. 3.35-3.38), the observed reaction orders with respect to hydrogen, oxygen and hydrogen peroxide can be analyzed as shown in Table 3.3.

Table 3.3. Limits of the reaction orders of the forward reactions. H=hydrogen, O=oxygen, P=hydrogen peroxide

Reaction	Hmin	Hmax	Omin	Omax	Pmin	Pmax
4	0	1	0	1	-2	0
5	0	1	-0.5	0.5	-2	0
6	-1	0	-1	0	-1	1
7	-0.5	0.5	-1	0	-1	1

As the table reveals, a wide variation of the reaction orders is at least theoretically possible. The important message is that, due to the adsorption phenomena, reaction orders of hydrogen and oxygen which are less than ½ and 1 can be expected.

The generation rates are formulated with the aid of the rate-limiting steps IV-VII corresponding to the overall reactions reported in Eqs. 1.1-1.4. The following expressions are obtained:

$$r_{H2O2} = r_4 - r_6 - r_7 \quad \text{(Eq. 3.39)}$$

$$r_{H2O} = r_5 + r_6 + r_7 \quad \text{(Eq. 3.40)}$$

$$r_{H2} = -r_4 - r_5 - r_7 \quad \text{(Eq. 3.41)}$$

$$r_{O2} = -r_4 - 1/2 r_5 + 1/2 r_6 \quad \text{(Eq. 3.42)}$$

$$r_{CO2} = 0 \quad \text{(Eq. 3.43)}$$

The generation rate expressions were inserted into the mass balances of the components, i.e. to equations 3.14 and 3.15.

3.4.4 Estimation of kinetic parameters

The mass balance equations are solved with respect to each liquid-phase concentration during the estimation of the kinetic parameters. The following objective function (Q) was minimized to obtain the best fit to the experimentally recorded hydrogen peroxide and water concentrations:

$$Q = \sum_t \left(c_{i\,\mathrm{exp},t} - c_{i,t} \right)^2 \quad \text{(Eq. 3.44)}$$

where $c_{i,exp,t}$ and $c_{i,t}$ denote the concentrations experimentally recorded and predicted by the model, respectively at any sampling time. The objective function is minimized by a hybrid simplex-Levenberg-Marquardt algorithm implemented in Modest software (Haario 2007). The differential equations, i.e. the mass balances, are solved numerically during the parameter estimation by a robust backward difference algorithm for stiff differential equations.

The parameters obtained are then checked with different methods. The standard statistical analysis gives the standard errors of the parameters as well as their mutual correlations (the correlation matrix). The identification of each parameter is studied by preparing sensitivity plots, in which the objective function is plotted as a function of one of the parameters, while the other parameter values are kept fixed to the same value, which gives the objective function minimum.

The overall fit of the model is characterized by the degree of explanation (R^2), which is defined as follows:

$$R^2 = 1 - \frac{\Sigma (c_{i\,\mathrm{exp},t} - c_{i,t})^2}{\Sigma (c_{i\,\mathrm{exp},t} - c_{iav,t})^2} \quad \text{(Eq. 3.45)}$$

As revealed by Eq. 3.45, R^2 compares the model performance with the simplest possible model, namely the average of all experimental values.

3.4.5 Parameter estimation results and model simulations

The equations derived in the former two sections have been implemented in the Modest software (Haario 2007). For convenience, they are summarized in the following:

$$D = \sqrt{K_{H2} * cH_2} + \sqrt{K_{O_2} * cO_2} + (K_{3eq} * \sqrt{K_H * K_O} * \sqrt{cH_2 * cO_2}) + \\ + (K_{H_2O_2} * cH_2O_2) + (K_{H_2O} * cH_2O) + 1.0d0 \qquad \text{(Eq. 3.46)}$$

$$z = \frac{1.0d0}{Temp} - \frac{1.0d0}{Tmean} \qquad \text{(Eq. 3.47)}$$

$$k_4 = A_4^{\frac{-Ea_4}{R*z}} \qquad \text{(Eq. 3.48)}$$

$$k_5 = A_5^{\frac{-Ea_5}{R*z}} \qquad \text{(Eq. 3.49)}$$

$$k_6 = A_6^{\frac{-Ea_6}{R*z}} \qquad \text{(Eq. 3.50)}$$

$$k_7 = A_7^{\frac{-Ea_7}{R*z}} \qquad \text{(Eq. 3.51)}$$

$$r_4 = k_4 * \frac{\frac{cH_2 * cO_2 - cH_2O_2}{K_{eq_4}}}{D^2} \qquad \text{(Eq. 3.52)}$$

$$r_5 = k_5 * \frac{\frac{cH_2 * \sqrt{cO_2} - cH_2O}{K_{eq_5}}}{D^2} \qquad \text{(Eq. 3.53)}$$

$$r_6 = k_6 * \frac{\frac{cH_2O_2 - (cH_2O * \sqrt{cO_2})}{K_{eq_6}}}{D^2} \qquad \text{(Eq. 3.54)}$$

$$r_7 = k_7 * \frac{\frac{(cH_2O_2 * \sqrt{cH_2}) - (\sqrt{cH_2} * \sqrt{cO_2} * cH_2O)}{K_{eq_7}}}{D^2} \quad \text{(Eq. 3.55)}$$

$$r_{H_2O_2} = r_4 - r_6 - r_7 \quad \text{(Eq. 3.56)}$$

$$r_{H_2O} = r_5 + r_6 + r_7 \quad \text{(Eq. 3.57)}$$

$$r_{H_2} = -r_4 - r_5 + r_7 \quad \text{(Eq. 3.58)}$$

$$r_{O_2} = -r_4 - (0.5d0 * r_5) + (0.5d0 * r_6) \quad \text{(Eq. 3.59)}$$

$$r_{CO_2} = 0.0d0 \quad \text{(Eq. 3.60)}$$

$$\rho B = \frac{mcat}{VL} \quad \text{(Eq. 3.61)}$$

$$ds(1) = \frac{1.0d0}{(\alpha * KGL_{H_2} + 1.0d0) * (r_{H_2} * \rho B + x_0 H_2 G * \beta)} \quad \text{(Eq. 3.62)}$$

$$ds(2) = \frac{1.0d0}{(\alpha * KGL_{O_2} + 1.0d0) * (r_{O_2} * \rho B + x_0 O_2 G * \beta)} \quad \text{(Eq. 3.63)}$$

$$ds(3) = \frac{1.0d0}{(\alpha * KGL_{CO_2} + 1.0d0) * (r_{CO_2} * \rho B + x_0 CO_2 G * \beta)} \quad \text{(Eq. 3.64)}$$

$$ds(4) = r_{H_2O_2} * \rho B \quad \text{(Eq. 3.65)}$$

$$ds(5) = r_{H_2O} * \rho B \quad \text{(Eq. 3.66)}$$

Data of experiments at -5°, 0° and 10° are used, corresponding to Figures 3.1-3.3. Parameters include Arrhenius constants for reaction 4 to 7 (Eqs. 3.48-3.51) and adsorption equilibrium constants.

The best fit values of the parameters are reported in Table 3.4.

With this first model attempt and parameter estimates, the experimental data are reproduced semi-quantitatively, as shown in Figure 3.5.

It is evident that some important features of the experimental data are not explained yet. The lack of a conclusive model for VLE might be one of the causes, but failing to predict the maximum of H_2O_2 production is a major limitations to extend the validity of the model. It definitely indicates some lack of explanation in the kinetics, where future efforts must concentrate.

Table 3.4. Best fit values of the model parameters

Parameters	Best fit
A_4	9.87
A_5	0.967E+03
A_6	0.399E+05
A_7	0.187E+03
Ea_4	0.516E+05
Ea_5	0.487E+05
Ea_6	0.529E+05
Ea_7	0.511E+05
KH_2	0.324E-04
KO_2	3.58
KH	1.82
KH_2O_2	0.907E-05
KH_2O	89.1
KO	0.935
K3eq	0.259

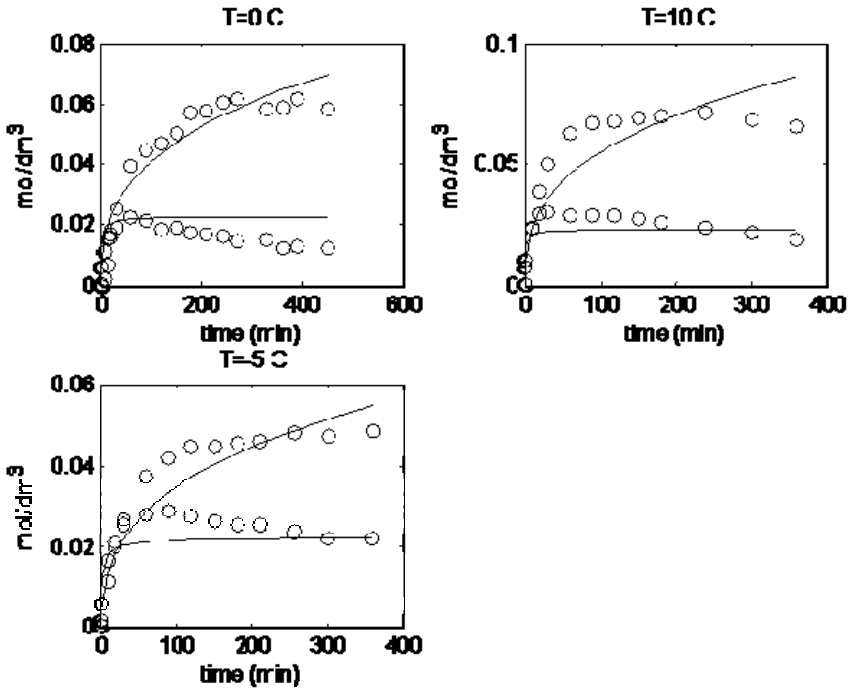

Figure. 3.5.Model of experimental data, upper curve is water and lower one is H_2O_2

3.5 Conclusions

The direct synthesis of hydrogen peroxide from molecular hydrogen and oxygen over a supported palladium catalyst was studied in a laboratory-scale semibatch reactor. The catalyst was in a form of finely dispersed slurry in the reactor to reduce the internal and external mass transfer resistances. Experiments carried out under kinetic control revealed that hydrogen peroxide was successfully formed on the catalyst surface, but it was decomposed as the reaction time was prolonged. The mass balances of the components were considered in detail, taking into account the enrichment of carbon dioxide in the system during semibatch operation. A Langmuir-Hinshelwood rate mechanism was proposed, based on the competitive adsorption of hydrogen and oxygen on the palladium surface. The surface reactions leading to the formation of hydrogen peroxide and water were assumed to be rate determining, after which the rate equations describing the system were derived and the kinetic parameters were estimated by nonlinear regression analysis. The model fairly fits the experimental data but requires further refinement to be confidently used to predict the behavior of batch and flow reactors.

Notation

A	interfacial area
A’	frequency factor
c	concentration
c*	concentration of a surface species
D	denominator in rate expression
E_a	activation energy
K	equilibrium constant
K’	merged equilibrium constant
k	reaction rate constant
k’	merged rate constant
N	flux
n	amount of substance
n’	flow of amount of substance (molar flow)
P	total pressure
Q	objective function
R	gas constant
R^2	degree of explanation
r	reaction rate
r_i	component (*i*) production rate
T	temperature
t	time
V	volume
V’	volumetric flow rate
x	mole fraction
α	gas-to-liquid volume ratio
β	parameter in mass balance
ν	stoichiometric number

Subscripts and superscripts

av	average
G	gas
i, j	component indices
L	liquid
P	reaction route
t	time
0	inlet property

Chapter 4

Direct Synthesis of hydrogen peroxide in a Trickle Bed Reactor (TBR).

4.1 Introduction

Pd is the most used and well known catalyst for the direct synthesis of H_2O_2. The main problem is that Pd also promotes the decomposition of the hydrogen peroxide, triggering a competition between H_2O_2 formation and consumption.
In this chapter a study on Hydrogen peroxide direct synthesis using a new continuous reactor approach is presented. A Trickle Bed Reactor was built to perform the experiments on the direct synthesis. The catalyst chosen for these experiments was palladium supported on sulfated-ceria (Pd-CeS). The aim of the work is to show how a systematic study on the reactor is needed to enhance the performance of the catalyst in hydrogen peroxide direct synthesis
H_2O_2 decomposition experiments are also performed in order to verify how the examined catalytic system, under specified conditions, affects H_2O_2 reduction and decomposition to yield water.

4.2 Experimental

4.2.1 Materials

$(NH_4)_2Ce(NO_3)_6$ (Sigma-Aldrich), $(NH_4)_2SO_4$ (Merck), were used for sample synthesis as received. Methanol for HPLC was used as reaction medium (J.T. BAKER 99,99%), potassium iodide (sigma-aldrich), Hydranal-Composite 2 (Fluka), dry methanol for KFT (Fluka), Acetic Acid (Sigma-Aldrich), Sodium Thiosulfate penta-hydrate 99,5% (Sigma-Aldrich), Starch (Sigma-Aldrich), Potassium dichromate (Riedel de Haën), H_2O_2 30% w/w (Merck).

4.2.2 Catalyst preparation

Ceria support substrate was synthesized by precipitation with urea from $(NH_4)_2Ce(NO_3)_6$ aqueous solution. The solution was continuously mixed for 6 hour at 100°C, the precipitate was washed twice in boiling deionized water and dried in oven at 110°C overnight. These materials were impregnated by an incipient wetness method with a proper amount of $(NH_4)_2SO_4$ to yield an 8% wt anion loading. Impregnated supports were calcined in flowing air (50 ml/min) at 650°C for 3 hour. Afterwards, calcined supports were impregnated via incipient wetness with H_2PdCl_4 aqueous solution to give a nominal 2.5% wt Pd-loaded catalyst, and finally calcined again at 500°C in flowing air for 3 hour. The catalyst was crushed and sieved (0.5-1 mm). Pure SiO_2 was crushed and sieved (0.5-1mm). 0.16 grams of Pd-CeS were mixed with 0.2 grams of SiO_2 and used as the catalytic bed in the continuous reactor. The catalyst was than reduced for 1 hour with a 20 ml/min flow of pure hydrogen (1bar, 25 °C) (Menegazzo 2008).

4.2.3 Reactor set-up for the experiments

The reactor set-up is described in detail in Section 2.3. Briefly, an AISI 316 stainless steel trickle-bed reactor was realized, with a catalyst bed up to 20 cm long in it. An external cooling system allows for working temperature between -20°C and 60°C. Three mass flow controllers (MFC) are used to feed the gases into the reactor. Every MFC is connected to a gas cylinder: N_2, CO_2/ H_2 97.5/2.5%, and O_2. The pressure inside the reactor is controlled and regulated with a back pressure controller (BPC). The liquid phase is fed in through a syringe pump. The catalyst bed (7 mm) is placed between two quartz wool plugs. From the bottom 37 mm of quartz wool, 7 mm of catalyst and inert particles, 26 mm of quartz wool and 140 mm of quartz sand (sieved under 0,2 mm).

4.2.5 H_2O_2 experiments and analyses

Preliminary H_2O_2 **decomposition** experiments are carried out at 10 bar and -10°C, with 0.5% H_2O_2 in methanol as the liquid phase. The concentration of H_2O_2 might appear quite low, but it is consistent with values achievable at the present with the available catalysts. H_2, N_2 and CO_2 compose the gas phase for hydrogenation experiments, with 2%, 18% and 80% (mol/mol), respectively. For decomposition experiments, only N_2 and CO_2 are used, with a composition of 20% and 80% (mol/mol), respectively. The liquid flow rates chosen are: 0.5, 1 and 2 ml/min.

Different values for the total gas flow rates are examined: 0.1, 1, 2, 2.7, 4, 6, 9 and 12 ml/min, at temperature and pressure conditions reported above.

The experiments of **direct synthesis** are carried out at 10 or 20 bar and -10°C, with methanol as the solvent. H_2, O_2 and CO_2 are fed into the reactor with the following composition: 2%, 18% and 80% (mol/mol), respectively. Liquid flow rates are: 0.5, 1 and 2 ml/min of methanol. The total gas flow rates tested are: 1, 2, 2.7, 4, 6, 9 and 12 ml/min, at a temperature of -10°C and a pressure of 10 bar. In the experiments carried out at 20 bar, the gas flow rates are: 1, 2, 2.7, 4, 6 ml/min.
Freshly produced catalyst is introduced into the reactor without pretreatments. Catalyst is then reduced in situ with a constant 20 ml/min flow of H_2 at room temperature. After this initial procedure, catalytic bed is prewetted for several hours (4 h) to ensure complete internal saturation and external wetting.
During experiments, small aliquots of the liquid phase are sampled through a valve positioned at the exit of the TBR, and used for water and hydrogen peroxide content determination. Specifically, H_2O_2 concentration is measured by iodometric titration, whereas water content is determined by volumetric Karl Fischer method. Water content is also measured in the reaction medium prior to each experiment, i.e. before feeding the oxygen. Protocol details are described in Section 1.4.

4.3 Results and discussion

4.3.1 H_2O_2 reduction and decomposition

The experiments of H_2O_2 reduction were carried out with the same catalyst and under the same operative conditions as the synthesis, to quantify the degree of hydrogen peroxide decomposition and hydrogenation. As reported in Section 1.2.4, there are several secondary reactions that are thermodynamically favored, leading to a decrease in H_2O_2 yield.
Results of decomposition and hydrogenation tests with different gas and liquid flow rates are shown in Figures 4.1-4.5. Results are shown as percentage of H2O2 disappeared in the outlet, with respect to the inlet. In addition, the inverse of the flow rate is used, which is proportional to the residence time.
Experiments were carried out with a solution of H_2O_2 in methanol (0.5% w/w), feeding a mixture of CO_2/N_2 (80%,20% mol), or a ternary $CO_2/H_2/N_2$ (80%,18%,2% mol) gas mixture.

The decomposition profile is similar in both cases, with and without H2. The presence of H2 always increase the amount of H2O2 that decomposes, up to approx 6%. At the beginning (short contact time in the reactor) the fractional decompositions are also comparable, but with a longer reaction time (lower flow rates), the reduction and simple decomposition behavior diverge. The experiments with CO_2 and N_2 only were designed to elucidate the effect of H_2O_2 decomposition alone, since hydrogenation is obviously not possible without H_2. Interestingly, the effect of H_2O_2 hydrogenation is always evident and quantifiable when comparing those results with the ones relative to the ternary gas mixture, proving that the catalyst is active for both reactions. Contact time clearly affect the amount of decomposition; at the lowers liquid flow rate tested decomposition can approach 20% of the available H2O2. Decomposition and hydrogenation also increase with longer gas contact time, except for the case of the highest liquid flow rate used, Figure 4.3. H_2 is continuously dissolved in the liquid phase, with no vapor-liquid equilibrium achievement and a noticeable pressure drop (0.5 bar), as measured by the back pressure controller. These results can be seen when an extremely low gas flow rate (0.1 ml/min) is used, and because of these issues and such a poor response, this flow rates combination is not considered further in subsequent experiments, when optimizing operative conditions.

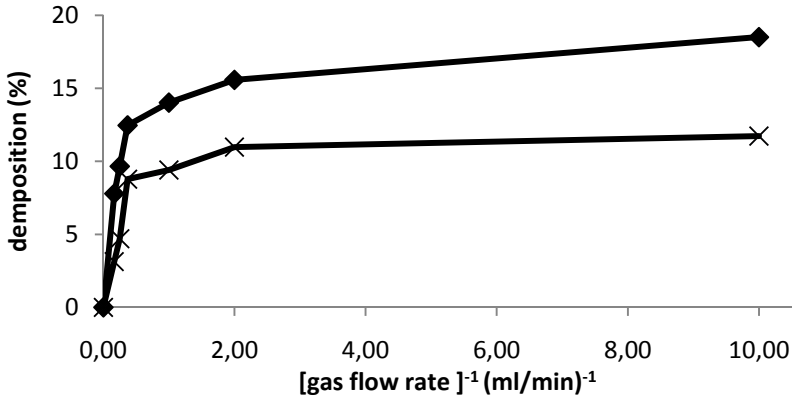

Figure 4.1. Comparison between decomposition and hydrogenation of 0.5% H_2O_2 in methanol with 0.5 ml/min liquid flow rate and different gas flow rates. $CO_2/H_2/N_2$ 80%/2%/18% respectively (diamonds), CO_2/N_2 80%/20% (X-shaped).

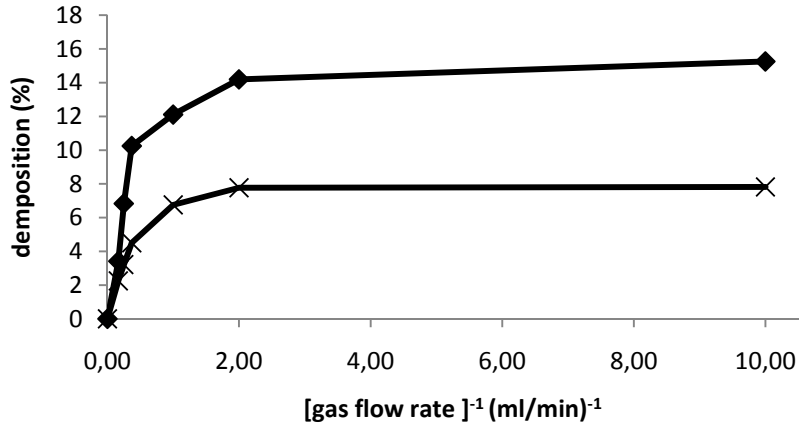

Figure 4.2. Comparison between decomposition and hydrogenation of 0.5% H_2O_2 in methanol with 1 ml/min liquid flow rate and different gas flow rates. $CO_2/H_2/N_2$ 80%/2%/18% respectively (diamonds), CO_2/N_2 80%/20% (X-shaped).

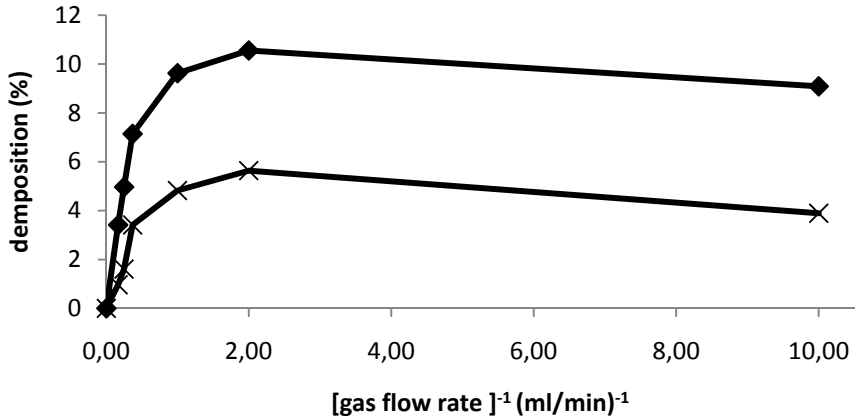

Figure 4.3. Comparison between decomposition and hydrogenation of 0.5% H_2O_2 in methanol with 2 ml/min liquid flow rate and different gas flow rates. $CO_2/H_2/N_2$ 80%/2%/18% respectively (diamonds), CO_2/N_2 80%/20% (X-shaped).

A comparison of the extent of H_2O_2 hydrogenation with different gas and liquid flow rates is reported in Figure 4.4. With the highest liquid flow rates the amount of H_2O_2 that undergoes hydrogenation is fairly limited, so suggesting that synthesis can be viable, particularly if its rate can be higher than decomposition and hydrogenation.

It is worth noticing that the maximum amount of hydrogen peroxide decomposed and hydrogenated is around 18%, which is achieved when both liquid and gas flow rates are lowest. These values provides an upper bound of hydrogen peroxide that can be decomposed, since H_2O_2 is present from the very beginning in the catalytic bed, and at a significant concentration, hardly achieved in the following synthesis experiments. When hydrogen peroxide synthesis is performed in the TBR, the extent of decomposition and hydrogenation is lower than what is measured in these

experiments, as H_2O_2 is being formed on the catalytic surface. Reasonably, in the first part of the bed decomposition and hydrogenation can be neglected because the concentration of hydrogen peroxide is approximately zero.

As a result, we can conclude that:

i) if the amount of water formed during H_2O_2 synthesis reaction, under the same operative conditions, is higher than the maximum value of water obtained during the hydrogenation and decomposition experiments, the excess water formed is to be ascribed to the direct water formation reaction (Section 1.2.4, Eq. 1.2), which competes with H_2O_2 synthesis.

ii) the gas flow rate cannot be too low; its increase leads to limitation in decomposition and reduction and must mach the similar reduction of H2O2 expected, to identify an optimum condition.

iii) too high a hydrogen concentration in the liquid phase with this catalyst promotes unwanted water formation.

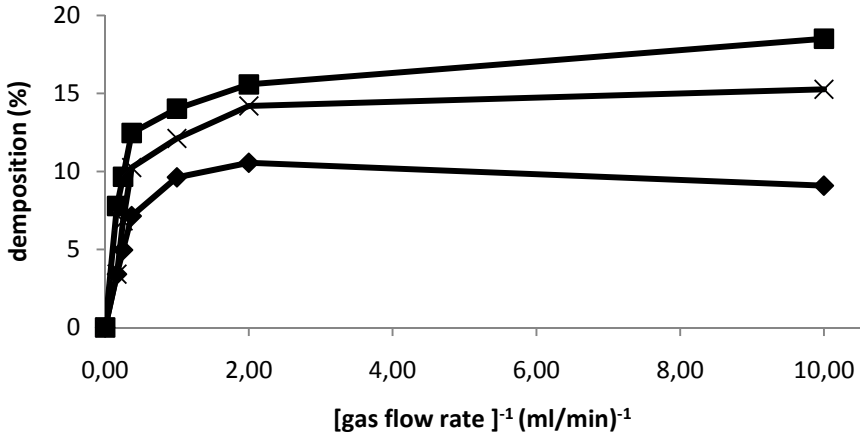

Figure 4.4. Hydrogenation and decomposition of 0.5% of H_2O_2 in methanol. Comparison between different liquid flow rates: 0.5 ml/min MeOH (squares), 1 ml/min MeOH (X-shaped), 2 ml/min MeOH (diamonds).

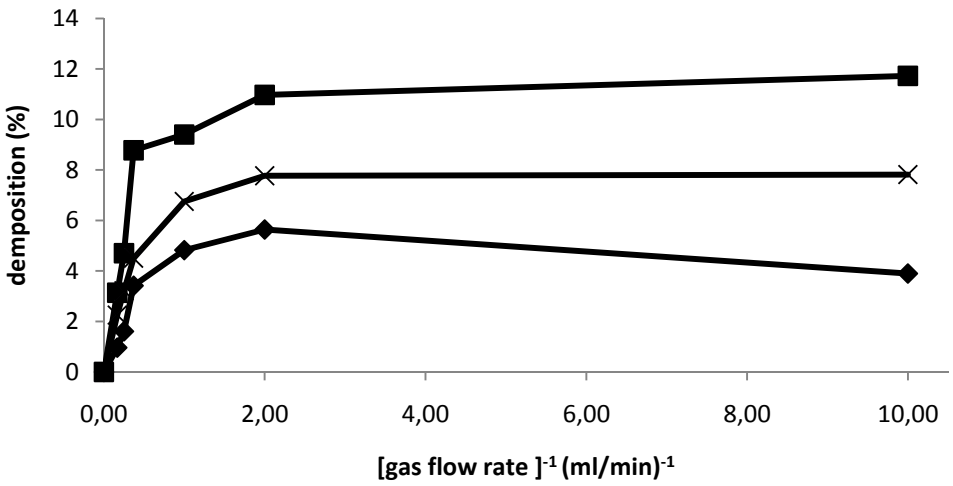

Figure 4.5. Simple decomposition of 0.5% of H_2O_2 in methanol. Comparison between different liquid flow rates: 0.5 ml/min MeOH (squares), 1 ml/min MeOH (X-shaped), 2 ml/min MeOH (diamonds).

4.3.2 H_2O_2 synthesis

The major limitation of hydrogen peroxide direct synthesis is the low selectivity due to the competing reactions.

Preliminary tests of H_2O_2 decomposition were carried out to verify that the support substrate alone do not decompose H_2O_2. We used pure calcined sulfated ceria at 20°C, 1 bar for 5 hour (Menegazzo 2008).

As already explained, we carried out the synthesis in methanol. Most oxidation reactions involving hydrogen peroxide as a reagent are carried out in organic solvents, often in methanol. Accordingly, direct synthesis of H_2O_2 in this alcoholic solvent could be an advantage if its subsequent use requires it, thus avoiding separation and concentration steps.

The results of the experiments to produce hydrogen peroxide from its elements are shown in Figures 4.6-4.9. Different gas and liquid flow rates are investigated to elucidate the effect of the relative contact times with the catalytic bed.

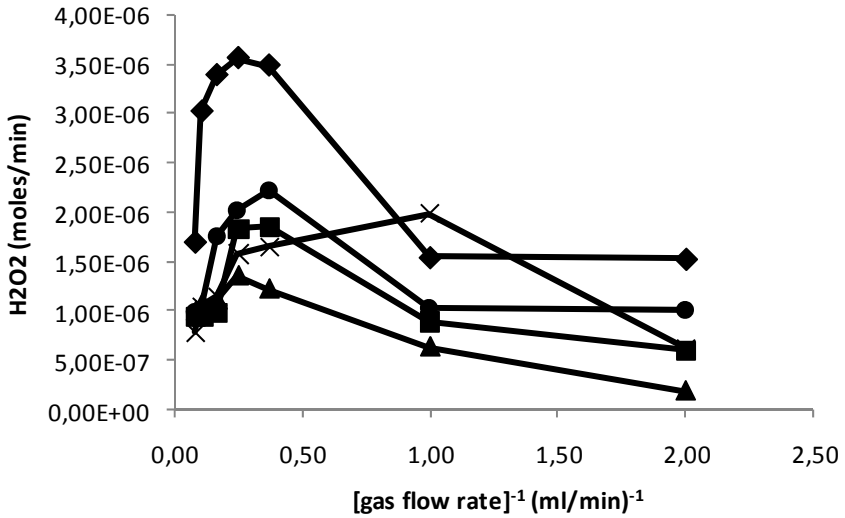

Figure 4.6. Production rate of H_2O_2. Combined effect of gas and MeOH flow rates: 0.3 ml/min (X-shaped), 0.5 ml/min (diamonds), 0.75 ml/min (circles), 1 ml/min (squares), 2 ml/min (triangles).

The results of Figure 4.6 show that production rate for all of the five different liquid flow rates tested has a similar profile, exhibiting a maximum at varying the gas flow rate, i.e. an optimum gas flow rate can be identified for every liquid flow rates examined.

Production rate is the lowest with the highest liquid flow rate (2 ml/min). In contrast, the maximum production rate of hydrogen peroxide is measured with a small flow rate of 0.5 ml/min, but not the lowest liquid flow rate tested (0.3 ml/min), implying that its effect is not linear and goes through an optimum.

Figure 4.7 shows selectivity results. It is worth highlighting that:

1) for every liquid flow rate there is an optimal gas flow rate value giving a maximum in selectivity;
2) selectivity doesn't vary monotonically with the gas flow rate;
3) with the highest liquid flow rate, the maximum of selectivity is achieved at the highest gas flow rate;
4) longer contact times decrease selectivity dramatically;
5) maximum selectivity can be achieved with liquid flow rates of 1 and 0.75 ml/min;
6) good production rate doesn't always imply high selectivity.

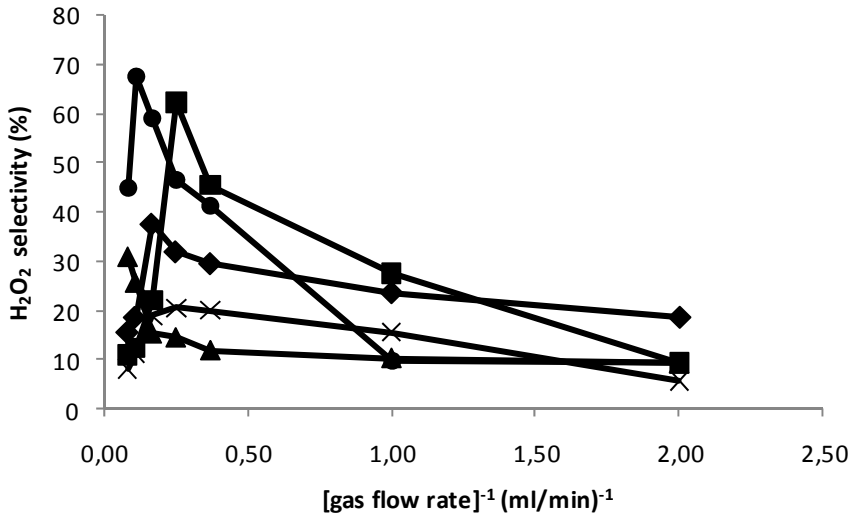

Figure 4.7. Selectivity of hydrogen peroxide. Combined effect of gas and MeOH flow rates: 0.3 ml/min (X-shaped), 0.5 ml/min (diamonds), 0.75 ml/min (circles), 1 ml/min MeOH (squares), 2 ml/min (triangles).

Selectivity is a crucial issue in hydrogen peroxide synthesis process. As previously discussed, if selectivity is lower than 80%, considering the results from hydrogenation and decomposition experiments (Section 4.3.1), excess water formation is due to the parallel reaction that yields water. With a longer contact time, this reaction (Section 1.2.4, Eq. 1.2) is more likely to happen. Thus, water formation reaction cannot be neglected with this reactor set-up if the contact time between liquid and solid phase is longer.

All the results above and the consequent considerations give important indications for engineering hydrogen peroxide direct synthesis process. Particularly, the mechanism usually proposed to explain the reaction network of hydrogen peroxide direct synthesis neglects the parallel water formation reaction, but in this study it is demonstrated that this assumption is not valid.

If the experimental results are analyzed at a fixed gas flow rate, a maximum in the profiles of selectivity and productivity can also be seen, varying the liquid flow rate, as shown in Figures 4.8-4.9 for 2.7 ml/min.

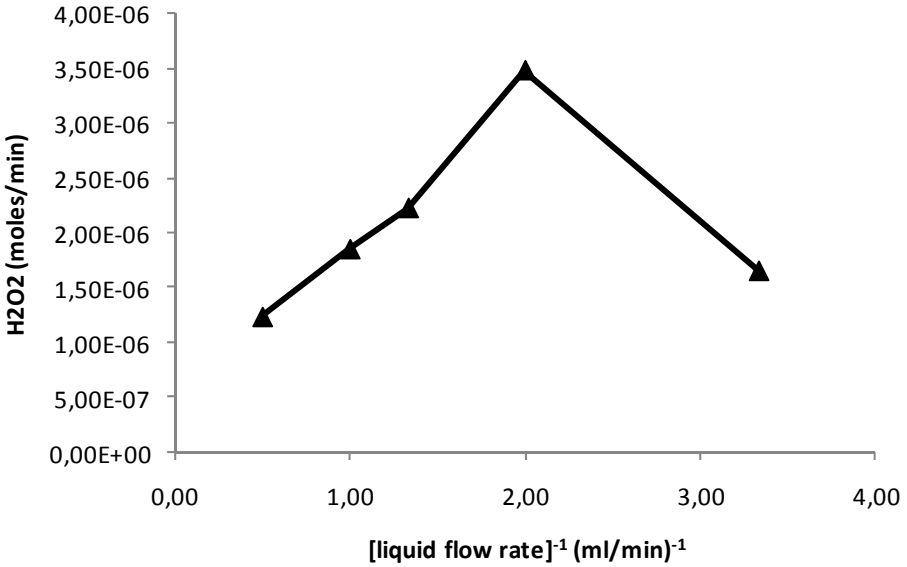

Figure 4.8. Production rate of H_2O_2 with a gas flow rate of 2.7 ml/min ,-10°C, 10 bar, varying the liquid flow rate.

It must be noted that the maximum of productivity, Figure 4.8, is not achieved at the same liquid flow rate that yields the maximum of selectivity, Figure 4.9.

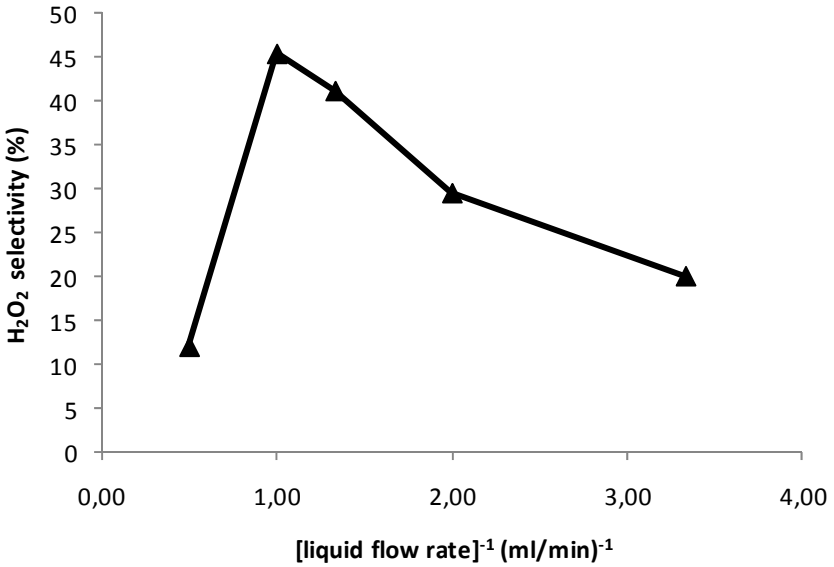

Figure 4.9. Selectivity of H_2O_2 with a gas flow rate of 2.7 ml/min,-10°C, 10 bar, varying the liquid flow rate.

The liquid flow rate are immediately related to different contact times with the catalyst and perhaps also its thorough wetting. Continuous operation easily allows to control gas and liquid residence time, enabling to operate under conditions corresponding to a maximum in both hydrogen peroxide productivity and selectivity. Reactions reported in Eq. 1.3 and Eq. 1.4 (Section 1.2.4) always occur during the experiments, as palladium can catalyze H_2O_2 production but also its decomposition

and reduction. The aim is to limit as much as possible the secondary reactions leading to water formation, and to promote the reaction of H_2O_2 synthesis. From the results shown in Figures 4.6-4.9, it is evident how a short enough contact time is required to achieve a good selectivity for hydrogen peroxide, but it cannot be excessively short otherwise productivity is compromised. On the other hand, a long contact time, which would be required to maximize productivity, results in a detrimental effect on selectivity.

The amount of catalyst and the length of the catalytic bed also appears to play a significant role in the process. Varying gas and liquid flow rates, thus altering residence times inside the reactor has a similar effect than changing the catalytic bed length.

Direct water formation reaction is usually ascribed to a palladium oxidated state. However, the actual oxidation state in the presence of both O_2 and H_2 is difficult to predict, also considering their different concentration in the liquid due to the reaction course and a different solubility. The simultaneous presence of hydrogen and oxygen dissolved in the liquid phase can lead to modification of catalyst oxidation state during the reaction. In accordance to the experimental procedure and catalyst design:

1) the catalyst is reduced for one hour before reaction begins, thus palladium is in its reduced form (oxidation state 0);
2) after pressurizing the reactor with a mixture of CO_2/H_2 (97.5%/2.5% respectively), the catalyst is expected to be still in its reduced form;
3) liquid phase is then fed into the reactor, and palladium remains in metallic form, since only H_2 and carbon dioxide are present along with methanol;
4) finally, the oxygen is fed into the reactor in excess with respect to hydrogen: at this stage, the oxidation state becomes questionable.

In the first part of the catalytic bed it is reasonable to assume that only reactions of H_2O_2 direct synthesis and water formation occur, being only H_2 and O_2 available. It is known that water formation takes place on PdO (palladium in oxidation state II and bound to oxygen). When oxygen is fed in large excess, catalyst surface is presumably covered with oxygen, and hydrogen cannot be adsorbed in dissociative form on the metal species. It is reported that if palladium is completely oxidized (Pd II), water formation or hydrogen peroxide synthesis cannot be observed. As previously shown, in the experimental set-up illustrated in this study, water and hydrogen peroxide formation occurs. We conclude that the irregular form of the palladium cluster doesn't allow for an entire surface coverage of O_2. When palladium is in oxidation state II, its surface only is involved, and not the inner part of the cluster.

Based on the experimental results above we see that: 1) selectivity is always less than 70%, decomposition and hydrogenation are up to around 20%, therefore direct water formation is always present; 2) when the contact time is either too long or too short, selectivity is very low; 3) the catalyst oxidation state is difficult to predict, but some assumptions can be inferred from the formation of water.

From these considerations it is possible to hypothesize a reaction mechanism as follows.

1) When contact time between liquid and solid phases is **long**, there is plenty of time for all the reactions to occur. The large excess of oxygen covers the cluster of metallic palladium with a higher efficiency in comparison to low contact time conditions. Therefore catalytic surface available for dissociative adsorption of hydrogen is smaller, and hence the chance to have direct synthesis decreases. Hydrogen is more likely to react with the oxygen present on the palladium surface than with the inner part of the palladium cluster. On the other hand, the larger the amount of oxidized palladium the greater the possibility to have direct water formation, rather than H_2O_2 synthesis.

2) When the contact time between liquid and solid phases is **short**, there is not enough time for dissociative hydrogen adsorption on the catalyst surface to take place. Only a few hydrogen molecules can react, and therefore the productivity decreases drastically. Adsorption of oxygen is also limited with shorter contact time, but it is more favorable owing to its large excess. Hence production rate is very low as well as selectivity because water formation is still more likely to happen.

3) For **intermediate** conditions of gas and liquid flow rates, production rate is higher and selectivity achieves very interesting values. Gas solubilization in the liquid phase plays a key role, and at the proper rate, it ensures hydrogen adsorption in a dissociative way on the palladium clusters. Oxygen still oxidizes the metal surface, but controlling operative conditions such liquid and gas flow rates can limit this phenomenon, for a reduced water formation.

These observations allow to conclude that controlling the reaction network depends on catalysts, catalyst surface and operative condition. For good results, it is thus impossible to separate the catalyst from the reactor design and operation.

The reaction takes place in different ways with different operative conditions due to the alternative reaction pathways. The enthalpies and Gibbs free energies of all the reactions involved indicate that they are all thermodynamically favored. Nevertheless, catalysts and operative conditions play a major role in driving the reactions towards high selectivity for hydrogen peroxide, as demonstrated in this chapter. The results presented show without any doubt that H_2O_2 direct synthesis

reaction requires specific care to the reactor design and operation, in order to achieve improved process performances, perhaps more than developing a selective catalyst,.

4.3.3 H_2O_2 synthesis: effect of pressure

The effect of pressure on the reaction, with its related change in gas solubility, has been studied observing the hydrogen peroxide productivity and selectivity. Results from experiments carried out at 10 bar and 20 bar are shown in Figures 4.10-4.15; the temperature is always -10°C. The volumetric gas flow rate (ml/min) is the same for the 10 and 20 bar experiments. Recall that at the higher pressure, 20 bar, the same volumetric flow rate measured at P = 1 bar imply a larger mass flow rate. A higher pressure also leads to an increase in gas solubility in the liquid phase. Therefore, with a larger amount of gas in the reaction medium, more reagents are available to the catalyst to be converted into the products.

Productivity results are presented in Figures 4.10-4.12. A similar profile for data at 10 and 20 bar is observed, with a clear maximum of productivity when the gas flow rates increases. Again, the best results are not at the highest gas flow rate. The absolute value of the maximum is higher with lower liquid flow rate, Figure 4.10, at which conditions the effect of pressure is larger. We can also observe that the higher pressure shift the maximum of productivity to lower gas flow rates, but the shift decreases with higher liquid flow rates, Figure 4.12. At the same time, the role of pressure with small gas flow rates is to support an increase of productivity. This is quite clear except for the case of 0.5 ml/min liquid flow rate and the smaller gas flow rate, where an inversion have been measured. The inverse is observed at large gas flow rate, where an increase of pressure apparently leads to a smaller productivity. In other words, we can say that the gain in productivity achieved with smaller liquid flow rates is reduced by a larger pressure.

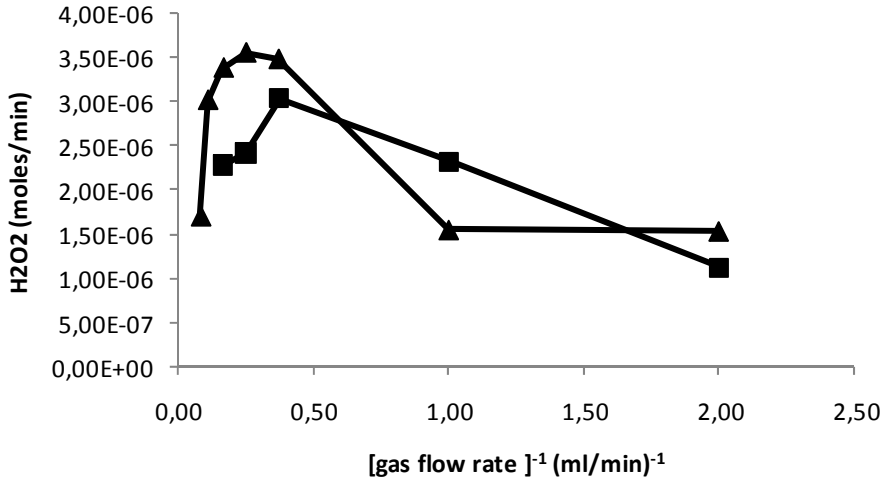

Figure 4.10. Production rate of H_2O_2. Liquid flow rate of 0.5 ml/min and T=-10°C, P=10 bar (triangles), 20 bar (squares).

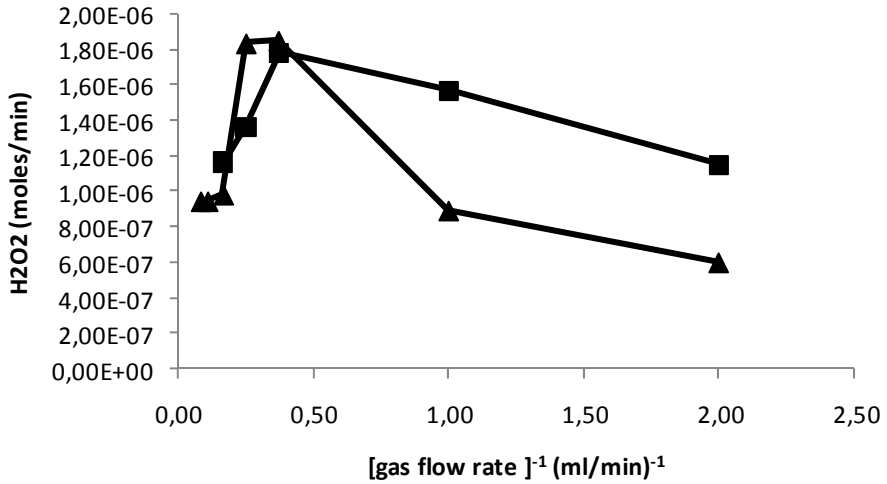

Figure 4.11. Production rate of H_2O_2. Liquid flow rate of 1 ml/min and T=-10°C, P=10 bar (triangles), 20 bar (squares).

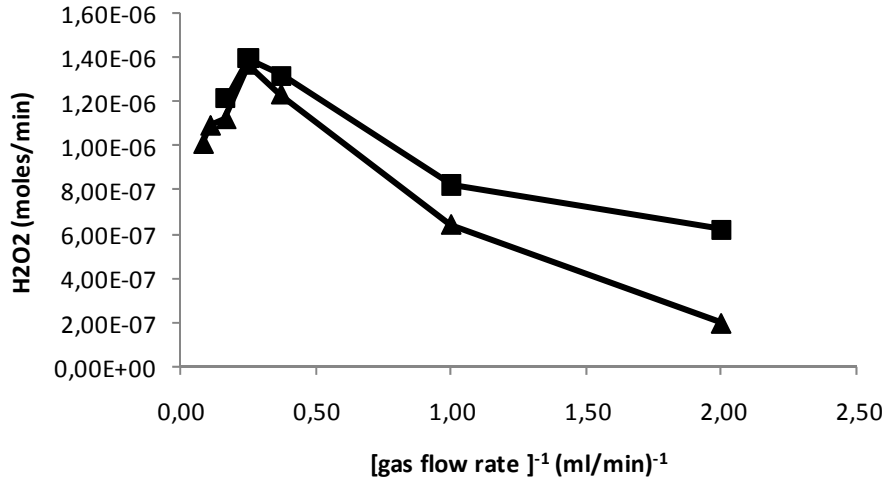

Figure 4.12. Production rate of H_2O_2. Liquid flow rate of 2 ml/min and T=-10°C, P=10 bar (triangles), 20 bar (squares).

On the other hand, results for **selectivity** are quite different when comparing experiments at different pressure conditions, as shown in Figures 4.13-4.15. Interestingly, we always measured a significant increase in selectivity with pressure and a clear shift of the best operating conditions. The net increase due to pressure varies with flow rates, also because of the shift in the maximum. The difference between the maximum values for each case (achieved at different flow rates) could be extremely high. For a liquid flow rate of 0.5 ml/min maximum selectivity is enhanced by 30% (Figure 4.13). For a flow rate of 1 ml/min methanol, the increase in maximum selectivity is 5% (Figure 4.14), whereas the largest difference is achieved with a liquid flow rate of 2 ml/min, when the maximum selectivity value raises up to a 50% (Figure 4.15), achieving a very high selectivity value of 80%. As anticipated, unfortunately the highest selectivity is achieved at conditions where the productivity is lower, Figure 4.12.

These results may be reasonably attributed to the higher gas solubility with increasing pressure, showing the critical importance of this parameter, which influences the gas concentration in the liquid phase. Thus, the gas solubility plays a major role in the direct synthesis process, and the right amount of gases in the liquid phase is one of the key factor to control in order to enhance hydrogen peroxide selectivity. It is also worth noticing how the peak of selectivity is reached with a lower gas flow rate at 20 bar compared to 10 bar. The reason here is to be identified in the increased number of H_2 and O_2 moles at a higher pressure for the same volumetric gas flow rate, and in the augmented solubility of the gases. Also, in the reactor's environment the presence of the reagents influence the activity of the catalyst.

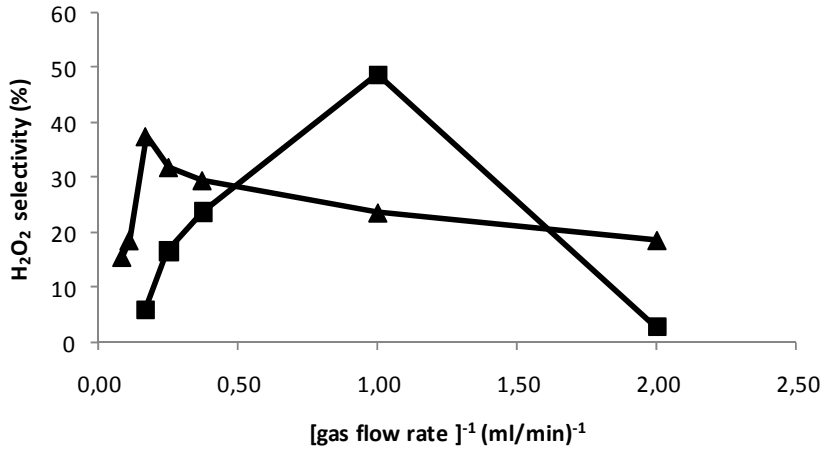

Figure 4.13. Selectivity of H_2O_2. Liquid flow rate of 0.5 ml/min and T=-10°C, P=10 bar (triangles), 20 bar (squares).

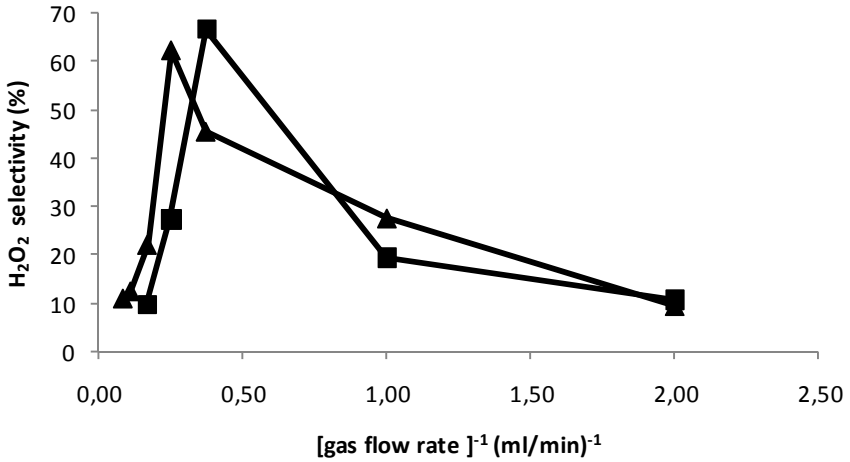

Figure 4.14. Selectivity of H_2O_2. Liquid flow rate of 1 ml/min and T=-10°C, P=10 bar (triangles), 20 bar (squares).

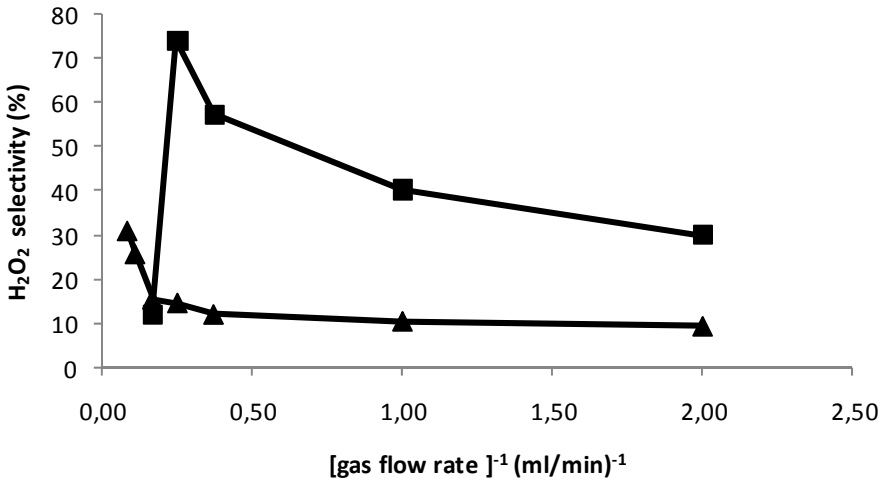

Figure 4.15. Selectivity of H_2O_2. Liquid flow rate 2 ml/min and T=-10°C, P=10 bar (triangles), 20 bar (squares).

4.3.4 Catalyst stability and reusability

To make hydrogen peroxide direct synthesis a viable process on an industrial scale, beside conditions that yield high productivity and selectivity, a stable catalyst is required, which enables a constant yield in H_2O_2. In this section a systematic study on the catalyst stability and reusability is presented. The experimental set-up is the continuous, trickle bed reactor described in Section 2.3. We carried out five cycles composed of 1) 4 hours start up, 2) 12 hours operation, and 3) 8 hours (overnight) decompression and conditioning with N_2 are performed, for a total of approx 5 days (12h) of operation in a sequence.

The first step in the procedure consists of an initial 4 hours system start up, which ensures reaching steady state conditions and complete catalyst wetting. In this stage, the pressure is set at 10 bar and a flow of CO_2 and H_2 is introduced into the reactor at room temperature. Then the syringe pump and the mass flow controller are started to feed methanol. The temperature is then gradually decreased to -10°C, which is the selected operative condition, and the valve controlling the flow of oxygen is opened. Continuous, steady state conditions are achieved within 4 hours.

Step 2) in the cycle is the actual experiment, and after the start up period catalyst stability can be evaluated in real experimental, H_2O_2 forming conditions. Three sampling points are introduced, which correspond to time 0, 6, and 12 hours.

The third and last step consists in decompression of the reactor down to atmospheric pressure, and overnight (8 hours) flushing with a flow of pure nitrogen.

This three step compression-decompression cycle is repeated 5 times, and productivity and selectivity are measured for each of the samples collected. Results are shown in Figures 4.16 and 4.17.

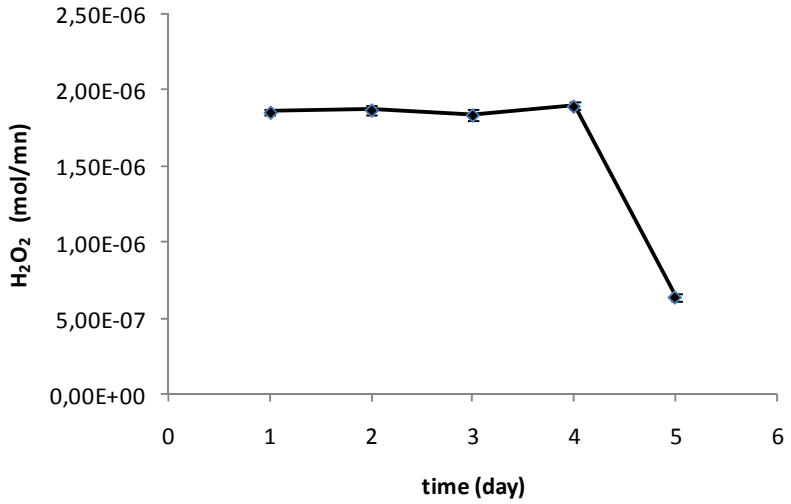

Figure 4.16. Stability of hydrogen peroxide production rate at 10 bar and -10°C, with a gas flow rate of 2.7 ml/min and a liquid flow rate of 1 ml/min.

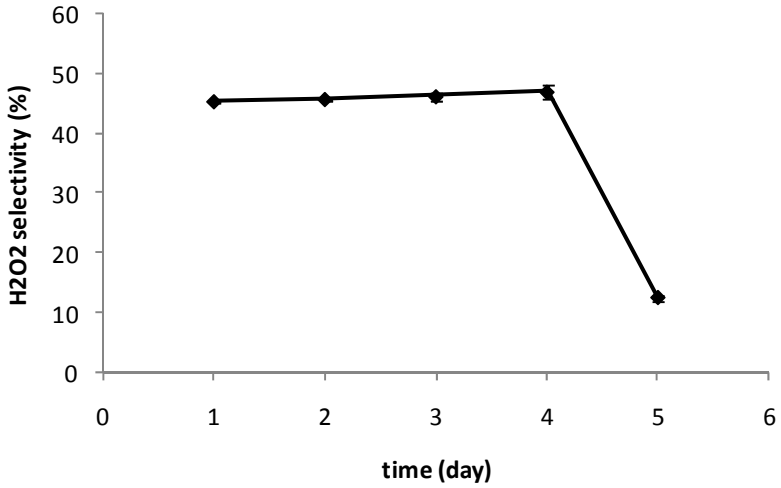

Figure 4.17. Stability of hydrogen peroxide selectivity at 10 bar and -10°C, with a gas flow rate of 2.7 ml/min and a liquid flow rate of 1 ml/min.

Every point in the graphs corresponds to the mean daily value resulting from the three samples (0,6,12h) of that specific day. It is evident how a good and stable catalyst performance is achieved during the first four days, in terms of both productivity (Figure 4.16) and selectivity (Figure 4.17). Importantly, the values are about constant both within the same day and among different days, and the error is minimal (<2%), highlighting a reproducible catalyst behaviour. However, a marked drop in the measured parameters occurs after the fifth cycle. The explanation was clear once the reactor was opened and the catalytic bed sectioned.

Catalyst appeared disaggregated. After the first four days, the catalyst exhibits an intact structure, but at the end of the fifth day it shows an extensive breakup with a powdery appearance as opposed to compact particles. This is probably caused by the repeated compression-decompression cycles, which can induce considerable stress on the catalyst structure and lead to its collapse. However, catalyst deactivation phenomena don't seem to be the issue, since selectivity is low, as well as productivity, which indicates that more H_2O_2 is decomposed into water. Most likely a greater number of active sites on the catalytic surface are exposed, due the higher surface/volume ratio, leading to a shift in the balance between hydrogen peroxide formation and decomposition reaction rates towards the latter.

Therefore repeated compression-decompression cycles prove to be detrimental for the catalyst performance, and, from an industrial perspective, some improvements need to be made in order to enhance the catalyst mechanical properties. However, it

also seem plausible that when safely performing the reaction on an industrial scale, continuous operation can be carried out for several days, avoiding re-compression of the system.

4. Conclusions

The results presented in this chapter collect measurements in a TBR with Pd-CeS catalyst. They provide evidence on the importance of designing a proper reactor set-up and experiments to engineer hydrogen peroxide direct synthesis process. Particularly, different pressure and flow rates (both gas and liquid) combinations allow achieving better H_2O_2 selectivity and production rate in comparison to previous results obtained under batch conditions, with the same catalyst (Menegazzo 2008).

TBR-based hydrogen peroxide synthesis by the direct combination of hydrogen and oxygen proves to be feasible with hydrogen oxygen ratios outside of the explosive range. This study indicates that Pd-CeS catalyst is suitable for hydrogen peroxide direct synthesis, with a significant increase in H_2O_2 selectivity achieved by using the catalyst in a TBR.

Selectivity up to 80% have been measures at the highest pressure tested (20bar), highest liquid flow rate (2 ml/min) and 6 ml/min gas flow rate (not the highest tested!). On the contrary, the maximum productivity measured is 0.0035 mmol/min with a small liquid flow rate (0.5 ml/min, again, not the lowest tested) and 2.7 ml/min gas flow rate .

These studies are promising for the ultimate goal of scaling-up the process for industrial application (continuous flow reactors with pellet or extruded catalyst formulations).

All the reactions present in the reaction network of hydrogen peroxide direct synthesis are shown to occur, and optimization of operative conditions is proved to minimize decomposition and hydrogenation as well as the reaction of direct water formation.

This study demonstrates the importance of reactor design and operation, and all the phenomena that influence catalyst behavior.

This systematic study on H_2O_2 decomposition, hydrogenation and synthesis implement a modern design for reaction mechanisms and reactor development, not ignoring any side reactions.

Promising preliminary results pave the way to further developments of a reactor operating under continuous flow able to maintain a constant H_2 concentration in the

liquid phase by feeding the reagent at the same rate at which it is consumed (starvation), and to guarantee an effective liquid–solid contact, without mechanically stressing the catalyst.

Chapter 5

Direct Synthesis of hydrogen peroxide in a Trickle Bed Reactor (TBR): comparison among Pd-based catalysts

5.1 Introduction

Pd is the most used and well known catalyst for the direct synthesis of H_2O_2. However, it also promotes the decomposition of the hydrogen peroxide, triggering a competition between its formation and consumption. Many attempts have been done to modify its functionality to make Pd more selective.

In this chapter we compare four catalysts based on palladium in the trickle-bed reactor already presented. The catalysts are based on different supports: silica (SiO_2), zirconia (Z), sulfated zirconia (ZS) and sulfated ceria (CeS). They have been developed at the University of Venice and tested there in a semi-batch reactor.

The aim of this study is to verify the influence of the reactor type and the operative conditions given the results presented in the previous chapter. Particularly, we want to confirm that suitable flow rates configuration can drive the reaction to better performances with respect to batch and semi-batch operations.

5.2 Experimental

5.2.1 Materials

$(NH_4)_2Ce(NO_3)_6$ (Sigma-Aldrich), $(NH_4)_2SO_4$ (Merck), were used for sample synthesis as received. Methanol for HPLC was used as the reaction medium (J.T. BAKER 99,99%). The other reagents are: potassium iodide (sigma-aldrich), Hydranal-Composite 2 (Fluka), dry methanol for KFT (Fluka), Acetic Acid (Sigma-

Aldrich), Sodium Thiosulfate penta-hydrate 99,5% (Sigma-Aldrich), Starch (sigma Aldrich), Potassium dichromate (riedel de haën), H_2O_2 30% w/w (Merck).

5.2.2 Catalysts preparation

Pd-SiO_2 catalyst. Silica support was prepared by "dry" impregnation with an aqueous solution of H_2PdCl_4 to give a nominal 2.5% wt. metal loaded catalyst. The sample prepared in this way was dried overnight at 110°C and finally calcined at 500°C in flowing air for 3 h.

Pd-Z catalyst. Zirconia support was prepared by precipitation from $ZrOCl_2$ at constant pH (pH 10), aged under reflux conditions, washed several times to remove excess of chloride ($AgNO_3$ test) and dried overnight at 110°C. The solution was continuously mixed and boiled for 6 h at 100°C, the precipitate was washed twice in boiling deionized water and dried overnight at 110°C. The support was impregnated by incipient wetness with H_2PdCl_4 aqueous solutions to give a nominal 2.5% wt metal loaded catalyst and finally calcined at 500°C in flowing air for 3 h (Melada 2006).

Pd-ZS catalyst. Zirconia support was prepared by precipitation from $ZrOCl_2$ at constant pH (pH 10), aged under reflux conditions, washed several times to remove excess of chloride ($AgNO_3$ test) and dried overnight at 110°C. The solution was continuously mixed and boiled for 6 h at 100°C, the precipitate was washed twice in boiling deionized water and dried overnight at 110°C. This material was then impregnated by an incipient wetness method with $(NH_4)_2SO_4$ in amounts necessary to yield an 8% wt anion loading. Impregnated supports were then calcined in flowing air (50 ml/min) at 650°C for 3 h. Calcined supports were impregnated by incipient wetness with H_2PdCl_4 aqueous solutions to give a nominal 2.5% wt metal loaded catalyst and finally calcined again at 500°C in flowing air for 3 h (Melada 2006).

Pd-CeS catalyst.
Ceria support substrate was synthesized by precipitation with urea from (NH4)2Ce(NO3)6 aqueous solution. The solution was continuously mixed for 6 hour at 100°C, the precipitate was washed twice in boiling deionized water and dried in oven at 110°C overnight. These materials were impregnated by an incipient wetness method with a proper amount of (NH4)2SO4 to yield an 8% wt anion loading. Impregnated supports were calcined in flowing air (50 ml/min) at 650°C for 3 hour. Afterwards, calcined supports were impregnated via incipient wetness with H2PdCl4 aqueous solution to give a nominal 2.5% wt Pd-loaded catalyst, and finally calcined

again at 500°C in flowing air for 3 hour. The catalyst was crushed and sieved (0.5-1 mm). Pure SiO2 was crushed and sieved (0.5-1mm). 0.16 grams of Pd-CeS were mixed with 0.2 grams of SiO2 and used as the catalytic bed in the continuous reactor. The catalyst was than reduced for 1 hour with a 20 ml/min flow of pure hydrogen (1bar, 25 °C) (Melada 2006).

All the catalysts were crushed and sieved (0.5-1 mm). Pure SiO_2 was crushed and sieved (0.5-1mm). 0.16 grams of either Pd-CeS or Pd-ZS were mixed with 0.2 grams of SiO_2 and used as catalytic bed in the continuous reactor. The catalyst was than reduced for 1 hour with a 20 ml/min flow of pure hydrogen (1bar, 25°C).

5.2.3 Reactor set-up for the experiments

The reactor set-up is described in detail in Section 2.3. Briefly, an AISI 316 stainless steel trickle-bed reactor was realized, with a catalyst bed up to 20 cm long in it. An external cooling system allows for working temperature between -20°C and 60°C. Three mass flow controllers (MFC) are used to feed the gases into the reactor. Every MFC is connected to a gas cylinder: N_2, CO_2/ H_2 97.5/2.5%, and O_2. The pressure inside the reactor is controlled and regulated with a back pressure controller (BPC). The liquid phase is fed in through a syringe pump. The catalyst bed (7 mm) is placed between two quartz wool plugs. From the bottom, we arranged 37 mm of quartz wool, 7 mm of catalyst and inert particles, 26 mm of quartz wool and 140 mm of quartz sand (sieved under 0,2 mm).

5.2.4 H_2O_2 synthesis

Direct synthesis experiments are carried out at 10 bar and -10°C, with methanol as the solvent. H_2, O_2 and CO_2 constitute the gas phase, and are fed into the reactor with a composition of 2%, 18% 80% (mol/mol) respectively. Liquid flow rates used are: 0.5, 1 and 2 ml/min. Total gas flow rates examined in this set of experiments at 10 bar are: 1, 2, 2.7, 4, 6, 9 and 12 ml/min.
During the experiments small aliquots of the liquid phase are sampled with a valve for the liquid sampling after the TBR, and used for water and hydrogen peroxide determination. H2O2 concentration is measured by iodometric titration, whereas water is determined by volumetric Karl Fischer method. The water content in the reaction medium before feeding the oxygen is determined prior to each experiment.

5.3 Results and discussion

5.3.1 Pd-SiO_2 catalyst

Palladium on silica is one of the catalyst that can be used for hydrogen peroxide direct synthesis (Liu 2006, Liu 2008, Liu 2009 and Park 2009). The catalyst bed is a homogeneous mixture of 40% Pd-SiO_2 catalyst and 60% pure silica (both crushed and sieved separately). Results for this catalyst are shown in Figures 5.1 and 5.2, for production rate and selectivity, respectively. A comparison between different liquid flow rates and different gas flow is carried out. The inverse of the gas flow rate is used as abcissa, which is proportional to the gas residence time.

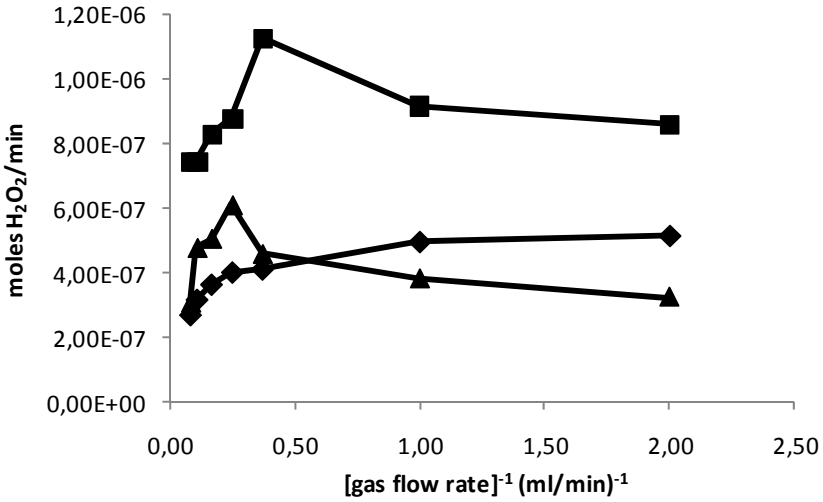

Figure 5.1. Production rate of hydrogen peroxide with Pd-SiO_2 catalyst. Comparison between different liquid flow rates: 0.5 ml/min of methanol (diamonds), 1 ml/min of methanol (squares)and 2 ml/min of methanol (triangles).

Results for the higher liquid flow rates (1 and 2 ml/min, squares and triangles) exhibit a similar trend: close to the highest gas flow rate, a maximum in hydrogen peroxide productivity is observed. On the contrary, the lowest liquid flow rate (0.5 ml/min) shows a gradual increase in H_2O_2 production rate as the gas residence time increases.

Similar considerations can be reported for selectivity, as shown in Figure 5.2, where a maximum for liquid flow rates of 1 and 2 ml/min and a monotonic increase for a liquid flow rate of 0.5 ml/min can be observed. Water is formed during the reaction, the highest amount being with a liquid flow rate of 0.5 ml/min (data not shown).

This fact confirms once more that the reaction pathway largely relies on the contact time between liquid and solid phase.

Apparently, the combination of gas and liquid flow rate that result in maximum productivity and selectivity is the same, which is not always the case with other catalysts, as shown in the following.

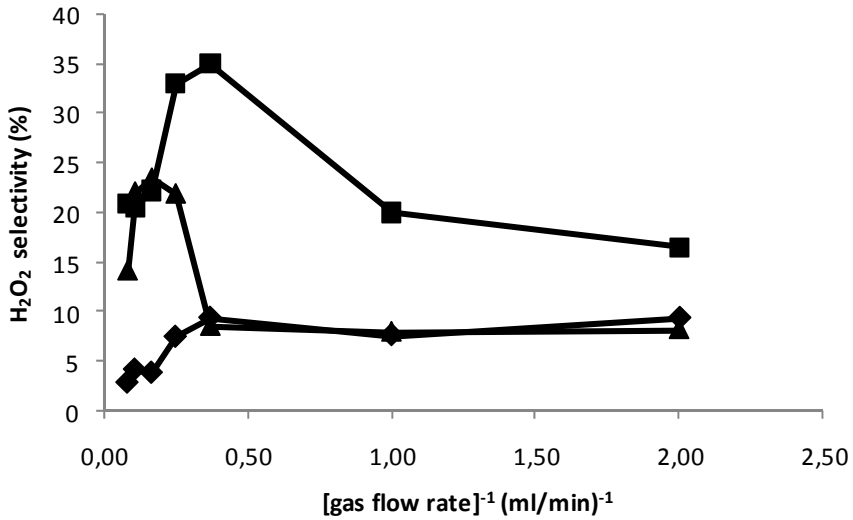

Figure 5.2. Selectivity for hydrogen peroxide with Pd-SiO_2 catalyst. Comparison between different liquid flow rates: 0.5 ml/min of methanol (diamonds), 1 ml/min of methanol (squares)and 2 ml/min of methanol (triangles).

5.3.2 Pd-Z catalyst

The second catalyst that was explored for hydrogen peroxide direct synthesis is a catalyst based on palladium with a zirconia (ZrO_2) substrate. This catalyst was previously tested in a semibatch-reactor. The catalyst was characterized by thermogravimetric/ differential scanning calorimetry analysis (Melada 2006). H_2O_2 production rate with this catalyst exhibits, for all the liquid flow rates tested, a maximum (Figure 5.3) determined by the gas flow rate used. The highest production rate is achieved with a liquid flow rate of 1 ml/min of MeOH..

Selectivity results are shown in Figure 5.4, and their interpretation give important information in order to maximize the catalyst performance by changing operative conditions in the reactor. This is feasible in the continuous, trickle bed reactor developed and implemented in this study. The maximum value for selectivity that can be reached is 60%, corresponding to a liquid flow rate of 2 ml/min and a total gas flow rate of 12 ml/min. However, the production rate of hydrogen peroxide in this case is not as high as with a liquid flow rate of 0.5 ml/min, and at the same time the production of water is very low (as can be seen from selectivity data). As a result, selectivity for hydrogen peroxide is quite high.

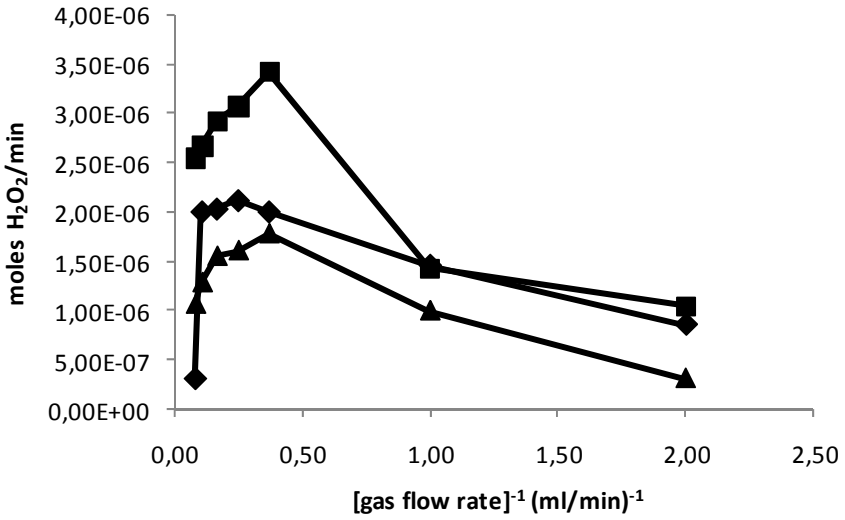

Figure 5.3. Production rate of hydrogen peroxide with Pd-Z catalyst. Comparison between different liquid flow rates: 0.5 ml/min of methanol (diamonds), 1 ml/min of methanol (squares)and 2 ml/min of methanol (triangles).

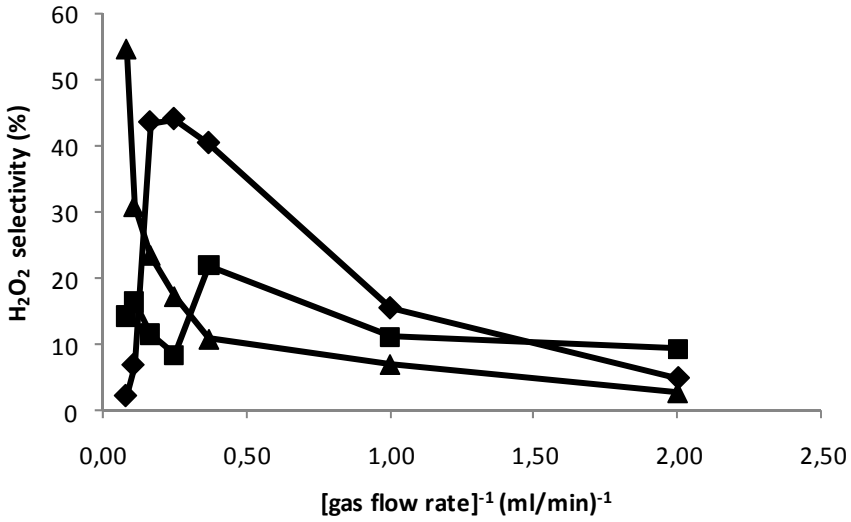

Figure 5.4. Selectivity for hydrogen peroxide with Pd-Z catalyst. Comparison between different liquid flow rates: 0.5 ml/min of methanol (diamonds), 1 ml/min of methanol (squares)and 2 ml/min of methanol (triangles).

When the contact time between liquid and solid phase is reduced (e.g. 1 ml/min of methanol) the production of hydrogen peroxide is the highest but also water formation is increased as clearly indicated by the drop in selectivity. This observation suggests that decomposition and hydrogenation of H_2O_2 occur at a higher rate in the catalyst bed with this liquid flow rate. The results for 1 ml/min of liquid flow rate, when compared with the ones relative to 2 ml/min methanol, show

that the concentration of hydrogen peroxide is higher, thus presumably the two reactions of reduction are slower.

Furthermore, looking at Figure 5.4, it is worth noticing how selectivity drops rapidly with 0.5 ml/min as the liquid flow rate, probably owing to the a faster water formation as opposed to H_2O_2 production, when contact time is too little. In the case of this PdZ catalyst, optimal flow rates configuration requires some trade-off between productivity and selectivity. In addition, it is surprising the large effect of both flow rates.

5.3.3 Pd-CeS catalyst

The catalyst consisting of palladium on sulfated ceria was extensively studied in Chapter 4. Some results are recalled in Figures 5.5 and 5.6 to allow for a comparison with the other catalytic systems. Figure 5.5 is indeed comparable to Figures 5.1 and 5.3, i.e. the production of hydrogen peroxide varies non-linearly with the gas flow rate, often showing a maximum.. With this catalyst, the production rate of H_2O_2 increases with decreasing liquid flow rates.

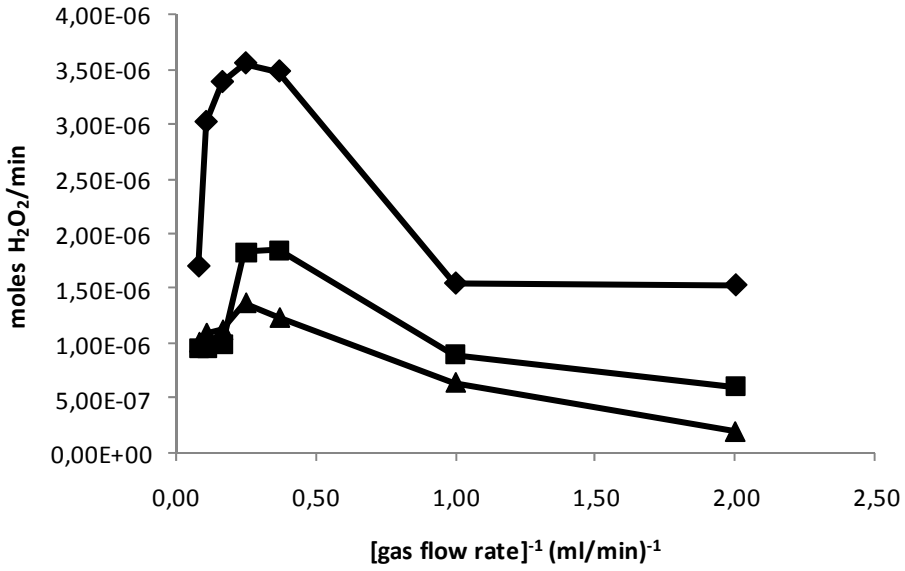

Figure 5.5. Production of hydrogen peroxide with Pd-CeS catalyst. Comparison of different liquid flow rates: 0.5 ml/min of methanol (diamonds), 1 ml/min of methanol (squares)and 2 ml/min of methanol (triangles).

H_2O_2 net production is negatively affected by several side reactions. Hydrogenation and decomposition can be as important as well as its direct synthesis path. This fact is clearly seen in Figure 5.6 where selectivity values are presented. In many

circumstances the selectivity is quite low, clearly indicating the significance of other reactions ineffective for H_2O_2 production.

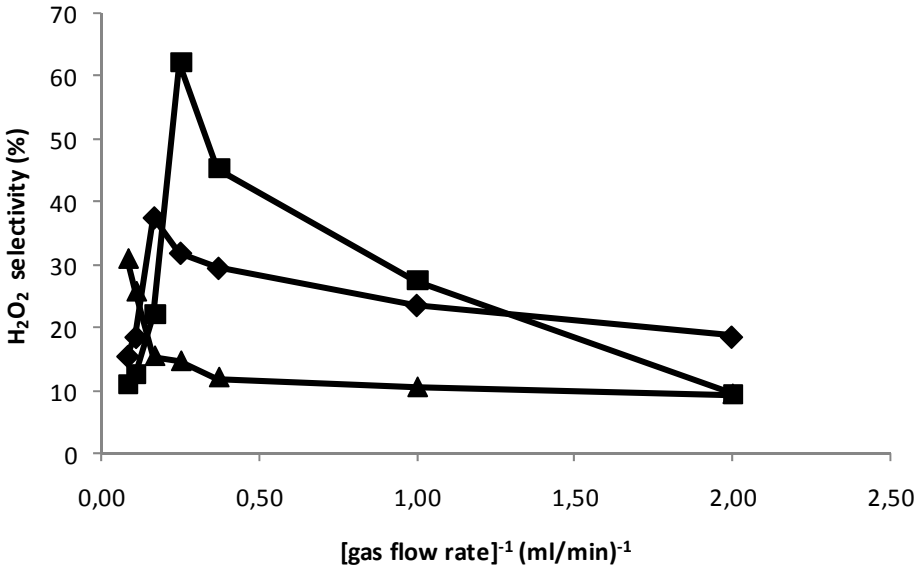

Figure 5.6. Selectivity of hydrogen peroxide with Pd-CeS catalyst. Comparison between different liquid flow rates: 0.5 ml/min of methanol (diamonds), 1 ml/min of methanol (squares)and 2 ml/min of methanol (triangles).

However, selectivity can be improved by changing the contact time between liquid and solid phase. The maximum in selectivity with this catalyst is 65% with a liquid flow rate of 1 ml/min and a gas flow rate of 4 ml/min. Therefore this catalyst can be used effectively for the synthesis in a TBR. The same catalyst was not so promising when tested in a semi-batch reactor; in TBR selectivity was enhanced up to 50% (Melada 2006). The contact time between liquid and solid phases thus influences the reaction pathway. Also, the concentration of hydrogen peroxide that forms and the duration of the contact with the catalyst is an important factor that can limit or suppress its reduction. In Figure 5.6 we see that the contact time obtained from a liquid flow rate of 1 ml/min and a gas flow rate of 4 ml/min allows to produce a good quantity of hydrogen peroxide with little quantity of water formed. On the other hand the selectivity achieved with 2 ml/min of liquid flow rate is poor, likely due to the low contact time between liquid and solid phases. With the liquid flow rate of 2 ml/min, water formation is expected to be very low as well as the production of hydrogen peroxide. In turn selectivity should be higher, with the shorter contact time. The latter is not true, making these results quite unexpected, but a reasonable explanation can be inferred. The water formed in this case is to be ascribed once more to reduction reactions, but also to direct formation from its elements (a reaction that runs in parallel with H_2O_2 formation). This consideration

becomes clearer if the results above are compared to the decomposition studies reported in Section 4.3.1.
Direct water formation is the last key step to be eliminated, or at least reduced, to drive the reaction mostly towards hydrogen peroxide formation. These results confirm the importance of developing both the reactor and the catalyst.

5.3.4 Pd-ZS catalyst

Sulfated zirconia was a further support considered for a palladium based catalyst. This catalyst shows very good properties for hydrogen peroxide direct synthesis, as previously assessed under semi-batch conditions (Melada 2006). It shows very good performances also with the trickle bed reactor. A significant hydrogen peroxide production is achieved with a liquid flow rate of 0.5 ml/min, as shown in Figure 5.7.

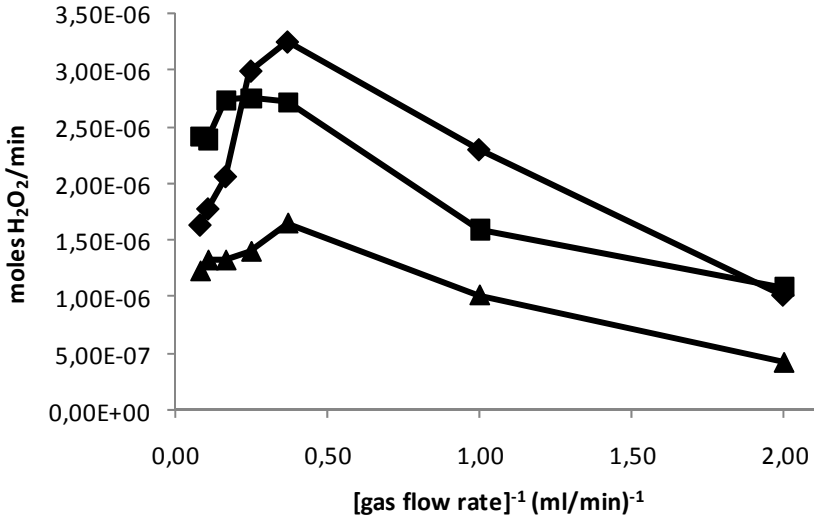

Figure 5.7. Production of hydrogen peroxide with Pd-ZS catalyst. Comparison between different liquid flow rates: 0.5 ml/min of methanol (diamonds), 1 ml/min of methanol (squares)and 2 ml/min of methanol (triangles).

Gas flow rate affects hydrogen peroxide production as with other catalyst, with a maximum for each of the liquid flow rate examined. The selectivity is shown in Figure 5.8. Notably, the maximum selectivity value is about 70% for all of the three liquid flow rates (0.5, 1 and 2 ml/min). This is a very interesting and industrially promising value, much higher than obtained in a semi-batch reactor, where the highest selectivity measured was about 50%. Hence, this particular combination between catalyst and reactor shows very interesting results, with a remarkable improvement of catalyst performance.

As previously reported, H_2O_2 production rate and selectivity often go to opposite directions when liquid and gas flow rates are changed. It is therefore of major importance to find a good compromise in terms of operative conditions, in order to have good selectivity while still achieving a satisfactory H_2O_2 production. With the Pd-ZS catalyst considered in this section, two combinations of liquid and gas flow rates are suitable for achieving good results in hydrogen peroxide direct synthesis, which correspond to 1 ml/min MeOH with 2.7 ml/min gas, and 0.5 ml/min MeOH and 2 ml/min gas. By choosing these operative conditions, which impact on the contact time between phases, values for both selectivity and production rate are very promising, showing how this reactor set-up, together with an appropriate catalyst, is well suited to enhance catalyst activity and reaction yield.

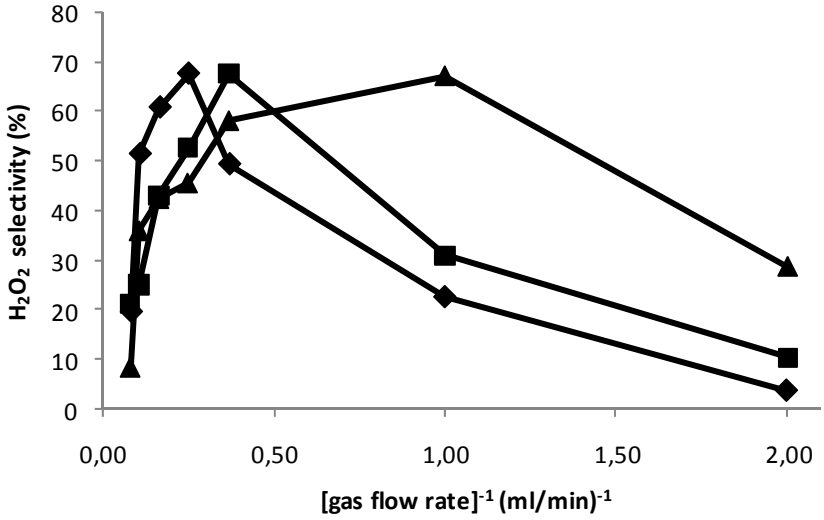

Figure 5.8. Selectivity for hydrogen peroxide with Pd-ZS catalyst. Comparison between different liquid flow rates: 0.5 ml/min of methanol (diamonds), 1 ml/min of methanol (squares)and 2 ml/min of methanol (triangles).

5.3.5 Production rate

A comparison among production rate with different catalysts operated at the same liquid flow rate, is shown in Figures 5.9-5.11. In Figure 5.9 the lowers liquid flow rate (0.5 ml/min methanol) is considered. The highest level of production rate with these operative conditions is achieved with palladium on sulfated ceria (Pd-ZS) catalyst. It provides similar results to the Pd-CeS catalyst. The least effective catalyst in this case is the one based on silica.

The earlier results obtained with a semi-batch reactor (Melada 2006) agree with this ranking just described. The catalyst based on sulfated zirconia confirms a quite good

performance, while the production rate with Pd-Z catalyst is not as high, due to the significant water formation compared to Pd-ZS catalyst.

In Figure 5.10 the experiments carried out with a liquid flow rate of 1 ml/min are presented. The best results in terms of hydrogen peroxide production rate are achieved with Pd-Z catalyst, with Pd-ZS still showing good activity in these conditions. However, the catalyst based on sulfated ceria doesn't provide a good performance in this case, and the catalyst based on silica remains the worst one.

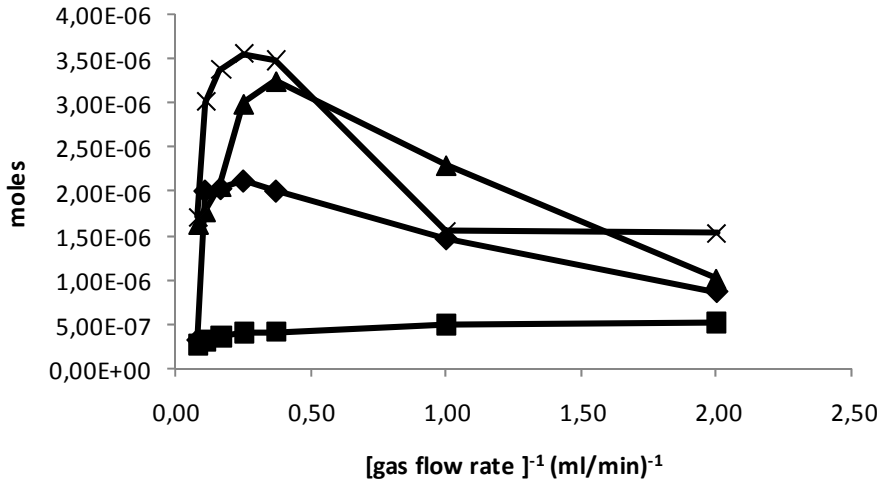

Fig. 5.9. Production rate of hydrogen peroxide with 0.5 ml/min MeOH. Comparison between different catalysts: Pd-Z (diamonds), Pd-SiO_2 (squares), Pd-ZS (triangles) and Pd-CeS (X-shaped).

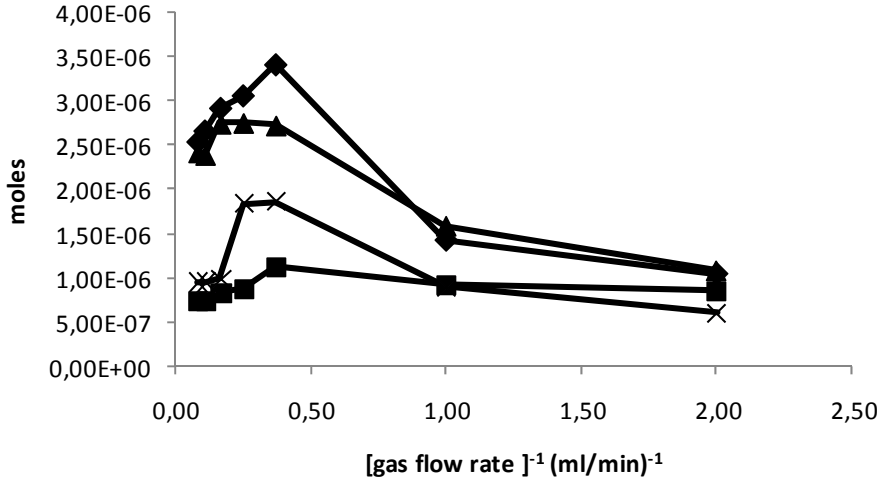

Figure 5.10. Production rate of hydrogen peroxide with 1 ml/min MeOH. Comparison between different catalysts: Pd-Z (diamonds), Pd-SiO_2 (squares), Pd-ZS (triangles) and Pd-CeS (X-shaped).

Comparing these results (Figure 5.10) with those presented earlier in Figure 5.9, it is worth highlighting how similar the hydrogen peroxide production rates that can be achieved with different catalysts by varying the operative conditions. 4 ml/min gas and 0.5 ml/min MeOH with Pd-CeS; 2.7 ml/min gas and 0.5 ml/min MeOH with Pd-ZS; 2.7 ml/min gas and 1 ml/min MeOH with Pd-Z gave comparable results in terms of H_2O_2 moles per minutes. As a consequence, reactor set-up and a proper choice of operative conditions can have an impact on the results as significant, if not more, as the catalyst properties. However, as reported in the literature, a big effort has been directed towards catalyst development, while little has been done on the reactor side to understand its role and study how it can affect the reaction pathway.
H_2O_2 production rate, with Pd-Z, Pd-SiO_2, Pd-ZS and Pd-CeS catalysts and a liquid flow rate of 2 ml/min, is reported in Figure 5.11.

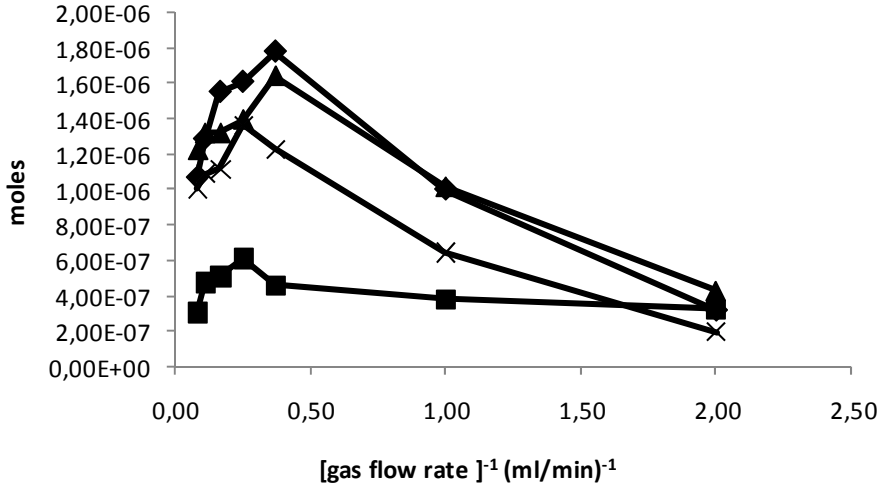

Figure 5.11. Production rate of hydrogen peroxide with 2 ml/min MeOH. Comparison between different catalysts: Pd-Z (diamonds), Pd-SiO_2 (squares), Pd-ZS (triangles) and Pd-CeS (X-shaped).

Immediately, it is evident that a higher liquid flow rate cause the production of hydrogen peroxide to be lower than before. The profile is still quite similar to the experiments with 1 ml/min methanol, but the absolute value of the H_2O_2 production is lower. This fact is to be attributed to the shorter contact time between liquid and solid phases, which reasonably leads to preferential direct water formation, as opposed to hydrogen peroxide.
Results with the Pd-Z and Pd-ZS catalysts are quite similar, the former being only slightly better. Sulfated ceria supported catalyst again shows a reasonable activity, but it's about halved compared with the lower liquid flow rate of 0.5 ml/min. The

Pd-SiO_2 catalyst is always the worst of the catalysts, its production of H_2O_2 is very low compared to the other catalysts.
The experiments show how it is possible to optimize hydrogen peroxide production and how, with different catalysts, to reach the same value of production rate by varying the operative conditions.
Production rate in itself though doesn't have all the information necessary to evaluate the industrial effectiveness of the process: it has to be always considered along with selectivity, to find the proper operative conditions in order to optimize H_2O_2 synthesis reaction .

5.3.6 Selectivity

Selectivity is the main issue in hydrogen peroxide direct synthesis. In Figures 5.12-5.14 selectivity results for four different catalysts varying liquid flow rate are presented.
Data with a liquid flow rate of 0.5 ml/min of methanol are shown in Figure 5.12.

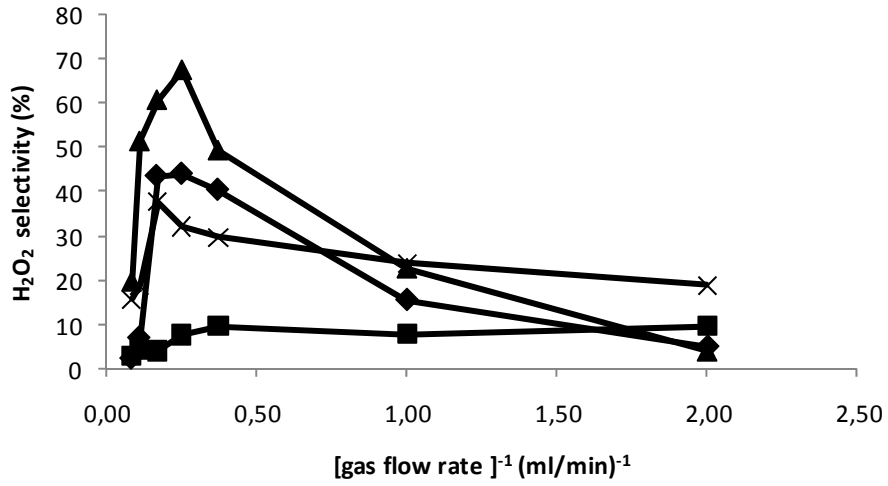

Figure 5.12. Selectivity for hydrogen peroxide with 0.5 ml/min MeOH. Comparison between different catalysts: Pd-Z (diamonds), Pd-SiO_2 (squares), Pd-ZS (triangles) and Pd-CeS (X-shaped).

Pd-ZS catalyst provides the best selectivity in this case (70%), showing a good activity for hydrogen peroxide direct synthesis, as previously reported. The best selectivity achieved with this catalyst in a semi-batch reactor was approx 50% (Melada 2006). However, a true comparison between the two results obtained with semi-batch and trickle bed reactors is not obvious, as other conditions differ. The semi-batch reactor was operated at 25 °C, 1 bar, with H_2SO_4, continuous flow of

gases through the liquid, liquid simply mixed by the gas flow, glass reactor, N_2 as the inert gas. The TBR operated at -10°C, 10 bar, continuous flow of gas and liquid, CO_2 as the inert gas.
Nevertheless, the aim of this study is to optimize conditions and reactor set-up to increase selectivity for hydrogen peroxide. This was achieved with a systematic work on operative conditions and reactors design.

As shown in Figure 5.12, with 0.5 ml/min liquid flow rate, results for the Pd-Z catalyst are quite good also with an higher selectivity measured compared to semi-batch conditions. On the other hand, palladium on both sulfated ceria and silica doesn't show a good selectivity for this liquid flow rate.

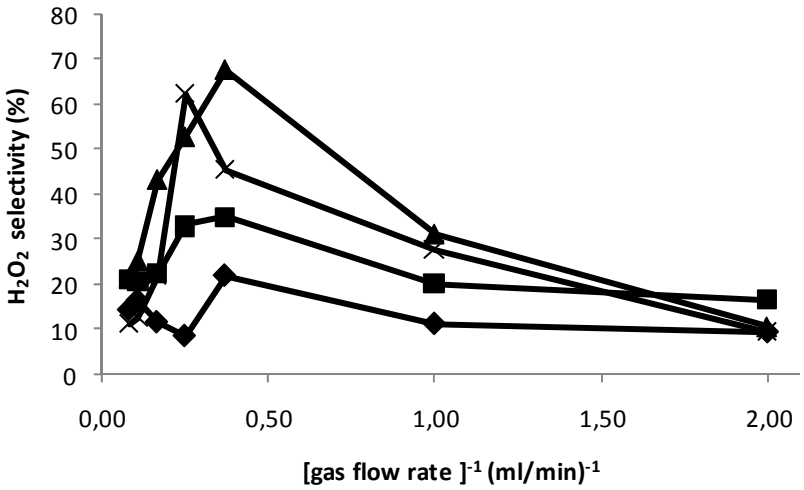

Figure 5.13. Selectivity for hydrogen peroxide with 1 ml/min MeOH. Comparison between different catalysts: Pd-Z (diamonds), Pd-SiO_2 (squares), Pd-ZS (triangles) and Pd-CeS (X-shaped).

Figure 5.13 shows the comparison between the four different catalysts with a liquid flow rate of 1 ml/min. In these experiments, as with 0.5 ml/min (Figure 5.12), the best catalyst is again the one based on sulfated zirconia. This catalyst provides a very good selectivity (70%) also with the higher liquid flow of rate of 1 ml/min. Similarly, Pd-CeS catalyst shows a good selectivity in this case too, about 63% of selectivity is achieved with an enhancement compared to the results in semi-batch conditions, where the selectivity was approx 40% (Melada 2006). Pd-CeS catalyst is comparable to Pd-ZS catalyst.
The importance of the reactor set-up can be easily understood from the pictures just presented: different catalysts give comparable results with different conditions.
Pd on silica still doesn't provide a satisfactory performance, and Pd on zirconia in this case shows bad selectivity as well.

Figure 5.14 shows the results corresponding to a liquid flow rate of 2 ml/min. It is noticeable how the only catalyst able to provide good selectivity, despite the very low contact time between liquid and solid phases, is the Pd-ZS catalyst. Other catalysts show very poor selectivity. Profiles relative to Pd-Z, Pd-CeS and Pd-SiO_2 catalysts are similar: with a high enough contact time selectivity is acceptable, but when the contact time is small selectivity drops down correspondingly. Selectivity for Pd-ZS catalyst shows a different trend with high selectivity in all the range of gas flow rates examined.

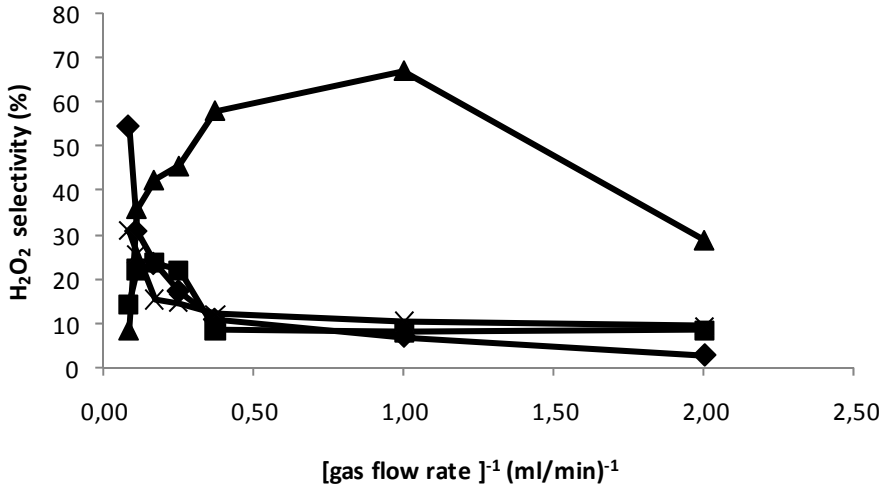

Figure 5.14. Selectivity for hydrogen peroxide with 2 ml/min MeOH. Comparison between different catalysts: Pd-Z (diamonds), Pd-SiO_2 (squares), Pd-ZS (triangles) and Pd-CeS (X-shaped).

5.3.7 Catalyst stability and reproducibility tests

In this section catalyst stability is investigated, and the results are reported in Figures 5.15 and 5.16. All the four catalysts show a good stability during a continuous 12 hours experiment. As shown in Figure 5.15, production rate is constant during the 12 hours experiments.

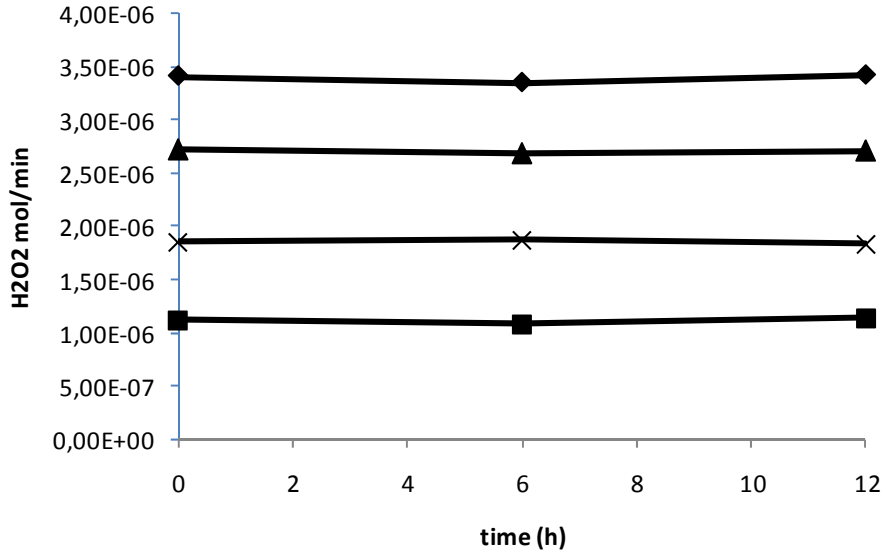

Figure 5.15. Stability of productivity for a long experiment (12 h) of hydrogen peroxide synthesis with 1 ml/min MeOH and a total gas flow rate of 2.7 ml/min . Comparison between different catalysts: Pd-Z (diamonds), Pd-SiO_2 (squares), Pd-ZS (triangles) and Pd-CeS (X-shaped).

The catalysts used for the experiments can be stressed and suffers pressurization and depressurization cycles. The importance to reuse the catalyst and its stability is fundamental for hydrogen peroxide direct synthesis from an industrial perspective, but in the literature usually tests are performed in batch reactors with the catalyst in powder form, which typically looses active metal after a few hour of experiment (Burato 2009).

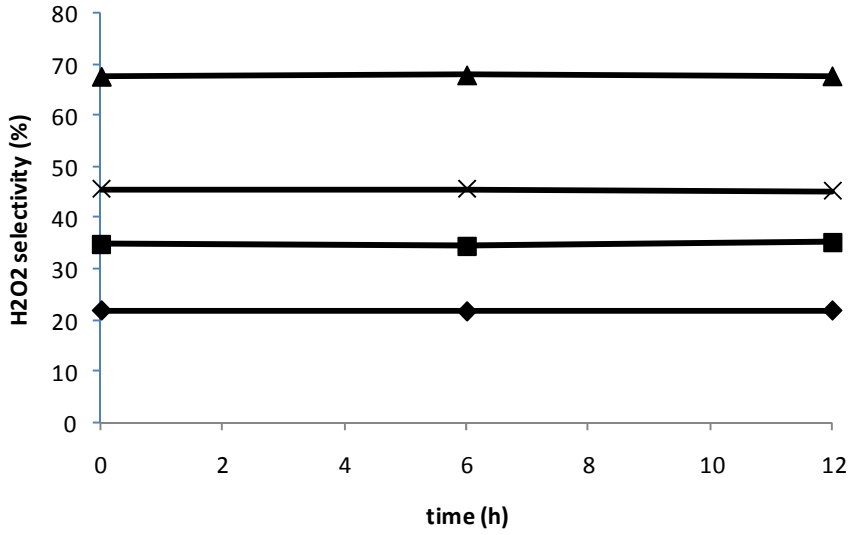

Figure 5.16. Stability of selectivity for a long experiment (12 h) of hydrogen peroxide synthesis with 1 ml/min MeOH and a total gas flow rate of 2.7 ml/min . Comparison between different catalysts: Pd-Z (diamonds), Pd-SiO_2 (squares), Pd-ZS (triangles) and Pd-CeS (X-shaped).

As a side information, results of Figures 5.15 and 5.16 provide an indication about the reproducibility of the whole experimental procedure, including the analytical steps. The error is always very small.

5.4. Conclusions

The most prominent achievement highlighted by this set of experiments is the dramatic enhancement of performances of the four catalysts examined in this chapter (Pd-SiO_2, Pd-Z, Pd-CeS, Pd-ZS) in comparison to previous results in semi-batch reactors. That confirms the working hypothesis of this Thesis that working on the operative conditions can significantly enhance catalysts performance. The crucial role of a continuous reactor is proved, highlighting its importance in optimizing hydrogen peroxide direct synthesis process. Obviously, an active catalyst is required to perform the reaction, but engineering the reactor/reaction system plays an extremely significant role in improving the process and marking a step further towards its application on an industrial scale.

A TBR is successfully used to improve and study the behavior of various catalysts under different operative conditions. Studying the process form a engineering point of view, and without using promoters or stabilizers in the reaction medium, provides clear information on how varying operative conditions impacts on the results. The issue of secondary unwanted parallel and series reactions is addressed, in order to limit them as much as possible for higher selectivity results.

Catalyst activity and durability are investigated, showing a good performance which also contribute in indicating the consistency and reproducibility of the results obtained.

Catalyst support substrate also plays an important role in the direct synthesis of hydrogen peroxide. Palladium supported on sulfated zirconia and sulfated ceria reveals very interesting behavior in the continuous reactor. The selectivity achieved is up to 70%, with a 40% enhancement in comparison to the semi-batch reactor results.

On the other hand, palladium on silica does not provide satisfying results, making it less attractive for a possible subsequent implementation on an industrial scale.

Therefore, to improve selectivity and productivity it is necessary to go beyond the catalyst properties, working on the process and engineer the reaction, by optimizing the reactor set-up and the operative conditions.

Chapter 6

Direct Synthesis of hydrogen peroxide in a Trickle Bed Reactor (TBR): bimetallic catalysts and H_2 concentration

6.1. Introduction

In this chapter a continuous reactor (Trickle Bed Reactor) is used to compare the behavior of different catalysts for hydrogen peroxide direct synthesis. Four different catalysts based on palladium, and palladium and gold, previously tested in a semi-batch reactor and a batch reactor, are chosen. The catalysts are supported on different substrates: a styrene-divinylbenzene copolymer with grafted SO_3^- groups (K2621), sulfated zirconia (ZS) and sulfated ceria (CeS). The present study wants to demonstrate the importance of the reactor and the operative conditions to maximize the efficiency of the catalyst on the reaction, with a particular attention to the effects of: a second metal in addition to palladium, the support substrate, flow rates and hydrogen concentration in the gas feed.

6.2. Experimental

6.2.1 Materials

$(NH_4)_2Ce(NO_3)_6$ (Sigma-Aldrich), $(NH_4)_2SO_4$ (Merck), are used for sample synthesis as received. Methanol for HPLC is used as the reaction medium (J.T. BAKER 99,99%), the other reagents are: potassium iodide (Sigma-Aldrich), Hydranal-Composite 2 (Fluka), dry methanol for KFT (Fluka), Acetic Acid (Sigma-Aldrich), Sodium Thiosulfate penta-hydrate 99,5% (Sigma-Aldrich), Starch (Sigma-Aldrich), Potassium dichromate (Riedel de Haën), H_2O_2 30% w/w (Merck), Acetone for HPLC (Sigma-Aldrich), Ethanol for HPLC (Sigma-Aldrich), Lewatit K2621 (Laxness), deionized water.

6.2.2 Catalyst preparation

Pd-ZS catalyst.

Zirconia support was prepared by precipitation from $ZrOCl_2$ at constant pH (pH 10), aged under reflux conditions, washed several times to remove excess of chloride ($AgNO_3$ test) and dried overnight at 110°C. The solution was continuously mixed and boiled for 6 h at 100°C, the precipitate was washed twice in boiling deionized water and dried overnight at 110°C. This material was then impregnated by an incipient wetness method with $(NH_4)_2SO_4$ in amounts necessary to yield an 8% wt anion loading. Impregnated supports were then calcined in flowing air (50 ml/min) at 650°C for 3 h. Calcined supports were impregnated by incipient wetness with H_2PdCl_4 aqueous solutions to give a nominal 2.5% wt metal loaded catalyst and finally calcined again at 500°C in flowing air for 3 h (Menegazzo 2008).

PdAu-ZS catalyst.

Zirconia support was prepared by precipitation from $ZrOCl_2$ at constant pH (pH 10), aged under reflux conditions, washed several times to remove excess of chloride ($AgNO_3$ test) and dried overnight at 110°C. The solution was continuously mixed and boiled for 6 h at 100°C, the precipitate was washed twice in boiling deionized water and dried overnight at 110°C. This material was then impregnated by an incipient wetness method with $(NH_4)_2SO_4$ in amounts necessary to yield an 8% wt anion loading. Impregnated supports were then calcined in flowing air (50 ml/min) at 650°C for 3 h. Calcined supports were impregnated by incipient wetness with H_2PdCl_4 and $HAuCl_4$ aqueous solutions to give a nominal 2.5% wt metal loaded catalyst and then calcined again at 500°C in flowing air for 3 h (Menegazzo 2008).

PdAu-CeS catalyst.

Ceria support substrate was synthesized by precipitation with urea from $(NH_4)_2Ce(NO_3)_6$ aqueous solution. The solution was continuously mixed for 6 hour at 100°C, the precipitate was washed twice in boiling deionized water and dried in oven at 110°C overnight. These materials were impregnated by an incipient wetness method with a proper amount of $(NH_4)_2SO_4$ to yield an 8% wt anion loading. Impregnated supports were calcined in flowing air (50 ml/min) at 650°C for 3 hour. Afterwards, calcined supports were impregnated via incipient wetness with H_2PdCl_4 and $HAuCl_4$ aqueous solution to give a nominal 2.5% wt Pd-loaded catalyst, and finally calcined again at 500°C in flowing air for 3 hour (Menegazzo 2008).

The three catalysts were crushed and sieved (0.5-1 mm). Pure SiO_2 was crushed and sieved (0.5-1mm). 0.16 grams of catalyst were mixed with 0.2 grams of SiO_2 and

used as catalytic bed in the continuous reactor. The catalyst was than reduced for 1 hour with a 20 ml/min flow of pure hydrogen (1bar, 25 °C).

Pd-K2621 catalyst. K2621 (LANXESS) is a commercial cross-linked polymeric matrix, a styrene-divinylbenzene copolymer with sulfonated groups. The particles diameters were between 0.5 and 1.5 mm. K2621 resin was washed 5 times with acetone (HPLC gradient grade, J.T.Baker), 5 times with deionized water, 5 times with 0.5 M NH_3 (Ammonia pro analysis, 25%, Merk), 5 times with deionized water and 10 times with 0.5 M H_2SO_4 (Sulfuric acid, baker analyzed, 95-97%, J.T.Baker). 50 ml of acetone were added to 5 g of resin and left overnight. The following day 5 ml of acetone were added to 0.1055 g of $Pd(OAc)_2$ (99.98% metals basis, Sigma-Aldrich) to achieve 1%wt of Pd in the resin. Pd salt was dissolved using a sonic bath. The solution with $Pd(OAc)_2$ was added dropwise to the resin suspension and concentrated to half volume in a rotavapor (Buchi). The colour of the resulting suspension was orange (due to PdII). 20 ml of acetone were added to the solution and dried again. This operation was repeated 3 times. After adding the last 20 ml of acetone for the third time, the colour of the suspension was clear. The temperature of the bath was approximately 313 K. The resin was washed with 150 ml of deionized water. Three drops of royal water were added to the water used to wash the catalyst, to maintain the metal in solution. The catalyst was reduced with 50 ml of ethanol (absolute ethanol, ETAX, EaS, ALTIA corporation) and 50 ml of water in a bath with reflux at approximately 361 K for 3 hours (Burato 2009). The colour of the catalyst, after the reduction, was dark grey. 0.16 grams of Pd-K2621 were mixed with 0.2 grams of K2621 and used as the catalytic bed in the continuous reactor. The catalyst was than reduced in situ (inside the reactor) for 1 hour with a 20 ml/min flow of pure hydrogen (1bar, 25 °C), ensuring complete removal of oxygen on the palladium surface.

6.2.3 Reactor set-up for the experiments

The reactor set-up is described in detail in Section 6.2.3. Briefly, an AISI 316 stainless steel trickle-bed reactor was realized, with a catalyst bed up to 20 cm long in it. An external cooling system allows for working temperature between -20°C and 60°C. Three mass flow controllers (MFC) are used to feed the gases into the reactor. Every MFC is connected to a gas cylinder: N_2, CO_2/ H_2 97.5/2.5%, and O_2. The pressure inside the reactor is controlled and regulated with a back pressure controller (BPC). The liquid phase is fed in through a syringe pump. The catalyst bed (7 mm) is placed between two quartz wool plugs. From the bottom 37 mm of quartz wool, 7

mm of catalyst and inert particles, 26 mm of quartz wool and 140 mm of quartz sand (sieved under 0,2 mm).

6.2.4 H_2O_2 synthesis

The experiments are carried out at 10 bar and -10°C, with methanol as the solvent for these experiments.

H_2, O_2 and CO_2 constitute the gas phase in the experiments of H_2O_2 synthesis, with a composition of either 2%, 18% 80% or 4%, 16%, 80%, respectively. The liquid flow rates examined are 0.5, 1 and 2 ml/min. Total gas flow rates are: 1, 2, 2.7, 4, 6, 9 and 12 ml/min at the conditions reported above.

During experiments, small aliquots of the liquid phase are sampled through a valve positioned at the exit of the TBR, and used for water and hydrogen peroxide content determination. Specifically, H_2O_2 concentration is measured by iodometric titration, whereas water content is determined by volumetric Karl Fischer method. Water content is also measured in the reaction medium prior to each experiment, i.e. before feeding the oxygen. Protocol details are described in Section 1.4.

6.3. Results and discussion

6.3.1 Pd-K2621 characterization

The water used to wash the catalyst is collected for ICP analysis (GENESIS, Spectro-Ametek). ICP analysis shows that only 12 ppb of Pd are still in solution, allowing to conclude that the amount of Pd incorporated in the resin closely matches the amount added to the solution used for preparation, with a 99.5% of resin palladiation achieved.

A Perkin-Elmer 5400 ESCA spectrometer is used for XPS analysis with monochromatized Al K radiation (photon energy 1486.6 eV) and a pass energy value of 35 eV. Samples are in contact with ambient air prior to analysis. Carbon 1s at 284.6 eV is used as energy reference to correct minor electric charging due to photoelectric effect. In the line fitting procedure, intensity ratios of p3/2:p1/2 and d5/2:d3/2 doublets are kept fixed at their theoretical values (3:2) and a mixture of Gaussian and Lorentzian line shapes is used. Sensitivity factors used in determining atomic concentration ratios for Pd 3d, C 1s, S 2p are 4.642, 0.296 and 0.570, respectively (Moulder 1970).

In all of the samples palladium is found to be present in two oxidation states. The observed binding energies are relative to PdO (336.2 eV) and Pd interacting with –

SO_3H groups (ca. 337.8 eV) (Blanco-Brieva et al, 2004). Figure 6.1 shows mostly PdO binding, while in Figure 6.2 it is noticeable how a higher percentage of palladium interacts with the $-SO_3H$ groups. Pd/S surface atomic concentration ratios are the highest in samples represented in Figure 6.2, which may partially explain why Pd is less bound to the $-SO_3H$ groups in Figure 6.1.

XPS analysis shows that the formation of an oxidized film around the catalyst is always present even after the reduction treatment of the catalyst.

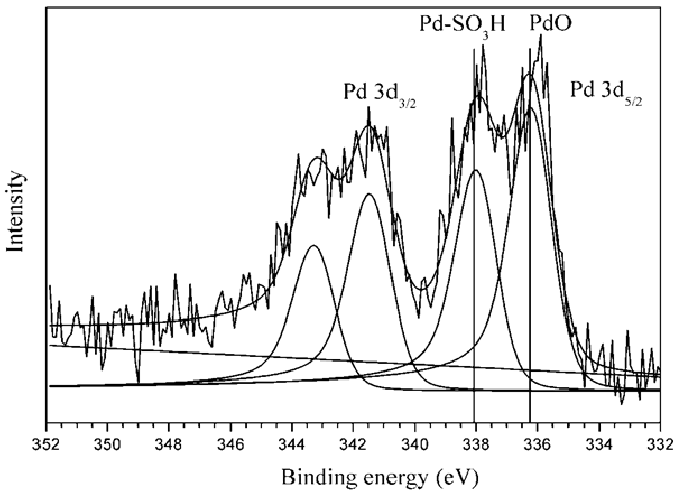

Figure 6.1. XPS analysis for Pd-K2621 catalyst before reduction treatment.

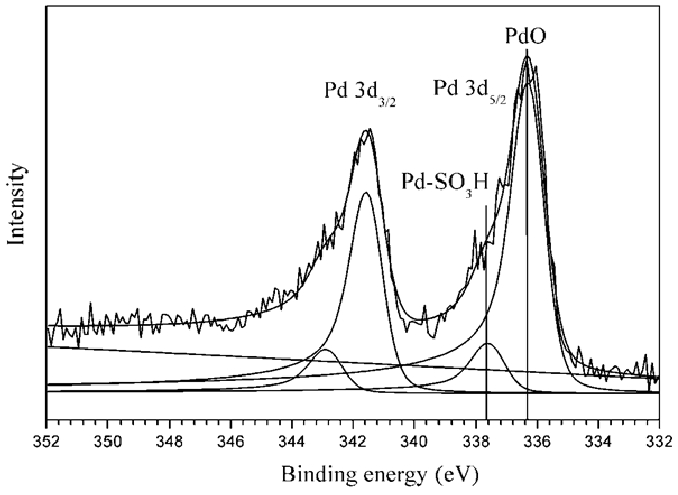

Figure 6.2. XPS analysis for Pd-K2621 catalyst after reduction treatment.

TEM images (Figures 6.3-6.6) show the particle size of the palladium cluster before and after the reduction treatment. The results show how after reduction (Figures 6.5-6.6) cluster size increases in accordance with TCS (template controlled synthesis) theory (Zecca 2008), which says that when the metal is loaded in a cross-linked polymer, the clusters that form with the reduction treatment increase their size until they reach the size of the hole in the cross-linked matrix.
TEM analysis also shows that the resin template is not homogeneous, and both big and small nanoclusters form. It is important to notice that the nanoclusters formed during palladium loading in the resin by ion exchange method are successively agglomerated into bigger clusters after the reduction treatment.

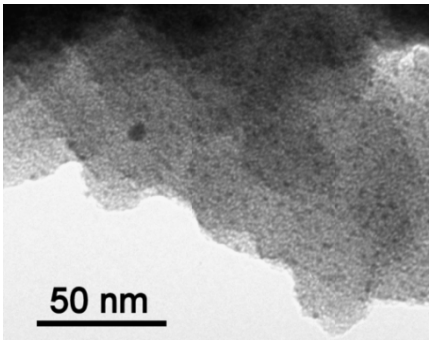

Figure 6.3. TEM analysis for Pd-K2621 catalyst before reduction treatment.

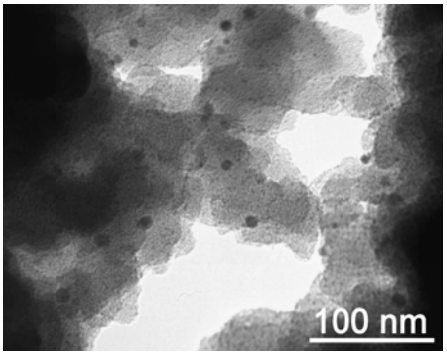

Figure 6.4. TEM analysis for Pd-K2621 catalyst before reduction treatment.

EDX analysis is also performed and the result is that the average concentration of palladium in the support is 3.3±1.3% wt. before reduction, and 3.4±1.1% wt. after reduction. The aim was to load about 1 wt.% of palladium on the resin, but owing to the very high resin affinity with water it was difficult to reach the specified percentage loading.

There are no such results in the literature, to measure the amount of palladium loaded on the catalyst, which is usually only calculated from weights. This method is far more precise, considering that an accurate estimation of the resin weight is difficult to make, due to its highly hygroscopic behavior.
The characterization of this catalyst with organic support shows the importance to have both XPS and TEM results, in order to gain thorough information on the catalyst, as was previously made for the catalysts with inorganic support (Melada 2006, Menegazzo 2008).

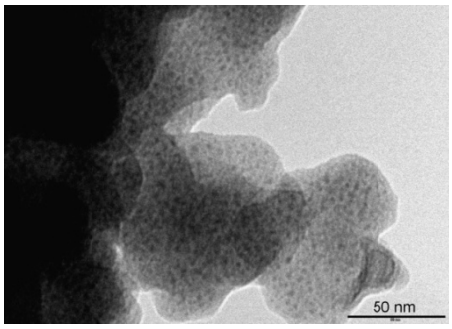

Figure 6.5. TEM analysis for Pd-K2621 catalyst after reduction treatment.

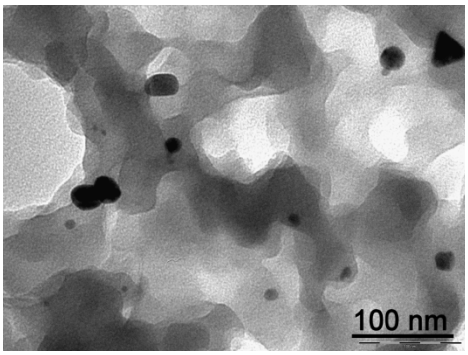

Figure 6.6. TEM analysis for Pd-K2621 catalyst after reduction treatment.

6.3.2 Pd-K2621

The differences between the experiments carried out with a hydrogen concentration of 2% and 4% in the gas phase with the catalyst based on organic support are presented in Figures 6.7-6.12. Results in Figure 6.7 show how the a different hydrogen concentration doesn't significantly affect hydrogen peroxide production rate. Indeed the results corresponding to the two concentrations of hydrogen are very close, both the trend and values are comparable. Gas flow rate though influences in a non linear way, passing through a maximum, hydrogen peroxide production. Figure

6.8 reports H_2O_2 selectivity for the two cases: i) 2% of H_2 in the gas phase ii) 4% of H_2 in the gas phase; both with a liquid flow rate of 0.5 ml/min. The results exhibit a similar profile for case i) and ii) but the values are not as close as for the production rate. This fact allows for further considerations: when the production rate is comparable but selectivity is higher for one of the cases, this means that in case ii) where selectivity is lower, production of water is higher comparison to case i). An explanation for the reaction pathway can be searched in the fact that when the hydrogen concentration is higher, there is more hydrogen solubilized in the liquid phase. H_2 can enhance hydrogen peroxide direct synthesis but also its hydrogenation to yield water. From the results, H_2O_2 formed in case ii) is more than in case i) but the reaction of hydrogenation, which occurs after H_2O_2 formation in the reaction network, is increased by the higher concentration of H_2 in the reaction environment. Also, if a higher concentration of H_2 is loaded, reaction kinetics are altered, and the reaction rate to yield hydrogen peroxide is increased. If this reaction proceeds faster, contact time between H_2O_2 and the catalyst is prolonged, and hence the possibility for H_2O_2 to be reduced is higher than in case i).

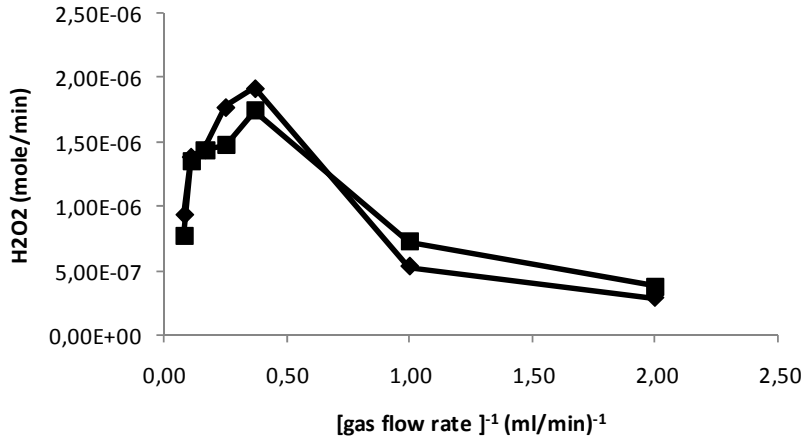

Figure 6.7. Production rate of hydrogen peroxide with 0.5 ml/min MeOH. Catalyst: Pd-K2621. Comparison between different concentrations of Hydrogen feed: 2% of hydrogen in gas phase (diamonds), 4% of hydrogen in gas phase (squares).

This catalyst presents also a high degree of porosity, thus the contact between liquid and solid phase becomes more intimate: indeed the liquid is allowed to pass through the catalyst porosity for a longer contact compared to a catalyst based on an inorganic support. As a result, this catalyst is not very suitable for hydrogen peroxide direct synthesis in a trickle bed reactor due to the large exposure of H_2O_2 formed to the active metal loaded in the resin.

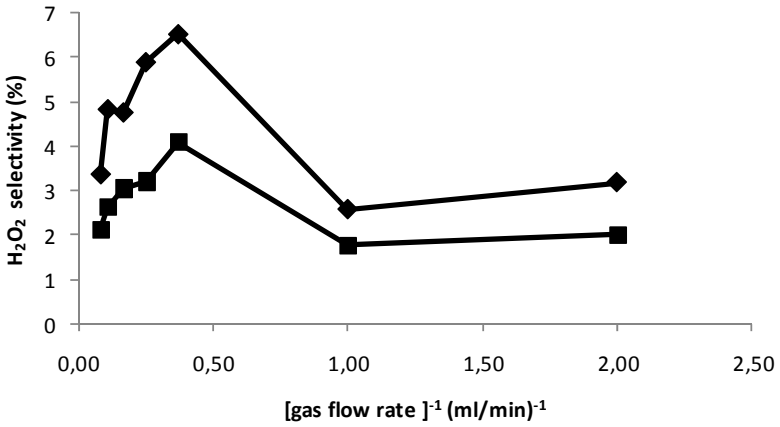

Figure 6.8. Selectivity of hydrogen peroxide with 0.5 ml/min MeOH. Catalyst: Pd-K2621 Comparison between different concentrations of Hydrogen feed: 2% of hydrogen in gas phase (diamonds), 4% of hydrogen in gas phase (squares).

Figure 6.9 reports the results of the comparison between different concentrations of hydrogen with a liquid flow rate of 1 ml/min. Hydrogen peroxide production rate is higher in the case with the highest concentration of H_2 in the environment. This result shows that the contact time between solid and liquid phase is always the key-step to improve catalyst performance.

With Pd-K2621 catalyst, decreasing residence time in the catalyst bed is needed to inhibit or reduce the reaction of H_2O_2 reduction. These considerations are confirmed by Figure 6.10, where selectivity data are reported. When the gas flow rate is the lowest, the amount of H_2 in the reaction environment is not high, that is that there's a low H_2 concentration in the liquid phase. It is thus reasonable to suppose that all the hydrogen reacts in the first part of the catalyst bed, so in the reaction network the hydrogenation reaction can be neglected. Hence the only water forming reaction in this case is H_2O_2 decomposition. On the other hand, when the gas flow rate is increased, the H_2 concentration in the environment has a significant impact. More reagent is available for the direct synthesis reaction to occur. If the contact time between liquid and solid phase is too high (as with a liquid flow rate of 0.5 ml/min), selectivity is low as shown in Figure 6.8, but with a higher liquid flow rate (i.e. 1 ml/min) contact between liquid and solid is quite fast and selectivity is increased, as shown in Figure 6.10.

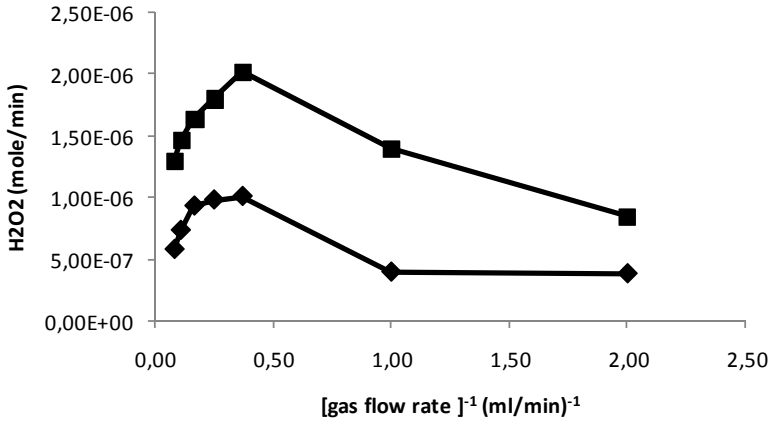

Figure 6.9. Production rate of hydrogen peroxide with 1 ml/min MeOH. Catalyst: Pd-K2621 Comparison between different concentrations of Hydrogen feed: 2% of hydrogen in gas phase (diamonds), 4% of hydrogen in gas phase (squares)

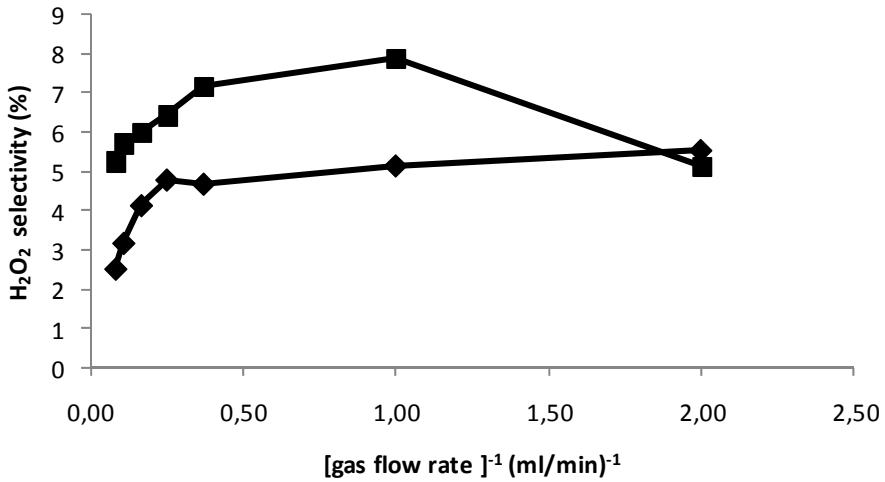

.

Figure 6.10. Selectivity of hydrogen peroxide with 1 ml/min MeOH. Catalyst: Pd-K2621. Comparison between different concentrations of Hydrogen feed: 2% of hydrogen in gas phase (diamonds), 4% of hydrogen in gas phase (squares).

In Figures 6.11 and 6.12 results with the highest liquid flow rate investigated are reported. The production of H_2O_2 is the largest with the highest concentration of H_2 used. This result is similar to the one with a liquid flow rate of 1 ml/min. Experiments carried out with a liquid flow rate of 1 and 2 ml/min permit to achieve better production rate and selectivity compared to the experiments carried out with 0.5 ml/min of MeOH. All together the results analyzed show how important it is to control the reaction pathway, taking into account catalyst porosity as well. If the reagents present a too elevated hydrogen content, and the contact between the liquid phase and the catalyst is too long, a significant reduction of the direct synthesis

reaction occurs, as the final effect. This is because once H_2O_2 forms, it is immediately reduced to water by the conspicuous amount of H_2 still in solution, reaction that happens on the active catalyst surface, and it's favoured by a prolonged contact time and a high catalyst porosity.

Pd-K2621 catalyst has good properties for the H_2O_2 direct synthesis, but due to its great porosity it is not recommended for using in a TBR. However, it is reasonable to hypothesize that reducing metal content in the catalyst, or loading a smaller amount of catalyst in the reactor could be beneficial in terms of achieving higher production rate and selectivity in the reactor set-up studied here.

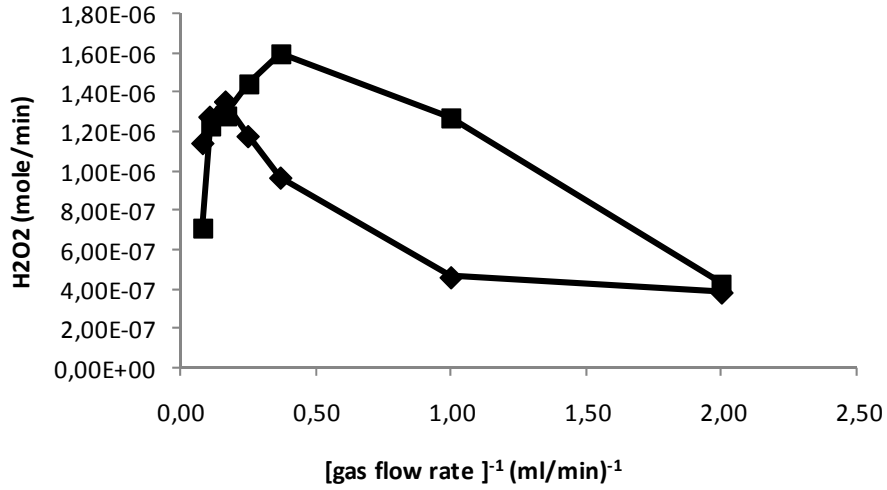

Figure 6.11. Production rate of hydrogen peroxide with 2 ml/min MeOH. Catalyst: Pd-K2621. Comparison between different concentrations of Hydrogen feed: 2% of hydrogen in gas phase (diamonds), 4% of hydrogen in gas phase (squares).

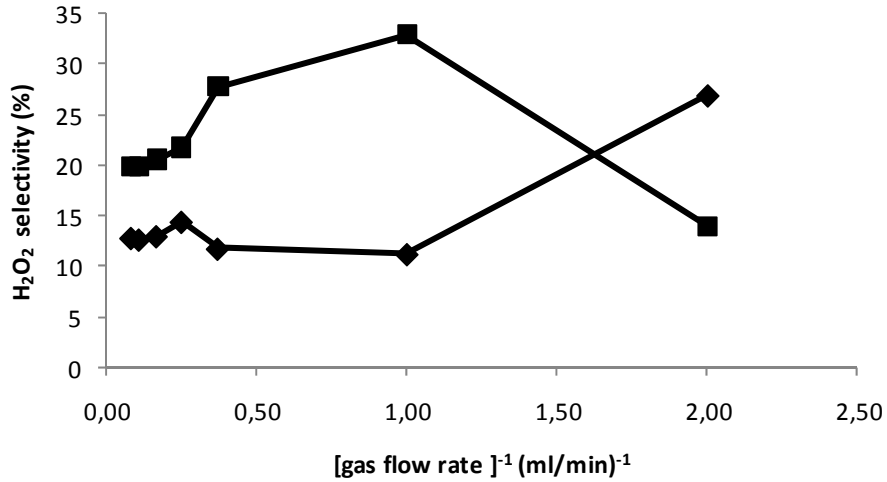

Figure 6.12. Selectivity of hydrogen peroxide with 2 ml/min MeOH. Catalyst: Pd-K2621. Comparison between different concentration of Hydrogen feed: 2% of hydrogen in gas phase (diamonds), 4% of hydrogen in gas phase (squares).

6.3.3 Pd-ZS

In Figures 6.13-6.18 results of the experiments performed loading a Pd-ZS catalyst in the TBR are presented. The effect of varying the concentration of H_2 in the gas phase is investigated.

As shown in Figure 6.13, hydrogen peroxide production rate is larger when hydrogen concentration in the gas phase is 2%. When the reactor is operated with a liquid flow rate of 0.5 ml/min and 4% hydrogen in the gas feed, this catalyst provides a not satisfying performance. Selectivity results are presented in Figure 6.14, and it is noticeable how the values corresponding to a 2% of H_2 in the gas flow are higher compared to those relative to a 4% of H_2.

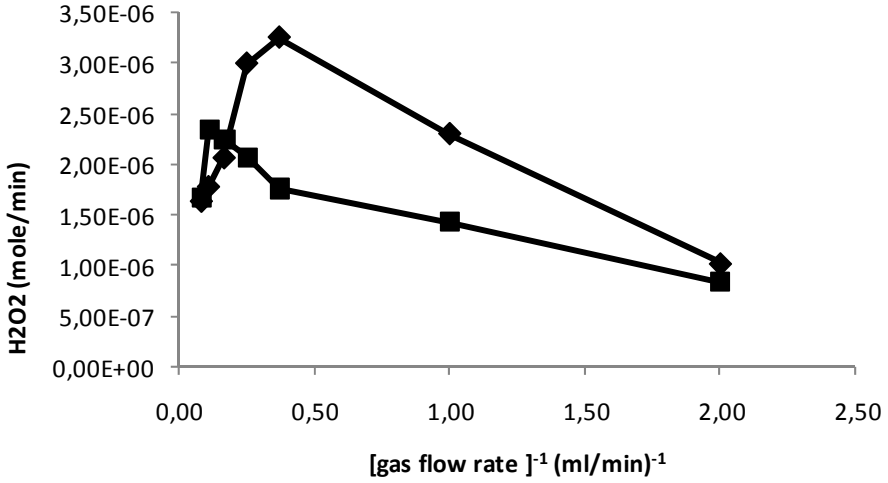

Figure 6.13. Production rate of hydrogen peroxide with 0.5 ml/min MeOH. Catalyst: Pd-ZS. Comparison between different concentrations of Hydrogen feed: 2% of hydrogen in gas phase (diamonds), 4% of hydrogen in gas phase (squares).

As shown in Figure 6.15, hydrogen peroxide production rate is quite similar for both 2% and 4% H_2, with 1ml/min of methanol as the liquid flow rate. However, a relevant difference between these conditions is manifest in Figure 6.16, where selectivity values are presented. This catalyst provides a better performance in terms of selectivity with a 2% hydrogen concentration in the gas flow, proving to be suited for H_2O_2 direct synthesis. With a 1ml/min liquid flow rate, the highest H_2 concentration makes H_2O_2 hydrogenation faster, promoting water formation as a consequence. The proper amount of hydrogen to be fed is thus one of the main issues in H_2O_2 synthesis. As demonstrated, a large excess of H_2 in the liquid phase plays an important role in H_2O_2 reduction.

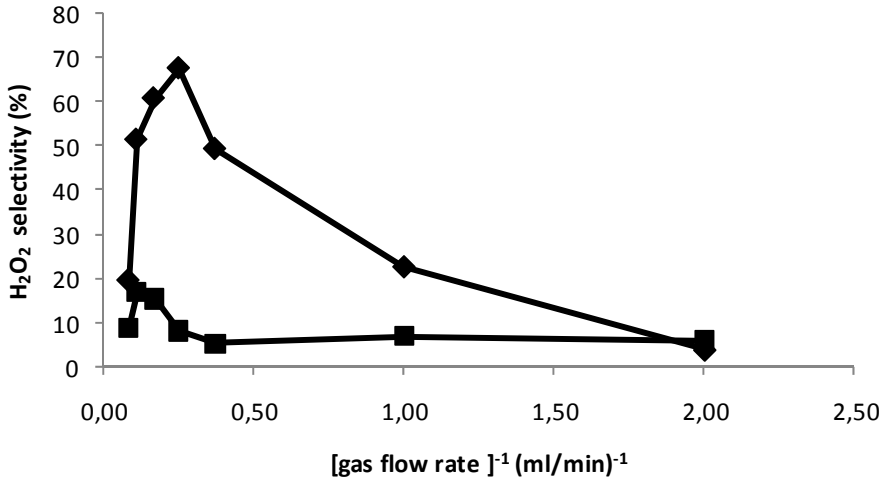

Figure 6.14. Selectivity of hydrogen peroxide with 0.5 ml/min MeOH. Catalyst: Pd-ZS. Comparison between different concentrations of Hydrogen feed: 2% of hydrogen in gas phase (diamonds), 4% of hydrogen in gas phase (squares).

Similar considerations can be deduced from the results reported in Figures 6.17 and 6.18, where a liquid flow rate of 2 ml/min was used.

Selectivity and production rate can be maximized by operating under optimized operative conditions.

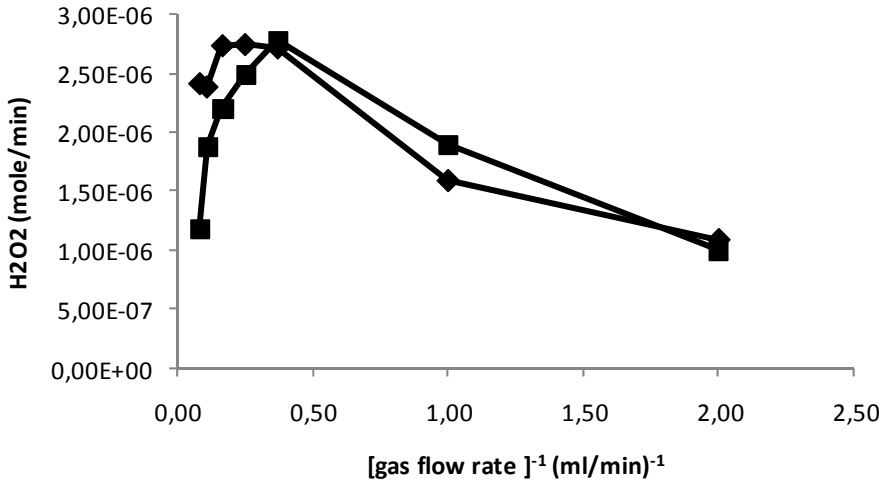

Figure 6.15. Production rate of hydrogen peroxide with 1 ml/min MeOH. Catalyst: Pd-ZS. Comparison between different concentrations of Hydrogen feed: 2% of hydrogen in gas phase (diamonds), 4% of hydrogen in gas phase (squares).

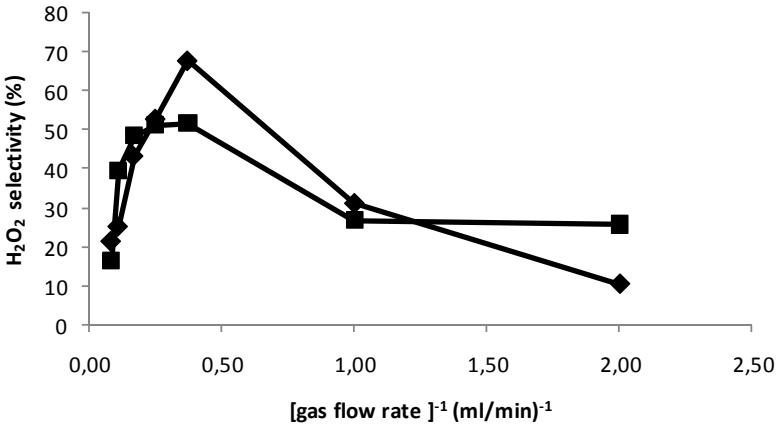

Figure 6.16. Selectivity of hydrogen peroxide with 1 ml/min MeOH. Catalyst: Pd-ZS. Comparison between different concentrations of Hydrogen feed: 2% of hydrogen in gas phase (diamonds), 4% of hydrogen in gas phase (squares).

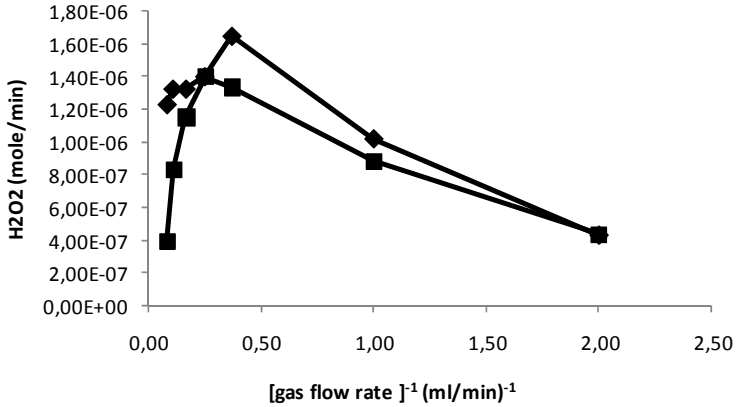

Figure 6.17. Production rate of hydrogen peroxide with 2 ml/min MeOH. Catalyst: Pd-ZS. Comparison between different concentrations of Hydrogen feed: 2% of hydrogen in gas phase (diamonds), 4% of hydrogen in gas phase (squares).

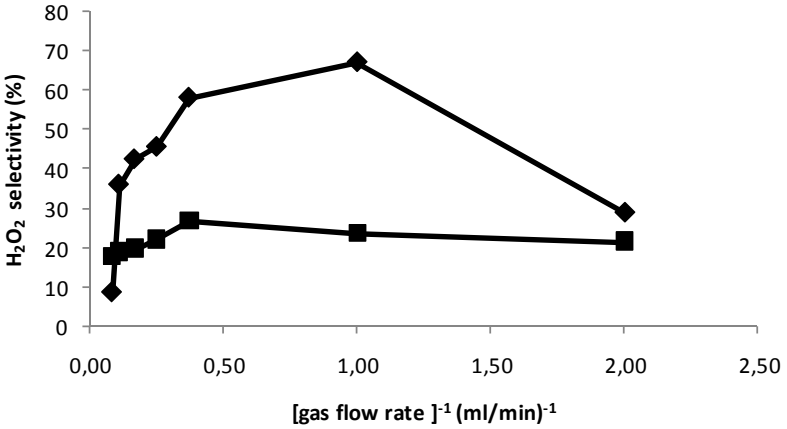

Figure 6.18. Selectivity of hydrogen peroxide with 2 ml/min MeOH. Catalyst: Pd-ZS. Comparison between different concentrations of Hydrogen feed: 2% of hydrogen in gas phase (diamonds), 4% of hydrogen in gas phase (squares).

6.3.4 PdAu-ZS

The effect of hydrogen concentration may vary depending on the catalyst: some catalysts require more H_2 dissolved in the liquid phase to have a higher H_2O_2 production rate. In Figures 6.19-6.22 H_2O_2 production rate and selectivity results for a PdAu-ZS catalyst are presented. Addition of gold enhances catalyst performance compared to a catalyst based on the same support but with palladium only as the active metal (i.e. Pd-ZS, Section 6.3.3). In Figure 6.19 experiments with 2% and 4% H_2 in the gas phase, and 0.5 ml/min as the liquid flow rate are compared. The experiments carried out with the highest concentration of H_2 show a better production rate: the trend for the two concentrations is similar, but about twice as much H_2O_2 is produced. However, selectivity (Figure 6.20) is not very satisfying due to the high contact time between liquid and solid phase.
The relevant consideration though is that with this catalyst the highest concentration of hydrogen gives a very high production rate of H_2O_2, as opposed to the catalysts previously employed.

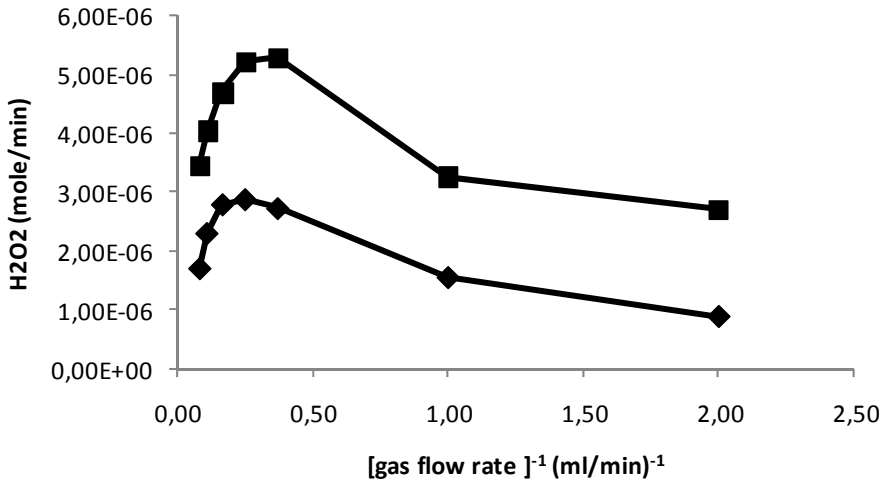

Figure 6.19. Production rate of hydrogen peroxide with 0.5 ml/min MeOH. Catalyst: PdAu-ZS. Comparison between different concentrations of Hydrogen feed: 2% of hydrogen in gas phase (diamonds), 4% of hydrogen in gas phase (squares).

In Figure 6.21 the production rate is still very high with a liquid flow rate of 1 ml/min, and it is comparable to the production rate achieved with a liquid flow rate of 0.5 ml/min. Figure 6.22 reports values for selectivity, which is quite good and notably it is improved in comparison to the results with the lower liquid flow rate (0.5 ml/min, Figure 6.20). This outcome confirms once again how manipulating operative conditions can lead to a significant improvement in catalyst performance, promoting H_2O_2 synthesis and limiting its hydrogenation and decomposition.

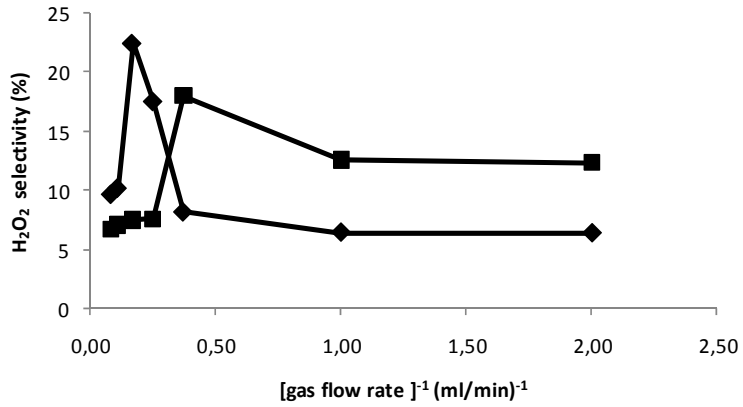

Figure 6.20. Selectivity of hydrogen peroxide with 0.5 ml/min MeOH. Catalyst: PdAu-ZS. Comparison between different concentrations of Hydrogen feed: 2% of hydrogen in gas phase (diamonds), 4% of hydrogen in gas phase (squares).

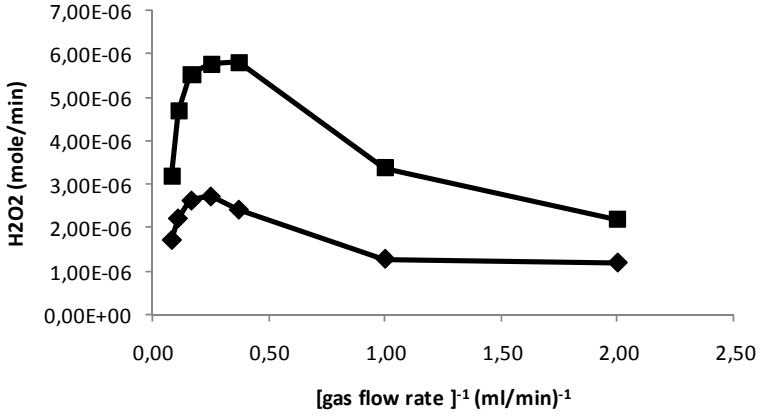

Figure 6.21. Production rate of hydrogen peroxide with 1 ml/min MeOH. Catalyst: PdAu-ZS. Comparison between different concentrations of Hydrogen feed: 2% of hydrogen in gas phase (diamonds), 4% of hydrogen in gas phase (squares).

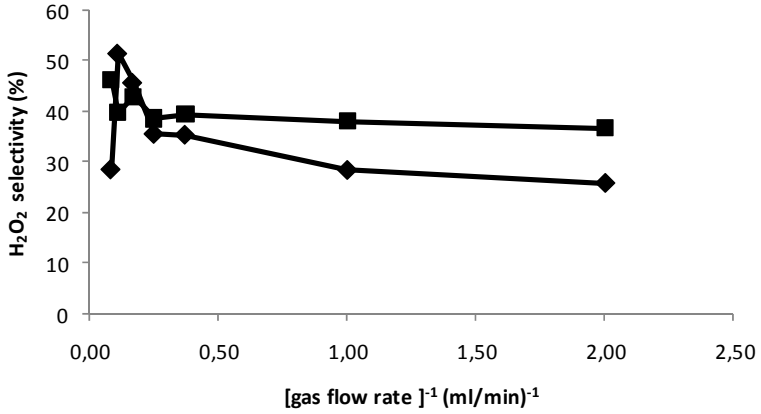

Figure 6.22. Selectivity of hydrogen peroxide with 1 ml/min MeOH. Catalyst: PdAu-ZS. Comparison between different concentrations of Hydrogen feed: 2% of hydrogen in gas phase (diamonds), 4% of hydrogen in gas phase (squares).

In Figures 6.23 and 6.24 results with the highest flow rate examined (2 ml/min) are reported. As shown in Figure 6.23, H_2O_2 production rate is still the highest with 4% H_2 in the gas flow; these values though are not as high as with the lower liquid flow rates (Figures 6.19 and 6.21), but an outstanding result for selectivity is achieved, which corresponds to a 90%. These conditions are therefore remarkable to promote H_2O_2 synthesis, using this gold and palladium catalyst on sulfated zirconia substrate. This value for selectivity is very close to what can be reached with the standard anthraquinone process, where the selectivity is usually about 98%.

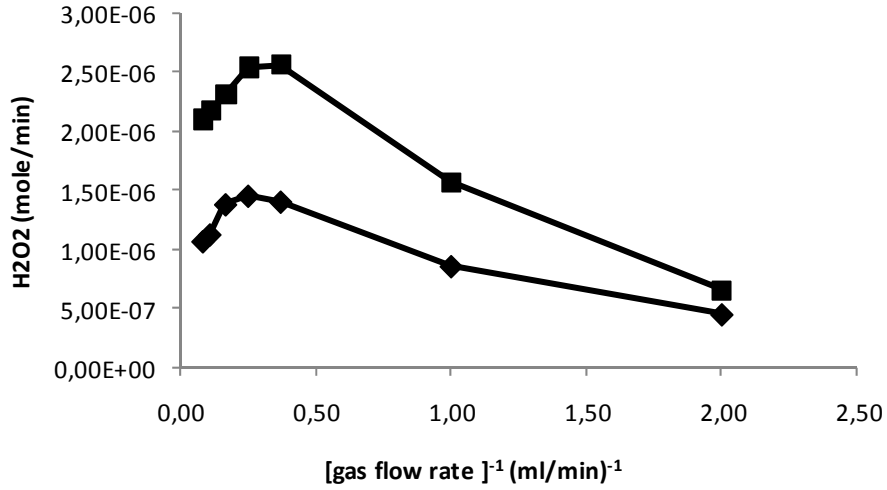

Figure 6.23. Production rate of hydrogen peroxide with 2 ml/min MeOH. Catalyst: PdAu-ZS. Comparison between different concentrations of Hydrogen feed: 2% of hydrogen in gas phase (diamonds), 4% of hydrogen in gas phase (squares).

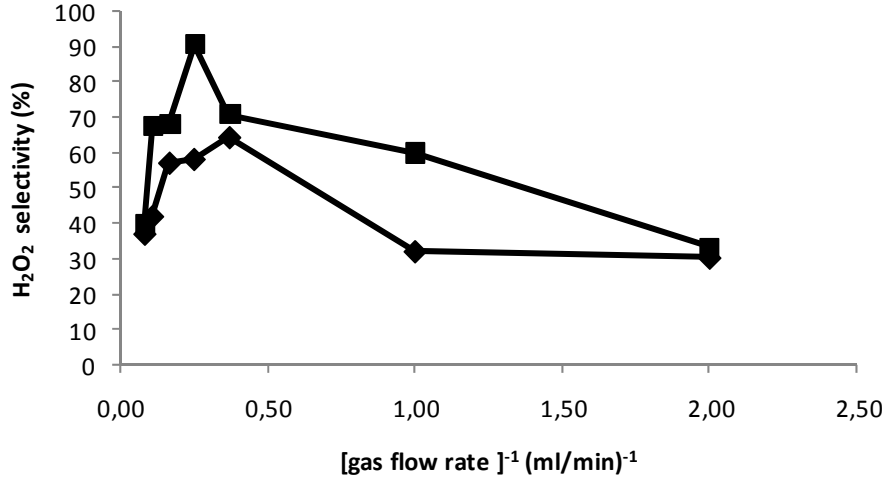

Figure 6.22. Selectivity of hydrogen peroxide with 2 ml/min MeOH. Catalyst: PdAu-ZS. Comparison between different concentrations of Hydrogen feed: 2% of hydrogen in gas phase (diamonds), 4% of hydrogen in gas phase (squares).

6.3.5 PdAu-CeS

In this section a bi-metallic catalyst based on palladium and gold on sulfated ceria is investigated.

Figure 6.25 shows, with a liquid flow rate of 0.5 ml/min, no relevant differences when H_2 concentration is either 2% or 4% in the total gas flow fed into the reactor. A reason for this is that when the contact time between liquid and solid phase is long enough, hydrogen concentration doesn't significantly impact on the production rate. However, in relation to selectivity, as shown in Figure 6.26, a conspicuous difference between the two hydrogen concentration exists. The production rate with PdAu-CeS catalyst is constant, but the reaction rates are different. When the concentration of H2 is the highest, H_2O_2 direct synthesis reaction rate is higher than in the case with 2% H_2, but, on the other hand, H_2 concentration also affects hydrogenation series reaction, increasing its rate (thus reducing selectivity) with increasing H_2 concentration.

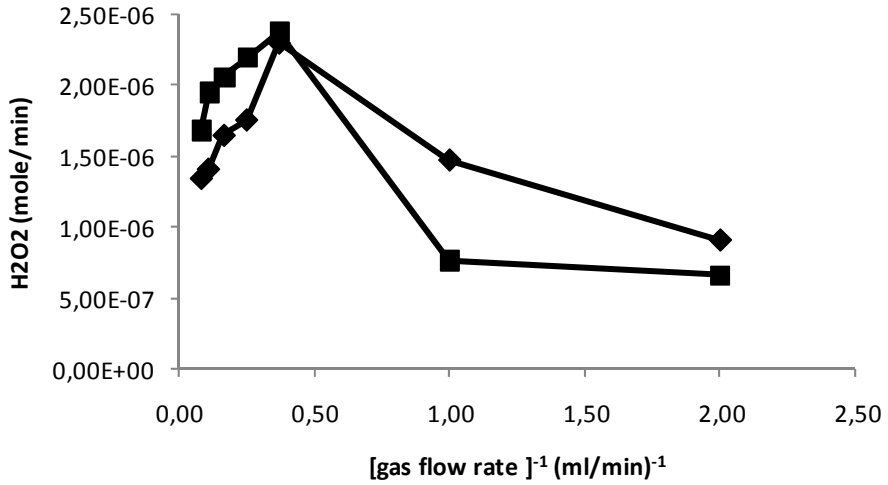

Figure 6.25. Production rate of hydrogen peroxide with 0.5 ml/min MeOH. Catalyst: PdAu-CeS. Comparison between different concentrations of Hydrogen feed: 2% of hydrogen in gas phase (diamonds), 4% of hydrogen in gas phase (squares).

As shown in Figure 6.27, H_2O_2 production rate is higher when 4% of hydrogen is used, with a liquid flow rate of 1 ml/min. Thus PdAu-CeS catalyst works well with more hydrogen; however selectivity is not enhanced by high hydrogen concentrations dissolved in the liquid phase, as shown in Figure 6.28.

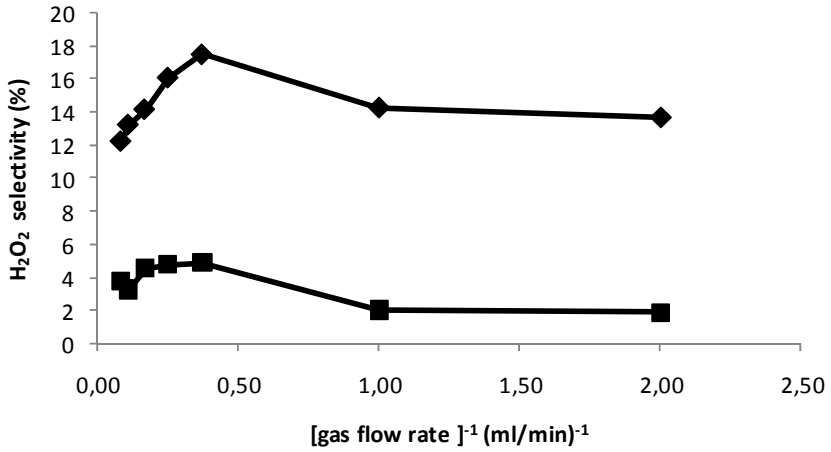

Figure 6.26. Selectivity of hydrogen peroxide with 0.5 ml/min MeOH. Catalyst: PdAu-CeS. Comparison between different concentrations of Hydrogen feed: 2% of hydrogen in gas phase (diamonds), 4% of hydrogen in gas phase (squares).

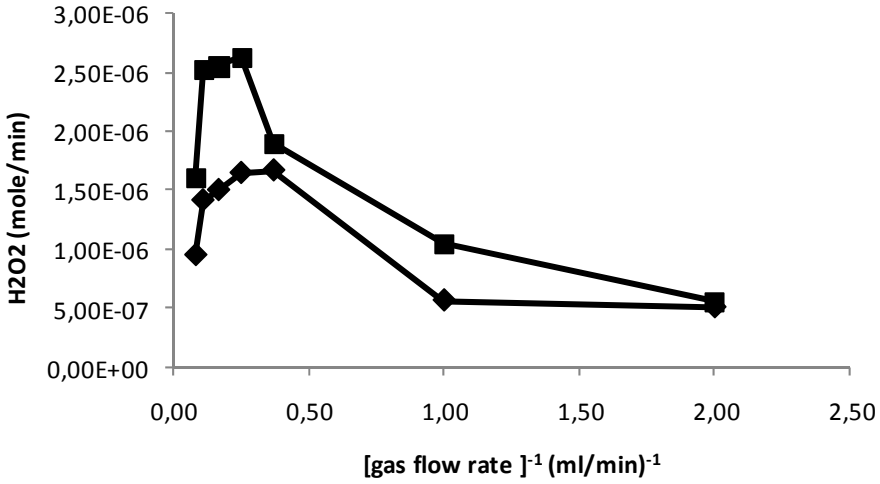

Figure 6.27. Production rate of hydrogen peroxide with 1 ml/min MeOH. Catalyst: PdAu-CeS. Comparison between different concentrations of Hydrogen feed: 2% of hydrogen in gas phase (diamonds), 4% of hydrogen in gas phase (squares).

When contact time is too short (i.e. with a liquid flow rate of 2 ml/min), production rate is about halved in comparison to the lower liquid flow rates, as shown in Figure 6.29. On the other hand, there's a remarkable increase in selectivity (Figure 6.30), which reaches 70%, when H_2 concentration is 4% in the gas feed.

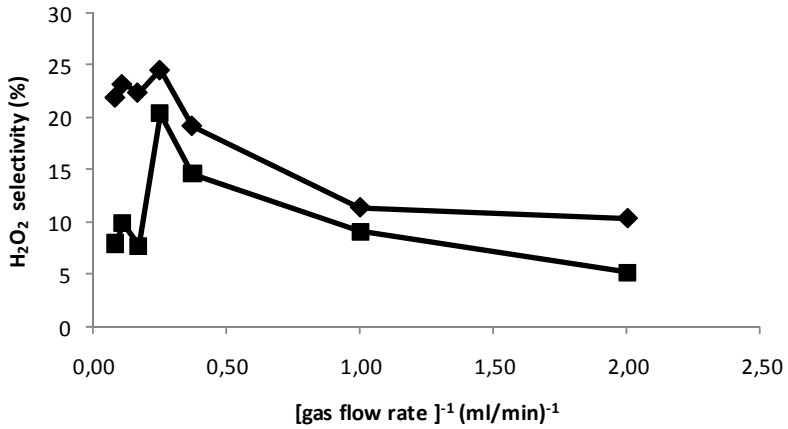

Figure 6.28. Selectivity of hydrogen peroxide with 1 ml/min MeOH. Catalyst: PdAu-CeS. Comparison between different concentrations of Hydrogen feed: 2% of hydrogen in gas phase (diamonds), 4% of hydrogen in gas phase (squares).

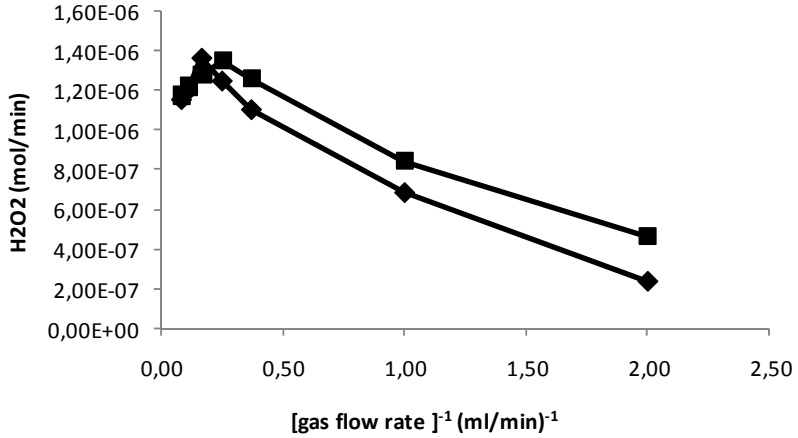

Figure 6.29. Production rate of hydrogen peroxide with 2 ml/min MeOH. Catalyst: PdAu-CeS. Comparison between different concentrations of Hydrogen feed: 2% of hydrogen in gas phase (diamonds), 4% of hydrogen in gas phase (squares).

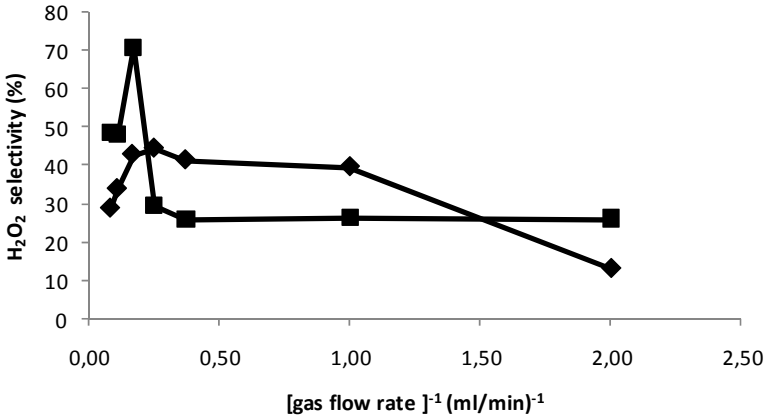

Figure 6.30. Selectivity of hydrogen peroxide with 2 ml/min MeOH. Catalyst: PdAu-CeS. Comparison between different concentrations of Hydrogen feed: 2% of hydrogen in gas phase (diamonds), 4% of hydrogen in gas phase (squares).

6.4 Production rate and selectivity optimization

In Figure 6.31 results from experiments with different catalysts are compared, when the liquid flow rate (2 ml/min MeOH) and the percentage of hydrogen in the gas flow (4% H_2) are kept constant. Bi-metallic PdAu on sulfated zirconia catalyst shows the highest production rate for this hydrogen concentration.

Figure 6.32 reports a comparison between the various catalysts when H_2 is fed at a concentration of 2%. It is worth noticing how changing operative conditions can affect catalyst behavior in different ways. For example, an increase in H_2 concentration leads to a decrease in H_2O_2 production rate for palladium supported on sulfated zirconia, but the opposite situation occurs when the catalyst based on palladium and gold on zirconia is loaded in the TBR. The quality of a catalyst is therefore strictly dependent on the operative conditions chosen for the reactor. However, when the gas flow rate is too low, there's no significant variation between the catalysts' response in terms of H_2O_2 production rate (Figures 6.31-6.32).

In the experimental set-up implemented for this study, no additives or stabilizers in the reaction medium are used, in order to gain clear information on how the operative conditions impact on the reaction pathway evolution. Stabilizers are used to suppress series reactions, but the aim here is to optimize conditions from an engineering point of view, before a further improvement that can be achieved by chemically altering reaction conditions by adding stabilizers or other additives.

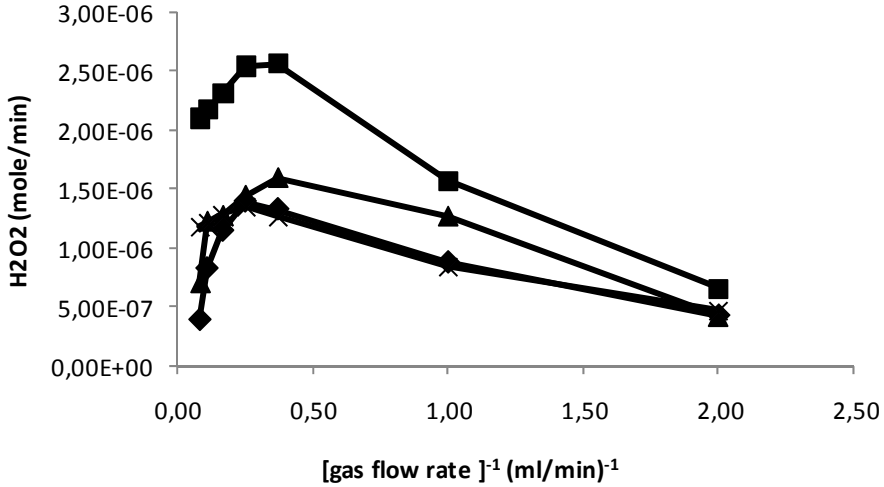

Figure 6.31. Production rate of hydrogen peroxide with 2 ml/min MeOH and 4% (mol/mol) hydrogen in the total gas flow. Comparison between different catalysts: Pd-ZS (diamonds), PdAu-ZS (squares) Pd-K2621 (triangles) PdAu-CeS (X-shaped).

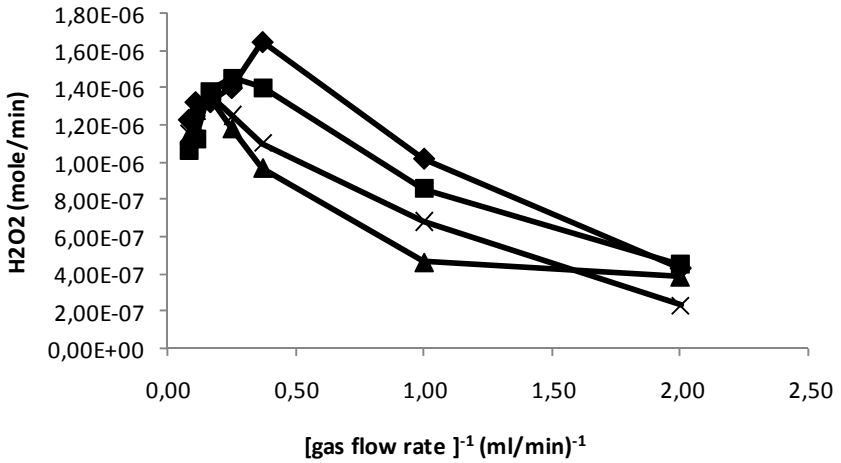

Figure 6.32. Production rate of hydrogen peroxide with 2 ml/min MeOH and 2% (mol/mol) hydrogen in the total gas flow. Comparison between different catalysts: Pd-ZS (diamonds), PdAu-ZS (squares) Pd-K2621 (triangles) PdAu-CeS (X-shaped).

To gain useful information on the reaction course, selectivity must be also taken into account, especially from an industrial perspective if this process has to be scaled up. Selectivity data are reported in figures 6.33 and 6.34. Catalysts behavior with different operative conditions is clearly not the same. The maximum selectivity value reached is about 90% with the PdAu-ZS catalyst, which is extremely high and very promising for industrial application. The experimental conditions in this case are: 2 ml/min MeOH as the liquid flow rate, 4% hydrogen in the total gas feed with 4 ml/min gas flow rate, 10 bar and -10°C (Figure 7.27). Importantly, to be noted is that H_2O_2 production rate is also the highest under these conditions (Figure 6.31).

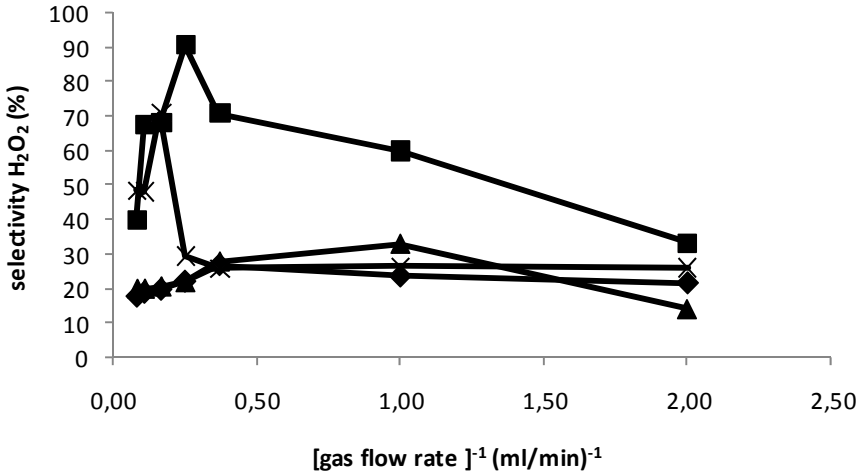

Figure 6.33. Selectivity of hydrogen peroxide with 2 ml/min MeOH and 4% (mol/mol) hydrogen in the total gas flow. Comparison between different catalysts: Pd-ZS (diamonds), PdAu-ZS (squares) Pd-K2621 (triangles) PdAu-CeS (X-shaped).

The same operative conditions for the other catalysts prove to be not satisfying.
Good results (70% selectivity) are also achieved with the catalyst based on palladium only and sulfated zirconia as the support substrate, with a gas flow rate of 2 ml/min with 2% hydrogen (Figure 6.32).
The catalyst based on organic support (i.e. Pd-K2621) shows poor results for hydrogen peroxide direct synthesis in the TBR set-up, even though it exhibits good selectivity in batch reactors (Blanco-Brieva 2004, Corain 2009). As shown in Figures 6.33 and 6.34, selectivity drastically decreases when this catalyst is used for continuous operation. In this case, its porosity is the major problem, since the liquid can pass through its polymeric structure with increased contact time and a subsequent enhancement of decomposition and hydrogenation reactions.

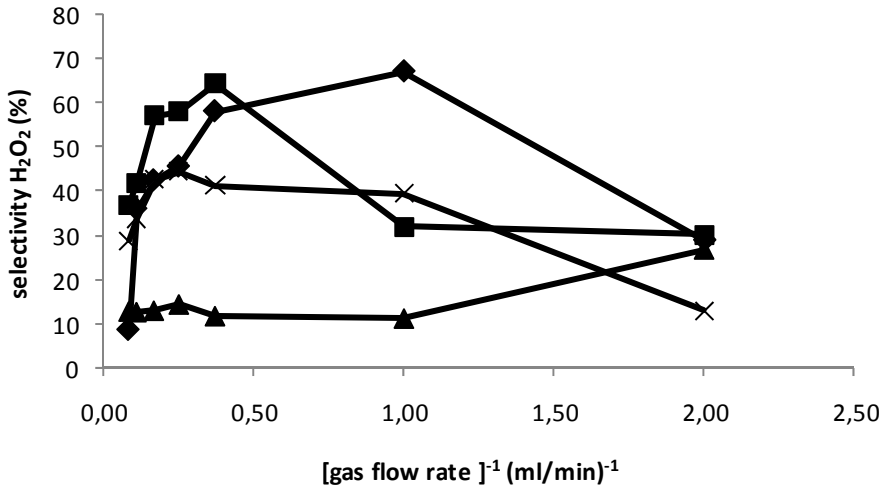

Figure 6.33. Selectivity of hydrogen peroxide with 2 ml/min MeOH and 2% (mol/mol) hydrogen in the total gas flow. Comparison between different catalysts: Pd-ZS (diamonds), PdAu-ZS (squares) Pd-K2621 (triangles) PdAu-CeS (X-shaped).

6.5 Catalyst stability

All the catalysts examined in this chapter show very good stability during a 72 hour experiment. The experiment consists of three iteration of the same cycle: 4 h reactor start-up to reach steady state conditions, 12 h synthesis reaction, 8 h depressurization and nitrogen flushing. Experimental details are described in Section 4.3.3.
Three samples are taken per day, and the mean production rate and selectivity values for one day are not significantly different from those relative to the other days (data not shown).

6.6 Conclusions

A continuous reactor for hydrogen peroxide synthesis is successfully used to enhance catalyst activity.

The findings presented in this chapter allow for some considerations.

1) A catalyst alone cannot be good or bad for hydrogen peroxide direct synthesis, independently from the reactor and its operative conditions. The catalyst based on K2621, due to the high porosity of the support, is not suited for continuous operation, with very low selectivity values achieved, even though the same catalyst performs very well in a batch reactor (Blanco-Brieva 2004, Corain 2009). The other catalysts examined, based on inorganic supports, exhibit a significantly improved behavior under continuous operation conditions, compared to experiments carried out in a semi-batch reactor.

2) Bimetallic catalysts prove to be very attractive for H_2O_2 direct synthesis. As the best results obtained are with a PdAu-ZS catalyst, it is advisable to consider a systematic study on this catalyst to further improve the reactor/reaction network system.

3) Hydrogen concentration in the gas phase has different effects on different catalysts: the catalyst based on PdAu-ZS shows better activity with a 4% H_2 compared to experiments carried out with 2% H_2. On the other hand, palladium supported on sulfated zirconia shows better activity with 2% hydrogen in the gas phase.

The other two catalysts show different behavior with 2% and 4% H_2 depending on the liquid flow rate. PdAu-CeS catalyst provides better selectivity with 2% H_2 with a liquid flow rate of 0.5 ml/min, than for a liquid flow rate of 1 ml/min the selectivity is practically not affected by hydrogen concentration, and finally with a liquid flow rate of 2 ml/min the selectivity is better with a 4% hydrogen concentration. This means that hydrogen concentration plays an important role on production rate and selectivity, but in combination with other operative conditions as the flow rate.

4) XPS and TEM analyses for Pd-K2621 catalyst show that palladium clusters form on the resin (TEM images) after the reduction treatment, and that these clusters are partially covered by oxygen (XPS analysis). These considerations are in accordance with the theory that the active phase of the catalyst for hydrogen peroxide direct synthesis is a mixture of Pd/PdO. This combination of metallic and oxidized palladium gives the catalyst those special properties required for the reaction to occur. Catalyst characterization shows that previous findings on this catalyst (Blanco-Brieva 2004, Corain 2009) are in agreement with this study.

5) Catalyst stability test shows how with a continuous reactor catalysts are preserved from mechanical stress and loosing of palladium during the reaction, which occur in

a batch reactor because of stirring. This result makes this process even more attractive from an industrial perspective, especially considering its scale-up, when every cost has to be minimized.

Chapter 7

Conclusions and future perspectives

7.1 Conclusions

The aim of this study was to investigate hydrogen peroxide direct synthesis process from an engineering point of view. Three reactor set-ups were developed and realized for H_2O_2 direct synthesis. A batch reactor was designed for catalyst testing under various conditions. A trickle bed reactor (TBR) was successfully developed and assembled to conduct continuous experiments of H_2O_2 synthesis. Continuous operation gathers a great interest from industry, but no process is yet commercially available. Finally a batch/semi-batch reactor was realized for kinetics studies.

Preliminary experiments with a Pd-K2621 catalyst were conducted in the batch reactor, showing the importance of engineering the process (manipulating VLE, developing a H2 feeding policy, acting on phases contact time) in order to improve hydrogen peroxide direct synthesis reaction performance. Firstly, hydrogen concentration in the reaction environment proved to be a critical aspect, with periodical top-ups required to maintain a satisfactory level of H_2O_2 production during batch experiments. The amount of catalyst and H_2/catalyst ratio were also investigated providing interesting and not immediately intuitive results.

Hydrogen peroxide synthesis cannot be studied without considering other series and parallel reactions which constitute the whole reaction network, since they are all thermodynamically favored, and the same catalyst is active for all of them. H_2O_2 undergoes decomposition and reduction to yield water, an unwanted by-product that lowers process selectivity. This issue was systematically investigated under continuous operation, in order to highlight reaction mechanisms and optimize conditions for minimal water formation.

Palladium is widely recognized as the more suitable catalyst for hydrogen peroxide direct synthesis, but a significant role is also played by the catalyst support substrate, as demonstrated in previous studies, by examining various organic and inorganic materials loaded with the active metal species. Here we tested several promising catalyst in the flow reactor. Sulfated zirconia provided the best results, owing to its acidic characteristics and functional groups which can stabilize hydrogen peroxide once formed. The addition of a second metal, namely gold, also contributed in enhancing catalytic performances, in terms of both H_2O_2 production rate and selectivity.

H_2/O_2 ratio was varied in the flow reactor to identify the best conditions for each catalyst. Considering six different catalysts, increasing hydrogen concentration did not necessarily result in improved production and selectivity. With bimetallic catalysts, a higher H_2 concentration produced better results, but this was not always the case for those catalysts based on palladium only, depending on the catalyst activity and on which reaction within the complex reaction network resulted more kinetically favored.

Operative conditions, particularly flow rates and the relative contact time between phases, were extensively investigated, in order to optimize the process for various catalyst-reactor systems. It was demonstrated how an engineering approach is required, since an active catalyst alone is not able to fulfill all the requirements for implementation on an industrial scale. This is extremely relevant especially for continuous operation, which is where all the industrial interest lies, and where this project mostly focused. The same catalysts proved to behave much more efficiently under suitable combinations of gas and liquid flow rates, enhancing selectivity up to more than 80%, an industrially interesting value.

Experimental studies on kinetics were also carried out to evaluate reaction rates, coupling the results with a theoretical model for the entire reaction network. Thermodynamic of the gas-liquid phase equilibria has been addressed also, with the aim of providing a suitable model to predict vapor-liquid equilibrium for the quaternary system investigated (CO_2, H_2, O_2, MeOH).

The results achieved with this work on hydrogen peroxide direct synthesis are very promising, and deserve further investigation to proceed in the direction of engineering continuous operation, with the aim of realizing a safe and cost-effective industrial process.

7.2 Future perspectives

From the results and experience achieved with this work, a new promising catalyst based on Pd and Au has already been selected, with a support substrate based on titania and zeolite. Operative conditions now need to be thoroughly investigated to optimize process performances in terms of H_2O_2 production and selectivity.

New reactor designs are also being considered, particularly a microreactor and a batch reactor with laminar flow conditions. The former will be able to provide an improved mass transfer between gas and liquid phase, and importantly it allows for intrinsically safe operation. The high surface area to volume ratio provides quenching capabilities for explosive reactions, allowing to operate at larger H_2 concentrations. An elevated A/V is also beneficial for a catalytic reaction. On the other hand, the batch reactor will allow to conduct new fundamental studies towards a better understanding of the complex reaction network involving H_2O_2 direct synthesis.

Moreover, experimental data on vapor-liquid equilibrium of the complex quaternary system need to be collected systematically to validate the thermodynamic model developed in this study.

Further investigation on the kinetic and mass transfer aspects need to be considered, with a particular attention to continuous operation in the trickle-bed, whose hydraulics is not so obvious.

Bibliography

Abate, S.; S. Melada; G. Centi; S. Perathoner; F. Pinna; G. Strukul (2006). Performances of Pd-Me (Me = Ag, Pt) catalysts in the direct synthesis of H_2O_2 on catalytic membranes. *Catalyaia Today*, **117**, 193–198.

Anastas, P.T.; Warner J.C. (1998). Green Chemistry: Theory and Practice. *Oxford University Press: New York*, USA.

Bernardotto G., Menegazzo F., Pinna F., Signoretto M., Cruciani G., Strukul G. (2009). New Pd–Pt and Pd–Au catalysts for an efficient synthesis of H2O2 from H2 and O2 under very mild conditions. *Applied Catalysis A: General*, **358**, 129–135.

Brieva, G.B.; E.C. Serrano; J.M.C. Martin; J.L.G. Fierro (2004). Direct synthesis of hydrogen peroxide solution with palladium-loaded sulfonic acid polystyrene resins. *Chemical Communications*, **2004**, 1184–1185.

Brill, W.F. (1987). (Halcon SD Group Inc.), US Patent 4, 661, 337.

Burato C., Campestrini S., Han Yi-Fan, Canton P., Centomo P., Canu P., Corain B. (2009). Chemoselective and re-usable heterogeneous catalysts for the direct synthesis of hydrogen peroxide in the liquid phase under non-explosive conditions and in the absence of chemoselectivity enhancers. *Applied Catalysis A: General,* **358** (2009) 224–231.

Burato, C.; P. Centomo; M. Rizzoli; A. Biffis; S. Campestrini; B. Corain (2006). Functional Resins as Hydrophilic Supports for Nanoclustered Pd(0) and Pd(0)-Au(0) Catalysts Designed for the Direct Synthesis of Hydrogen Peroxide. *Advanced Synthesis & Catalysis*, **348**, 255–259.

Burch, R.; P.R. Ellis (2003). An investigation of alternative catalytic approaches for the direct synthesis of hydrogen peroxide from hydrogen and oxygen *Applied Catalysis B: Environment*, **42**, 203–211.

Campos-Martin J.M.; Blanco-Brieva G.; Fierro J.L.G. (2006). Hydrogen Peroxide Synthesis: An outlook beyond the Anthraquinone Process. *Angew. Chem. Int. Ed*., **45**, 6962 – 6984.

Centi, G.; R. Dittmeyer; S. Perathoner; M. Reif (2003). Tubular Inorganic catalytic membrane reactors: advantages and performance in multiphase hydrogenation reactions. *Catalysis Today*, **79–80**, 139–149.

Choudhary, V.R.; C. Samanta (2006). Role of chloride or bromide anions and protons for promoting the selective oxidation of H_2 by O_2 to H_2O_2 over supported Pd catalysts in an aqueous medium. *Journal of Catalysis*, **238**, 28–38.

Choudhary, V.R.; C. Samanta; P. Jana (2007). Formation from direct oxidation of H_2 and destruction by decomposition/hydrogenation of H_2O_2 over Pd/C catalyst in aqueous medium containing different acids and halide anions. *Applied Catalysis A: General*, **317**, 234–243.

Choudhary, V.R.; C. Samanta; T.V. Choudhary (2006a). Direct oxidation of H_2 to H_2O_2 over Pd-based catalysts: Influence of oxidation state, support and metal additives. *Applied Catalysis A: General*, **308**, 128–133.

Choudhary, V.R.; S.D. Sansare; A.G. Gaikwad (2002c). Direct Oxidation of H_2 to H_2O_2 and Decomposition of H_2O_2 Over Oxidized and Reduced Pd-Containing Zeolite Catalysts in Acidic Medium. *Catalysis Letters*, **84**, 81–87.

Chuang, K.T. (1992). (Atomic Energy of Canada Ltd.), US Patent 5, 082, 647.

Chuang, K.T. (1992). (Atomic Energy of Canada Ltd.), US Patent 5, 082, 647.

Chuang, K.T.; B. Zhou (1993). (EKA Nobel AB), WO 9, 314, 025.

Chuang, K.T.; B. Zhou (1998). (EKA Nobel AB), US Patent 5, 846, 898.

Dalton, A.I.; E.J. Greskovich; R.W. Skinner (1983). (Air Products & Chemicals Inc.), US Patent 4, 389, 390.

Dalton, A.I.; R.W. Skinner (1982). (Air Products & Chemicals Inc.), US Patent 4, 336, 239.

Danciu, T.; E.J. Beckmann; T. Hâncu; R.N. Cochran; R. Grey; D.M. Hajnik; J. Jewson (2003). Direct Synthesis of Propylene Oxide with CO_2 as the Solvent. *Angewandte Chemie International Edition*, **2**,1140–1142.

De Frutos M. P., J. M. Campos-Martin, J. L. G. Fierro, E. Cano-Serrano, G. Blanco-Brieva (2003). (Repsol QuNmica S.A.), EP1344747.

Dissanayake, D.P.; J.H. Lunsford (2002). Evidence for the Role of Colloidal Palladium in the Catalytic Formation of H_2O_2 from H_2 and O_2. *Journal of Catalysis*, **206**, 173–176.

Dissanayake, D.P.; J.H. Lunsford (2003). The direct formation of H_2O_2 from H_2 and O_2 over colloidal palladium. *Journal of Catalysis*, **214**, 113–120.

Edwards, J.K.; A. Thomas; B.E. Solsona; P. Landon; A.F. Carley; G.J. Hutchings (2007). Comparison of supports for the direct synthesis of hydrogen peroxide from H_2 and O_2 using Au–Pd catalysts. *Catalysis Today*, **122**, 397–402.

Edwards, J.K.; B.E. Solsona; P. Landon; A.F. Carley; A. Herzing; C.J. Kiely; G.J. Hutchings (2005a). Direct synthesis of hydrogen peroxide from H_2 and O_2 using TiO_2-supported Au–Pd catalysts. *Journal of Catalysis*, **236**, 69–79.

Edwards, J.K.; B.E. Solsona; P. Landon; A.F. Carley; A. Herzing; M. Watanabe; C.J. Kiely; G.J. Hutchings (2005b). Direct synthesis of hydrogen peroxide from H_2 and O_2 using Au–Pd/Fe_2O_3 catalysts, *Journal of Materials Chemistry* , **15**, 4595–4600.

Fisher M., G. Karbel, A. Stammer, K. Flick, S. Quaiser, W. Harder, K. Massoume (2002). US Patent 6,375,920, assigned to BASF (Germany).

Foller P. C., R. T. Bombard (1995). *J. Appl. Electrochem*., **25**, 613 – 627.

Fu, F.; K.T. Chuang; R. Fiedorow (1992). Selective Oxidation of Hydrogen to Hydrogen Peroxide. *Studies in Surface Science and Catalysis*, **72**, 33–41.

Gaikwad, A.G.; S.D. Sansare; V.R. Choudhary (2002). Direct oxidation of hydrogen to hydrogen peroxide over Pd-containing fluorinated or sulfated Al_2O_3, ZrO_2, CeO_2, ThO_2, Y_2O_3 and Ga_2O_3 catalysts in stirred slurry reactor at ambient conditions. *Journal of Molecular Catalysis A: Chemical*, **181**, 143–149.

Germin, A.; J.P. Pirapad; V. Delattre; J. Van Weynbergh; C. Vogels (1996). (Solvay Interox), US Patent 5, 500, 202.

Gosser, L.W. (1987). (Du Pont), US Patent 4, 681, 751.

Gosser, L.W. (1989a). (Du Pont), US Patent 4, 889, 705.

Gosser, L.W. (Du Pont), EP 0 132,294 A1 (1985).

Gosser, L.W.: M.A. Paoli (1992). (Du Pont), US Patent 5, 135, 731.

Gosser, L.W.; J.A.T. Schwartz (1988). (Du Pont), US Patent 4, 772, 458

Gosser, L.W.; J.A.T. Schwartz (1989b). (Du Pont), US Patent 4, 832, 938.

Haas T., G. Stochniol, J. Rollmann (2006). US Patent 7,005,528 assigned to Degussa AG (Germany).

Harris C. R. (1949) (E. I. Du Pont de Nemours and Company), US Patent 2, 479, 111.

Hart W. H., S. J. Hsieh (1998). *Am. Inst. Chem. Eng. Symp*., **319**, 73 – 76.

Hass, T.; G. Stochniol; J. Rollmann (2004). (Degussa AG), US Patent 6, 764, 671.

Hass, T.; G. Stochniol; J. Rollmann (2004). (Degussa AG), US Patent 6, 764, 671.

Hass, T.; G. Stochniol; J. Rollmann (2006). (Degussa AG), US Patent 7, 005, 528.

Henkel, H.; W. Weber (1914). (Henkel & CIE), US Patent 1, 108, 752.

Henricson K. (1993). (Ahlstroem Oy), WO Patent 9, 321, 106.

Hiramatsu, Y.; Y. Ishiuchi; H. Nagashima (1991). (Mitsubishi Gas Chemical Company), EP 0 492, 064 A1.

Izumi, Y.; H. Miyazaki; S.I. Kawahara (1976). (Tokuyama Soda KK.) DE 2, 528, 601 A1.

Jennings S. R., D. J. Dollhopf, W. P. Inskeep (2000). *Appl. Geochem*., **15**, 35 – 243.

Jones C.W. (1999). Applications of Hydrogen Peroxide and Derivatives, *RSC Clean technology Monographs, RSC Publisher: Cambridge (UK).*

Kanada, T.; K. Nagai; T. Nawata (1992). (Mitsubishi Gas Chemical Company), US Patent 5, 104, 635.

Kawakmi, M.; Y. Ishiuchi; H. Nagashima; T. Tomita; Y. Hiramatsu (1995). (Mitsubishi Gas Chemical Company), US Patent 5, 399, 334.

Kitamura, M.; Y. Shimazu; M. Yako (2001). (Sumitomo Chemical Company) US Patent 6, 265, 574.

Kosaka K., Yamada H., Shishida K., Echigo S., Minear R. A., Tsuno H., Matsui S. (2001). *Water Res*., **35**, 3587 – 3594.

Krishnan, V.V.; A.G. Dokoutchaev; M.E. Thompson (2000). *Journal of Catalysis*, **196**, 366–374.

Landon, P.; J. Ferguson; B.E. Solsona; T. Garcia; S. Al-Sayari; A.F. Carley; A. Herzing; G.J. Hutchings (2006). Direct Synthesis of Hydrogen Peroxide from H_2 and O_2 Using Al_2O_3 Supported Au−Pd Catalysts. *Chemistry of Materials*, **18**, 2689 –2695.

Landon, P.; P.J. Collier; A.F. Carley; D. Chadwick; A.J. Papworth; A. Burrows; C.J. Kiely; G.J. Hutchings (2003). Direct synthesis of hydrogen peroxide from H_2 and O_2 using Pd and Au catalysts. *Physical Chemistry Chemical Physics*, **5**, 1917–1923.

Landon, P.; P.J. Papworth; C.J. Kiely; G.J. Hutchings (2002). Direct formation of hydrogen peroxide from H_2/O_2 using a gold catalyst. *Chemical Communications*, **2002**, 2058–2059.

Lewis, B.; G. Von Elbe (1961). *Combustion, Flames and Explosions of Gases*. Academic Press: New York.

Leyshon D. W., R. J. Jones, R. N. Cochran (1993). (ARCO Chemical Technology), US Patent 5, 254, 326.

Ligtenbarg A. G. J., R. Hage, B. L. Feringa (2003). *Coord. Chem. Rev.*, **237**, 89 – 101.

Liu Q., K. K. Gath, J. Chris Bauer, R. E. Schaak, J. H. Lunsford (2009). *Catal. Lett.*, **132**, 342–348.

Liu Q.; J.H. Lunsford (2006a). The roles of chloride ions in the direct formation of H_2O_2 from H_2 and O_2 over a Pd/SiO_2 catalyst in a H_2SO_4/ethanol system. *Journal of Catalysis*, **239**, 237–243.

Liu Q.; J.H. Lunsford (2006b). Controlling factors in the direct formation of H_2O_2 from H_2 and O_2 over a Pd/SiO_2 catalyst in ethanol. *Applied Catalysis A: General*, **314**, 94–100.

McIntyre, J.A. (1996). (Dow Chemical Company), US Patent 5, 512, 263.

Meiers, R.; W.F. Hölderich (1999). Epoxidation of propylene and direct synthesis of hydrogen peroxide by hydrogen and oxygen. *Catalysis Letters*, **59**, 161–163.

Melada, S.; F. Pinna; G. Strukul; S. Perathoner; G. Centi (2006a). Direct synthesis of H_2O_2 on monometallic and bimetallic catalytic membranes using methanol as reaction medium. *Journal of Catalalysis*, **237**, 213–219.

Melada, S.; R. Rioda; F. Menegazzo; F. Pinna; G. Strukul (2006b). Direct synthesis of hydrogen peroxide on zirconia-supported catalysts under mild conditions. *Journal of Catalysis*, **239**, 422–430.

Menegazzo F., Burti P., Signoretto M., Manzoli M., Vankova., Boccuzzi F., Pinna F., Strukul G. (2008). Effect of the addition of Au in zirconia and ceria supported Pd catalysts for the direct synthesis of hydrogen peroxide. *Journal of catalysis,* **257**, 369-381.

Nagashima, H.; Y. Ishiuchi; Y. Hiramatsu (1993). (Mitsubishi Gas Chemical Company), US Patent 5, 236, 692.

Nagashima, H.; Y. Ishiuchi; Y. Hiramatsu; M. Kawakami (1994). (Mitsubishi Gas Chemical Company), US Patent 5, 292, 496.

Paparatto G., G. De Alberti (2003). US Patent 6,649,140, assigned to Eni and Enichem (Italy).

Paparatto, G.; F. Rivetti; P. Andrigo; G. De Alberti (2003). (Eni S.p.A.), US Patent 6, 649, 140.

Paparatto, G.; F. Rivetti; P. Andrigo; G. De Alberti (2003b). (Eni S.p.A.), US Patent 6, 649, 140.

Paparatto, G.; R. D'Aloisio; G. De Alberti; P. Furlan; V. Arca; R. Buzzoni; L. Meda (2001). (Enichem S.p.A.), US Patent 6, 284, 213.

Parasher, S.; M. Rueter; B. Zhou (2006). (Headwaters Nanokinetix Inc.) US Patent 7, 045, 481.

Park S., Jung J. C., Seo J. G., Kim T. J., Chung Y.-M., Oh S.-H., Song I. K. (2009). Direct Synthesis of Hydrogen Peroxide from Hydrogen and Oxygen Over Palladium Catalysts Supported on SO3H-Functionalized SiO2 and TiO2. *Catal Lett*., **130**, 604–607.

Park, S.E.; L. Huang; C.W. Lee; J.S. Chang (2000). Generation of H_2O_2 from H_2 and O_2 over zeolite beta containing Pd and heterogenized organic compounds. *Catalysis Today*, **61**, 117–122.

Park, S.E.; Y. Yoo; W.J. Lee; J.S. Chang; Y.K. Park; C.W. Lee (1999). (Korea Research Institute of Chemical Technology), US Patent 5, 972, 305.

Penner S, Bera P, Pedersen S, Ngo LT, Harris JJW, Campbell CT (2006). *J Phys Chem B* 110:24577.

Pospelova, T.A.; N.I. Kobozev (1961). Palladium catalyzed synthesis of hydrogen peroxide form its elements. II. Active centres of palladium. *Russian Journal of Physical Chemistry*, **35**, 262–265.

Pospelova, T.A.; N.I. Kobozev (1961). Palladium catalyzed synthesis of hydrogen peroxide form its elements. III. Active centres for the catalytic decomposition of hydrogen peroxide on palladium. *Russian Journal of Physical Chemistry*, **35**, 584–587.

Pospelova, T.A.; N.I. Kobozev; E.N. Eremin (1961). Palladium catalyzed synthesis of hydrogen peroxide form its elements. I. Conditions for the formation of hydrogen peroxide, *Russian Journal of Physical Chemistry*, **35**, 143–147.

Pralus, C.; J.P. Schirmann (1991). (Atochem ELF SA), US Patent 4, 996, 039.

Reidl, H.J.; G. Pfleiderer (1939). (I.G. Farbenindustrie AG), US Patent 2, 158, 525.

Reis, K.P.; V.K. Joshi; M.E. Thompson (1996). Molecular Engineering of Heterogeneous Catalysts: An Efficient Catalyst for the Production of Hydrogen Peroxide. *Journal of Catalysis*, **161**, 62–67.

Rueter, M.; B. Zhou; S. Parasher (2006). (Headwaters Nanokinetix Inc.) US Patent 7, 144, 565.

Samanta, C.; V.R. Choudhary (2007b). Direct oxidation of H_2 to H_2O_2 over Pd/Ga_2O_3 catalyst under ambient conditions: Influence of halide ions added to the catalyst or reaction medium. *Applied Catalysis A: General*, **326**, 28–36.

Samanta, C.; V.R. Choudhary (2007c). Direct formation of H2O2 from H2 and O2 and decomposition/hydrogenation of H2O2 in aqueous acidic reaction medium over halide-containing Pd/SiO2 catalytic system. *Catalysis Communications*, **8**, 2222–2228.

Samanta, C.; V.R. Choudhary (2007d). Direct synthesis of H_2O_2 from H_2 and O_2 and decomposition/hydrogenation of H_2O_2 in an aqueous acidic medium over halide-modified Pd/Al_2O_3 catalysts.*Applied Catalysis A: General*, **330**, 23–32.

Samanta, C.; V.R. Choudhary (2008). Direct oxidation of H_2 to H_2O_2 over Pd/CeO_2 catalyst under ambient conditions: Influence of halide ions. *Chemical Engineerin Journal*, **136**, 126–132.

Schwartz, J.A.T. (1992). (DuPont), US Patent 5, 128, 114.

Schwartz, J.A.T. (1994). (DuPont), US Patent 5, 352, 645.

Tanev P. T., M. Chibwe, T. J. Pinnavaia (1994). *Nature*, **368**, 321 – 323.

Thompson, M.E.; V. Krishnan; A.G. Dokoutchaev; F. Abdel-Razzaq; S. Rice (1999). (University of Southern California), US Patent 5, 976, 486.

Tomita, T.; Y. Ishiuchi; M. Kawakami; H. Nagashima (1995). (Mitsubishi Gas Chemical Company), US Patent 5, 378, 450.

Van Weynbergh, J.; J.P. Schoebrechts; J.C. Colery (1995). (Solvay Interox), US Patent 5, 447, 706.

Voloshin Y., R. Halder, A. Lawal (2007). *Catal. Today*, **125**, 40.

Wang, X.; Y. Nie; J.L.C. Lee; S. Jaenicke (2007). Evaluation of multiphase microreactors for the direct formation of hydrogen peroxide. *Applied Catalysis A: General,* **317**, 258–265.

Wanngangrd, J. (1999). (EKA Chemicals AB), US Patent 5, 961, 948.

Webb, S.P.; J.A. McIntyre (1998). (Dow Chemical Company), US Patent 5, 800, 796.

Yamanaka, I.; T. Onizawa; S. Takenaka; K. Otsuka (2003). Direct and Continuous Production of Hydrogen Peroxide with 93 % Selectivity Using a Fuel-Cell System. *Angewandte Chemie Int. Ed.*, **42**, 3653–3655.

Zhou B., L.K. Lee (2001). US Patent 6,168,775, assigned to Hydrocarbon Techn. Inc. (US).

Zhou, B.; L.K. Lee (2001). (Hydrocarbon Technologies Inc.), US Patent 6, 168, 775.

Appendix A

Vapor-liquid equilibrium in multi-component systems

A.1 Equilibrium criterion

For multi-component systems, properties are not only function of P and T, but they also depend on composition. This is true for Gibbs free energy as well, which is particularly useful for describing vapor-liquid equilibrium (VLE) since it is itself a function of T and P:

$$dG = \left(\frac{\partial G}{\partial P}\right)_{T,n} dP + \left(\frac{\partial G}{\partial T}\right)_{P,n} dT + \sum_i \left(\frac{\partial G}{\partial n_i}\right)_{P,T,n_{j\neq i}} dn_i$$

When the composition is constant, it becomes:

$$\left(\frac{\partial G}{\partial P}\right)_{T,n} = V \quad \text{e} \quad \left(\frac{\partial G}{\partial T}\right)_{P,n} = -S$$

therefore:

$$dG = VdP - SdT + \sum_i \left(\frac{\partial G}{\partial n_i}\right)_{P,T,n_{j\neq i}} dn_i$$

$\left(\frac{\partial G}{\partial n_i}\right)_{P,T,n_{j\neq i}}$ is an important quantity, which is named chemical potential (symbol μ_i).

Both T and P are constant between the two phases of a system at equilibrium; also, for an enclosed system dn_i =0. Thus the equilibrium criterion is $dG = 0$. As a results:

$$\mu_i^L dn_i^L + \mu_i^V dn_i^V = 0$$

Since it is an enclosed system, the number of moles exiting the liquid phase are equal to those entering the vapor phase (and vice versa), that is $dn_i^L = -dn_i^V$. Therefore:

$$\mu_i^L dn_i^L - \mu_i^V dn_i^L = 0 \Rightarrow \mu_i^L = \mu_i^V$$

The *equality between chemical potentials* for each species between liquid and vapor phases is the *vapor-liquid equilibrium* criterion.
From the definition of fugacity it is:

$$RT\ d\ln\hat{f}_i \equiv d\mu_i$$

where $\hat{f}_i$ is the fugacity of the i component in the mixture. The equilibrium criterion thus becomes:

$$d\mu_i^L - d\mu_i^V = RT\ d\ln\left(\frac{\hat{f}_i^L}{\hat{f}_i^V}\right) \Rightarrow \hat{f}_i^L = \hat{f}_i^V$$

This is the **iso-fugacity criterion**, which will be useful to identify vapor-liquid equilibrium.

A.2 Ideal mixture, ideal solution, real solution

Typically, to model a gas mixture, three simplification levels are considered:

1) ***Ideal mixture***: an ideal combination of ideal gases, that can be treated as a single ideal gas;
2) ***Ideal solution***: a real combination of ideal gases, thus a combination of gases with similar molecules (hence negligible interactions), but formation of a liquid phase may occur;

3) ***Real solution***: a real combination of real gases, thus a combination of non-ideal gases (interactions are not neglected) with a non-ideal behaviour (liquid phase formation).

For those three levels more complex models are used.

It can be demonstrated that for an ideal gas behaviour (ideal mixture) it is:

$$\hat{f}_i^{ig} = y_i P$$

As previously discussed, an ideal gas doesn't condensate into a liquid phase. It is therefore reasonable to describe the deviation between ideal mixture and real solution by means of real fugacity-ideal fugacity ratio:

$$\hat{\varphi}_i \equiv \frac{\hat{f}_i}{y_i P} \Rightarrow \hat{f}_i = \hat{\varphi}_i y_i P$$

$\hat{\varphi}_i$ is the fugacity coefficient for the i component in the mixture (which is 1 for an ideal gas).

Similarly, deviation between real solution and ideal solution can be described by the fugacity of the i component in the real mixture ($\hat{f}_i$) divided by that in the ideal mixture, thus considering a pure component, at the same P and T conditions as in the mixture f_i :

$$a_i = \frac{\hat{f}_i}{f_i}$$

$$\gamma_i \equiv \frac{\hat{f}_i}{x_i f_i}$$

a_i is the i component activity, while γ_i is its activity coefficient.

Theoretically, activity could be used to describe both liquid and vapor phases (same as fugacity), but usually it is employed to describe the liquid phase only.

To be noted that, similarly to activity, it is possible to define a fugacity coefficient for ideal solutions:

$$\varphi_i \equiv \frac{f_i}{y_i P}$$

where φ_i is the fugacity coefficient of the pure i component at the same P and T as the mixture.

A.3 Approaches to describe the VLE

Iso-fugacity criterion can be written in terms of both fugacity coefficient and activity coefficient (the latter being usually employed for liquid phase only):

$$\begin{aligned} \hat{f}_i^V &= \hat{\varphi}_i^V y_i P \\ \hat{f}_i^L &= \hat{\varphi}_i^L x_i P \end{aligned} \quad \Rightarrow \quad \hat{\varphi}_i^V y_i P = \hat{\varphi}_i^L x_i P$$

or:

$$\begin{aligned} \hat{f}_i^V &= \hat{\varphi}_i^V y_i P \\ \hat{f}_i^L &= \gamma_i f_i P \end{aligned} \quad \Rightarrow \quad \hat{\varphi}_i^V y_i P = \gamma_i x_i f_i^L, \quad f_i^L = \varphi_i^{SAT} P_i^{SAT} \exp\left(\frac{V_i^L \left(P_i - P_i^{SAT} \right)}{RT} \right)$$

and these equations are applicable to real solutions.
Normally the first approach is referred to as the $\varphi - \varphi$ method, while the second as the $\gamma - \varphi$ method.
It is worth noticing how the EoS approach treats vapor and liquid phases the same way, that is it applies the same technique (the EoS indeed) for calculating both the liquid and vapor phases: it considers the deviation between ideal mixture and real solution.
On the other hand, the second approach uses EoS for the vapor phase, but it considers activity for the liquid phase, which represents the deviation between ideal and real solutions. To be remembered is that this deviation represents excess properties.

It can be now demonstrated that:

$$\ln \hat{\varphi}_i = \left[\frac{\partial \left(\frac{(A - A^{ig})_{T,V}}{RT} \right)}{\partial n_i} \right]_{T,V,n_{j \neq i}} - \ln Z$$

To solve the VLE with the $\varphi - \varphi$ method, the expression above must be applied to both liquid and vapor phases. To solve the quantity on the right hand side, an suitable equation of state (EoS) to describe the mixture is required. Typically equations of state with parameters valid for mixtures are used, for example:

$$Peng - Robinson: \quad Z = \frac{1}{1 - b_m \rho} - \frac{a_m}{b_m RT} \cdot \frac{b_m \rho}{1 + 2 b_m \rho - {b_m}^2 \rho^2}$$

Indeed a_m e b_m coefficients have to be in relation with the mixture, and are calculated as combinations of those relative to the pure species, employing classical mixing rules (but other ways also exist), for example:

$$a_m = \sum_{i=1}^{NC} \sum_{j=1}^{NC} z_i z_j \sqrt{a_i + a_j} (1 - k_{ij})$$

$$b_m = \sum_{i=1}^{NC} z_i b_i$$

where z_i is the generic i component fraction.

a_i and b_i are the parameters relative to the pure species, which can be calculated from critical temperature, critical pressure and saturation pressure for each component.

k_{ij} are the binary interaction parameters: they need to be regressed from experimental data of vapor-liquid equilibrium for bi-component systems. This approach can thus be seen as a correlation method for bi-component systems, and as a prediction method for multi-component systems.

In order to solve the problem with the $\gamma - \varphi$ method, activity coefficients have to be known. They can be calculated with the so-called excess free energy models (G^E models). It can be demonstrated that:

$$G^E = RT \sum_i x_i \ln \gamma_i$$

To be noted that excess Gibbs free Energy goes to 0 for ideal solutions, that is when $\gamma_i = 1$ (indeed excess properties describe the deviation between an ideal and a real mixture).
Different models for G^E are available:

- Polynomial (Margules, Van Laar, Wohl), with expressions like:

$$\frac{G^E}{RT} = \frac{\sum_k a_k x^k}{\sum_k b_k x^k}$$

  a_k e b_k parameters are temperature dependent and are regressed from experimental data.

- Wilson:

$$\frac{G^E}{RT} = f(x_i, \lambda_{ij}, \lambda_{ji}, T)$$

  Here there's an explicit temperature dependence; this is a correlation model for binary systems, and a prediction one for multi-component systems. It can successfully describe VLE, but not LLE.

- NRTL:

$$\frac{G^E}{RT} = f(x_i, \Delta g_{ij}, \Delta g_{ji}, T, k_{ij})$$

  There is an additional parameter in comparison to the other models, thus it is suited for LLE as well. It is still predictive for multi-component systems, but correlative for binary ones.

- UNIQUAC:

$$\frac{G^E}{RT} = f(x_i, \Delta \nu_{ij}, \Delta \nu_{ji}, T)$$

It is similar to NRTL, but with two parameters only.

There are also some G^E models, which are completely predictive, such UNIFAC o ASOG models (methods with group contributions).
The best EoS, mixing rules and G^E model have to be chosen for every specific system considered.

A.3.1 Simplifications

When ideal solutions are considered, the following expression can be demonstrated to be valid:

$$\frac{\Delta G_{mix}^{is}}{RT} = \sum_i x_i \ln(x_i) = \sum_i x_i \ln(\frac{\widehat{f}_i^{is}}{f_i})$$

and therefore:

$$\frac{\widehat{f}_i^{is}}{f_i} = x_i \quad \Rightarrow \quad \widehat{f}_i^{is} = f_i x_i$$

This is the ***Lewis/Randal laws***, and it is valid for ideal solutions.

Now, taking into account the iso-fugacity condition for ideal solutions, it is:

$$y_i f_i^V = x_i f_i^L$$

Following the $\varphi - \varphi$ approach, fugacities for pure vapor and liquid are:

$$f_i^V = \varphi_i^V P$$

$$f_i^L = \varphi_i^{SAT} P_i^{SAT} \exp\left(\frac{V_i^L \left(P_i - P_i^{SAT}\right)}{RT}\right) \quad \Rightarrow \quad y_i \varphi_i^V P = x_i \varphi_i^{SAT} P_i^{SAT} \exp\left(\frac{V_i^L \left(P_i - P_i^{SAT}\right)}{RT}\right)$$

For quite low pressures it is also:

$$\frac{\varphi_i^V}{\varphi_i^{SAT}} \approx 1$$
$$\exp\left(\frac{V_i^L\left(P_i - P_i^{SAT}\right)}{RT}\right) \approx 1 \quad \Rightarrow \quad y_i P = x_i P_i^{SAT}$$

This is ***Raoult's law***, which is valid for gases with negligible interactions and low pressures (<5 atm).
The following is ***Henry's law***:

$$y_i P = k_H x_i$$

Which says that the partial pressure for the i component in the gas phase (y_iP) is proportional to its composition in the liquid phase (x_i) through a constant (k_H). This is referred to as the Henry constant, which, beside temperature, depends on the different components, and has to be experimentally determined.
Raoult's and Henry's laws are in close relation: they are both valid for chemically similar gases at low pressures, but they apply to the two opposite extremes of the composition range. In other words, partial pressure of the most abundant component is proportional to its saturation pressure (Raoult's law), while partial pressure of the least abundant component is proportional to Henry's constant (Henry's law):

$$\text{Raoult's law:} \quad \lim_{x\to 1}\left(\frac{P_i}{x}\right) = P_i^{SAT}$$
$$\text{Henry's law:} \quad \lim_{x\to 0}\left(\frac{P_i}{x}\right) = k_H$$

VLE for real mixtures, in terms of activity, is:

$$\hat{\varphi}_i^V y_i P = \gamma_i x_i \varphi_i^{SAT} P_i^{SAT} \exp\left(\frac{V_i^L\left(P_i - P_i^{SAT}\right)}{RT}\right)$$

For a relatively low pressure it is:

$$\frac{\varphi_i^V}{\varphi_i^{SAT}} \approx 1$$
$$\exp\left(\frac{V_i^L\left(P_i - P_i^{SAT}\right)}{RT}\right) \approx 1 \quad \Rightarrow \quad y_i P = x_i \gamma_i P_i^{SAT}$$

This is the ***modified Raoult's law***, now valid for real solutions at low pressures.

A.4 VLE calculations

For a multi-component system at equilibrium, there are 4 degrees of freedom: T, P, x_i e y_i (the latter being vectors). Equilibrium condition corresponds to 1 equation, another one is $\sum_i z_i = 1$ (congruence equation). There are still 2 degrees of freedom to be saturated, and different calculation options are possible, depending on the information available:

1) Bubble P: T and x_i are known, P are y_i;
2) Bubble T: P and x_i are known, T are y_i;
3) Dew P: P and y_i are known, T and x_i are calculated;
4) Dew T: T and y_i are known, P and x_i are calculated;
5) Isothermal Flash: T, P and z_i (total composition) are known, x_i , y_i and L/F (liquid to liquid+vapor ratio) are calculated.

As an example, an isothermal flash calculation is reported. As previously said, two different approaches are possible:

1- $\varphi - \varphi$ *method*

In this case, VLE is described by the equation:

$$\hat{\varphi}_i^V y_i P = \hat{\varphi}_i^L x_i P$$

and an EoS for the mixture is required. The algorithm to be solved is as follows:

1) T, P and z_i are known, Raoult's law is used for an initial approximate estimation of x_i, y_i and L/F;
2) $\hat{\varphi}_i^L, \hat{\varphi}_i^V, k_i = \dfrac{\hat{\varphi}_i^L}{\hat{\varphi}_i^V}$ are calculated with the EoS;
3) The objective function $f_{ob} = \sum_i \dfrac{z_i(1-k_i)}{k_i + \dfrac{L}{F}(1-k_i)}$ is designed;
4) $f_{ob} = 0$?

   If not, a new value for L/F is assumed, following the criterion:

   $f_{ob} > 0 \Rightarrow L/F \uparrow$
   $f_{ob} < 0 \Rightarrow L/F \downarrow$

   and step 3 is repeated.

   If yes, it is possible to proceed to step 5.

5) x_i and y_i are calculated:

$$x_i = \frac{z_i}{k_i + \dfrac{L}{F}(1-k_i)}, \quad y_i = x_i k_i$$

6) If x_i, y_i and L/F are different in comparison to the previous iteration, step 2 has to be repeated with the new calculated values for x_i, y_i e L/F.
   If x_i, y_i and L/F are the same, then calculations are completed.

2- $\gamma - \varphi$ method

In this case, VLE is described by the equation:

$$\hat{\varphi}_i^V y_i P = \gamma_i x_i \varphi_i^{SAT} P_i^{SAT} \exp\left(\frac{V_i^L \left(P_i - P_i^{SAT}\right)}{RT}\right)$$

and an EoS for the mixture and a G^E model are required. The algorithm to be solved is as follows:

1) T, P and z_i are known, Raoult's law is applied for an initial approximate estimation of x_i, y_i and L/F $\varphi_i^{SAT}, P_i^{SAT}$ and $\exp\left(\frac{V_i^L\left(P_i - P_i^{SAT}\right)}{RT}\right)$ are thus calculated.
2) By EoS and the G^E model $\hat{\varphi}_i^V, \gamma_i$ e $k_i = \frac{\gamma_i f_i^L}{\hat{\varphi}_i^V y_i}$ can be calculated.
3) The objective function $f_{ob} = \sum_i \frac{z_i(1-k_i)}{k_i + \frac{L}{F}(1-k_i)}$ is designed.
4) $f_{ob} = 0$?
   If not, a new value for L/F is assumed, following the criterion:

   $f_{ob} > 0 \Rightarrow L/F \uparrow$
   $f_{ob} < 0 \Rightarrow L/F \downarrow$

   and step 3 is repeated.

   If yes, it is possible to proceed to step 5.

5) x_i and y_i are calculated:

$$x_i = \frac{z_i}{k_i + \frac{L}{F}(1-k_i)}, \quad y_i = x_i k_i$$

6) If x_i, y_i and L/F are different in comparison to the previous iteration, step 2 has to be repeated with the new calculated values for x_i, y_i e L/F.
   If x_i, y_i and L/F are the same, then calculations are completed.

A.5. Application

The aim is to realize a suitable model to predict liquid phase composition from T, P and z_i (composition for the whole system). The system is composed of: CO_2, O_2, H_2, MeOH. We consider a catalytic reaction with H_2O e H_2O_2 formation. Specifically, what we want to calculate is H_2 concentration in the liquid phase.
Reactor volume is 100 ml, and temperature is set at -10°C.
A first approximation is to consider that H_2O e H_2O_2 don't exit the liquid phase: their presence can be therefore neglected. This assumption is justified by the low temperature and the very small amount of those species.
For those species taken into account, their total amount is:

CO_2 = 0,2 moles
O_2 = 0,03 moles
MtOH = 1,2343 moles
H_2 = can be varied from 0,009 to 0,003 moles, with a step variation of 0,001 moles

A.5.1. The thermodynamic model

The first thing to be chosen is the equilibrium model. Pressure conditions, and the presence of polar species (methanol) and hydrogen, make the system a non-ideal one.
A $\varphi - \varphi$ model is chosen, and various equations of state have been tested. Best results are achieved with Peng-Robinson EoS, therefore all the calculations reported below are based on this model. Software aided calculations are performed, with "Aspen Property Excell Calculator", which is an Aspen tool.

Peng-Robinson equation of state is:

$$P = \frac{RT}{V-b} - \frac{a}{V(V+b)+b(V-b)} \quad (1)$$

where P is the pressure, R the gas constant, T the temperature and V the molar volume.

In relation to parameters *a* and *b*, for the attraction parameter *a* a quadratic mixing rule is chosen (Eq.3), while a linear one is used for *b* (Eq.2).

$$b = \sum_{i=1}^{NC} x_i b_i \quad (2)$$
$$a = \sum_{i=1}^{NC} \sum_{j=1}^{NC} x_i x_j \sqrt{a_i a_j} \left(1 - k_{ij}\right) \quad (3)$$
$$k_{ij} = k_{ji},\ k_{ii} = 0$$

Parameters for the pure species are calculated as follows:

$$b_i = 0.07780 \frac{R T_{C,i}}{P_{C,i}}$$
$$a_i = \alpha_i \cdot 0.45724 \frac{R^2 T_{C,i}^2}{P_{C,i}} \quad (4)$$

where $T_{c,i}$ and $P_{c,i}$ are critical temperature and pressure, respectively, of the *i* component. Parameter α_i is a function of temperature:

$$\alpha_i(T) = \left[1 + m_i\left(1 - T_{r,i}^{1/2}\right)\right]^2 \quad (5)$$
$$m_i = 0.37464 + 1.54226\omega_1 - 0.26992\omega_i^2 \quad (6)$$

with ω_i and $T_{r,i}$ being the acentric factor (Table A.1) and reduced temperature respectively, of the i component.

Component	ω_i
CO_2	0.22934
O_2	0.0222
H_2	-0.219
MeOH	0.5625

Table A.1: Acentric factors used for equilibrium calculations (Source: NIST)

However, for light gases at high reduced temperature ($T_{r,i}$>5), Eq. 5 is not valid: molecular attraction should disappear at high temperature and α decrease

asymptotically to 0. Therefore, for higher temperature than critic temperature, Boston-Mathias equation is used:

$$\alpha_i(T) = \left[\exp\left[c_i\left(1 - T_{r,i}^{d_i}\right)\right]\right]^2$$
$$d_i = 1 + \frac{m_i}{2} \qquad (7)$$
$$c_i = 1 - \frac{1}{d_i}$$

m_i is always calculated through Eq.6.

Binary interaction parameters k_{ij} are regressed from vapor-liquid equilibrium data in the literature (all the references are reported in Table A.2). When binary data are not available for the temperature of interest, parameters are expressed as a function of T and then interpolated or extrapolated.

Components	T [K]	Refs
CO_2 - H_2	278 - 290.15 - 298.15	1
MeOH - H_2	298.15 - 323.15 - 373.15	2
MeOH - CO_2	273.15 - 290	3
	258	4
	313 - 320.15	5
O_2 - CO_2	223.15 / 273.15	6
MeOH - O_2	298.34 - 323.32 - 348.29	7

Table A.2. Vapor-liquid equilibrium binary data from the literature, used to regress binary interaction parameters.

Figure A.1 shows regressed parameters at various temperatures, with the corresponding interpolation curves.

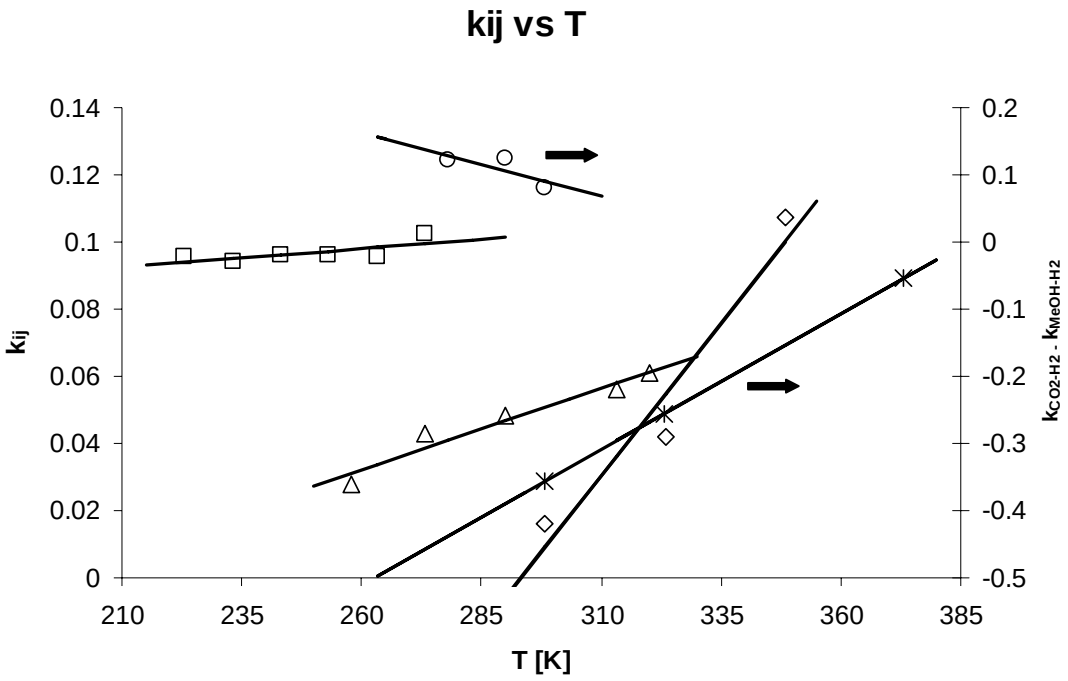

*Fig. A.1. Binary interaction parameters: □ CO_2-O_2, ○ H_2-CO_2, ◊ O_2-MeOH, Δ CO_2-MeOH, * H_2-MeOH.*

Interpolation polynomials are as follows:

$$k_{CO_2-MeOH} = -9.2512 \cdot 10^{-2} + 4.8027 \cdot 10^{-4} \cdot T \quad (8)$$

$$k_{H_2-MeOH} = -1.5550 + 4.0228 \cdot 10^{-3} \cdot T \quad (9)$$

$$k_{CO_2-H_2} = 0.6568 - 1.9000 \cdot 10^{-3} \cdot T \quad (10)$$

$$k_{O_2-MeOH} = -0.5338 \cdot + 1.8200 \cdot 10^{-3} \cdot T \quad (11)$$

$$k_{CO_2-O_2} = 6.9677 \cdot 10^{2} + 1.0912 \cdot 10^{-4} \cdot T \quad (12)$$

where T is the temperature in [K].

It is assumed that no interaction occurs between O_2 and H_2 which corresponds to $k_{H_2O_2} = 0$.

Vapor-liquid equilibrium binary data are then compared to the results from the thermodynamic model implemented. Figures A.2-A.6 show these results.

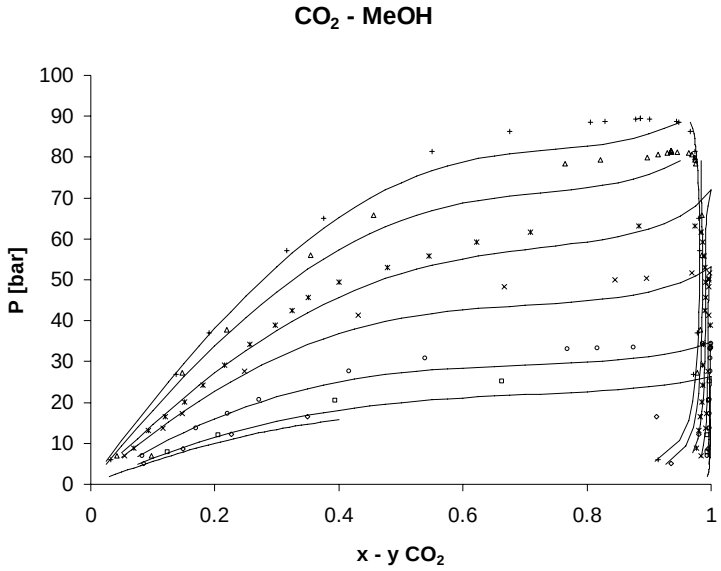

*Fig. A.2. Vapor-liquid equilibrium for CO_2-MeOH mixture: — Peng-Robinson, ◊ 258 K, □ 263.15 K, ○ 273.15 K, × 290 K, * 303.15 K, Δ 313.15 K, + 320.15 K*

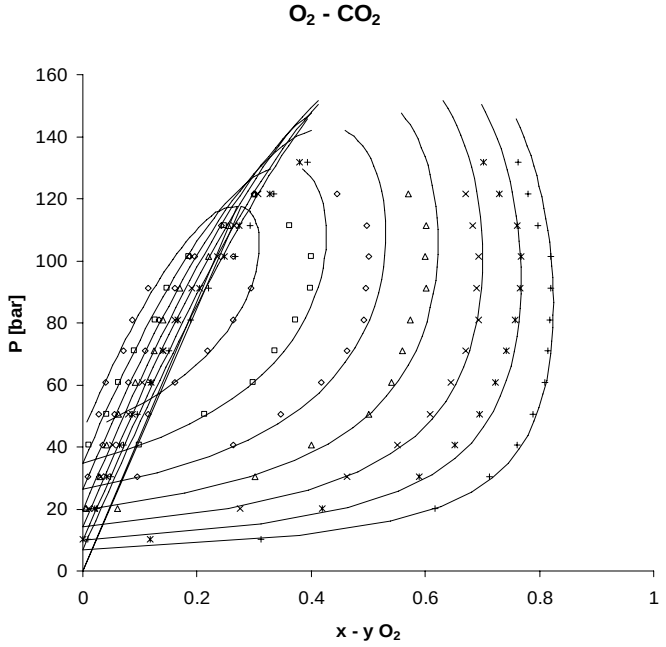

*Fig. A.3. Vapor-liquid equilibrium for O_2-CO_2mixture: — Peng-Robinson, + 223.15 K, * 233.15 K, × 243.15 K, Δ 253.15 K, ◊ 263.15 K, □ 273.15 K, ○ 283.15 K*

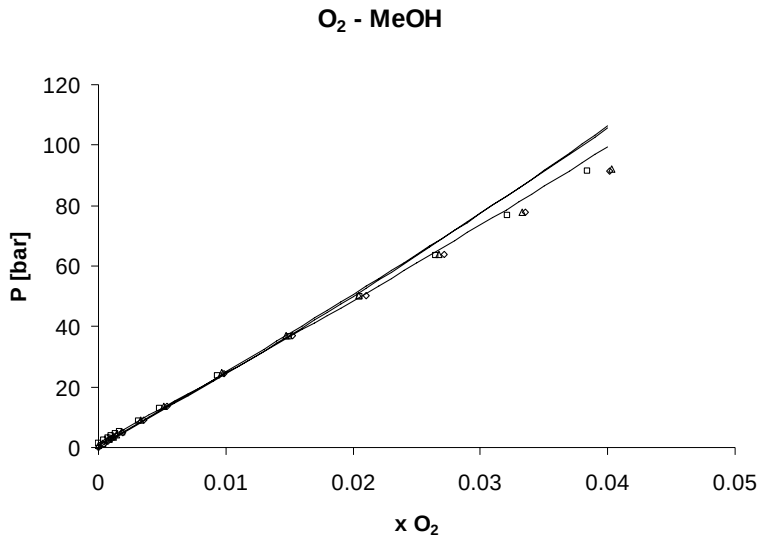

Fig. A.4. Vapor-liquid equilibrium for O_2-MeOH mixture: — Peng-Robinson, □ 248.29 K , ◊ 298.34 K, Δ 323.23 K, ○ 283.15 K

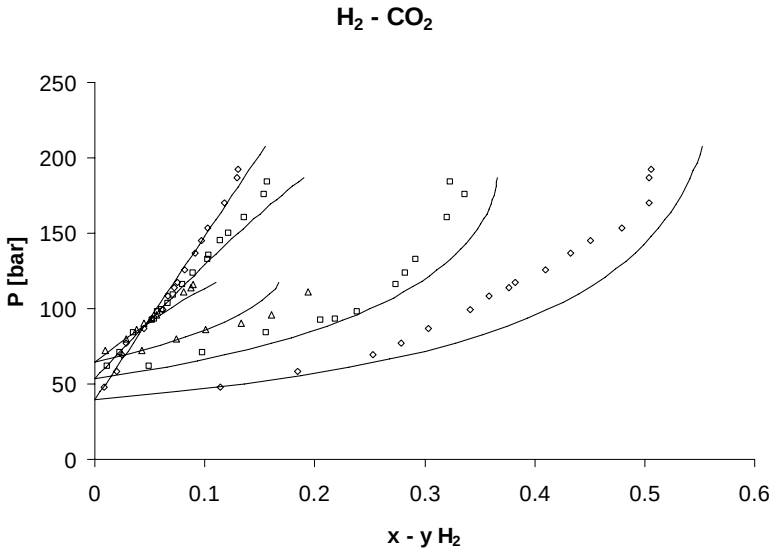

Fig. A.5. Vapor-liquid equilibrium for H_2-CO_2mixture: — Peng-Robinson, ◊ 278 K, □ 290.15 K, Δ 298 K

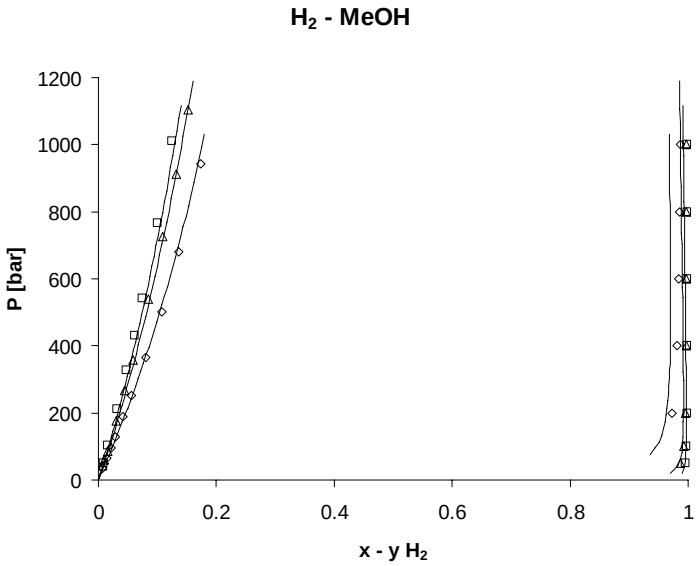

Fig. A.6. Vapor-liquid equilibrium for H_2-MeOH mixture: — Peng-Robinson, ◊ 373.15 K, Δ 323.15 K, □ 298.15 K

It is noticeable how a generally good prediction of binary systems is achieved. However, some imperfections are present when Peng-Robinson equation is applied to predict phase equilibrium for CO_2-MeOH system, especially for high pressure conditions and high CO_2 molar ratios in the liquid phase (Figure A.2). Some flaws are also noticeable for H_2-CO_2 system, in relation to H_2 composition in the gas phase (Figure A.5). This may lead to some difficulties when predicting multicomponent phase equilibrium at high pressure.

To verify the quality of the equation of state predictions, this model is tested with vapor-liquid equilibrium data for ternary CO_2-O_2-MeOH[9] and CO_2-H_2-MeOH[10,11] mixtures from the literature. Data comparison is carried out through the percentage of average absolute relative deviation (%AARD):

$$\%AARD_i = \frac{100}{ND}\sum_{d=1}^{ND}\frac{\left|x_{i,\exp}^{d} - x_{i,calc}^{d}\right|}{x_{i,\exp}^{d}} \quad (13)$$

where ND is the number of ternary data, while $x_{i,\exp}^{d}$ e $x_{i,calc}^{d}$ are experimental and calculated composition respectively, of the i component. Starting from vapor phase

composition, for each experimental ternary datum liquid phase composition is calculated; thus %AARD is calculated for liquid phase composition only of every *i* component.
Table A.3 reports binary parameters used for calculations.

Components	T [K]	k_{ij}	Comment
CO_2-MeOH	313	0.0579	Interpolated
	278	0.0410	Interpolated
O_2-MeOH	313	0.0361	Interpolated
O_2-CO_2	313	0.1038	Extrapolated
H_2-CO2	313	0.0618	Extrapolated
	278	0.1568	Extrapolated
H_2-MeOH	313	-0.2953	Interpolated
	278	-0.4367	Extrapolated

Table 3. Binary interaction parameters for CO_2-O_2-MeOH (@ T=313.15 K) and CO_2-H_2-MeOH (@ T=313.15 and 278 K) systems.

Figure A.6 shows the comparison between vapor-liquid equilibrium experimental and calculated data for CO_2-O_2-MeOH system at a temperature of 313.15 K. In Table A.4 liquid phase composition is reported, while Table A.5 presents the corresponding calculated %AARD.

T [K]	P [bar]	$x_{CO2,exp}$	$x_{O2,exp}$	$x_{MeOH,exp}$	$x_{CO2,calc}$	$x_{O2,calc}$	$x_{MeOH,calc}$
313.15	15.60	0.040	0.003	0.957	0.044	0.003	0.953
313.35	30.10	0.080	0.005	0.915	0.089	0.006	0.905
312.95	53.40	0.140	0.011	0.849	0.160	0.012	0.829

Table A.4. Experimental[9] and calculated liquid phase composition for CO_2-O_2-MeOH mixture, at a temperature of 313.15 K.

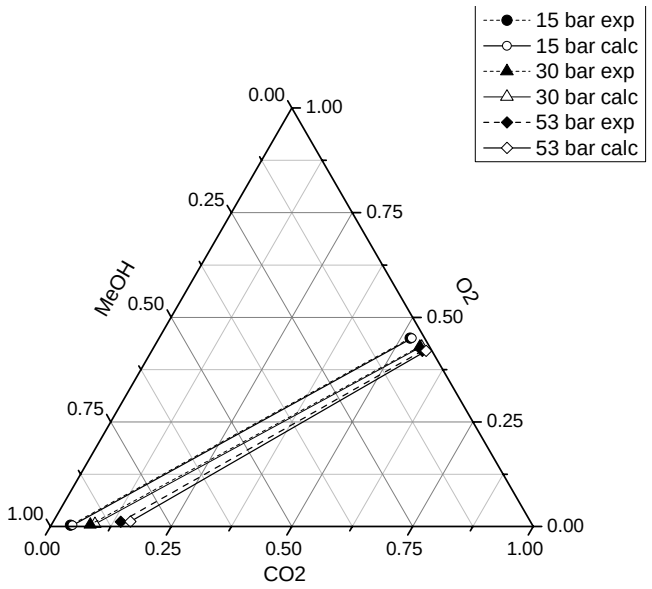

Fig. A.6. Vapor-liquid equilibrium for CO_2-O_2-MeOH system (T = 313.15 K, P = 15, 30 and 53 bar): comparison between Peng-Robinson and experimental data[9].

	%AARD		
T [K]	x_{CO2}	x_{O2}	x_{MeOH}
313.15	11.99	10.05	1.32

Table A.5. %AARD for CO_2-O_2-MeOH mixture at a temperature of 313.15 K.

Figures A.7 and A.8 show the comparison between experimental and calculated vapor-liquid equilibrium data for CO_2-H_2-MeOH system, at a temperature of 313.15 and 278 K, respectively. In Table A.6 liquid phase composition is reported, while Table A.7 presents the corresponding calculated %AARD.

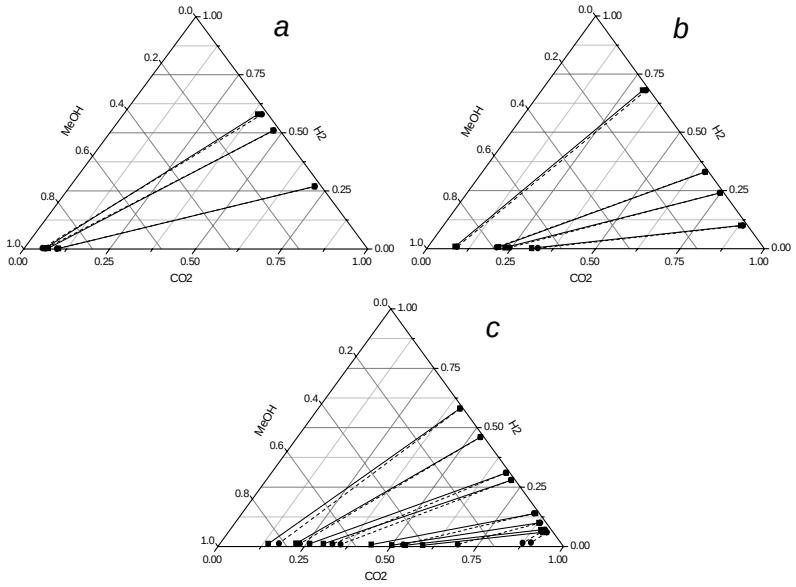

Fig. A.7. Vapor-liquid equilibrium for CO_2-H_2-MeOH system (T = 313.15 K): a) P = 25 bar, b) P = 60 bar, c) P = 90 bar; --- Peng-Robinson, — experimental[9].

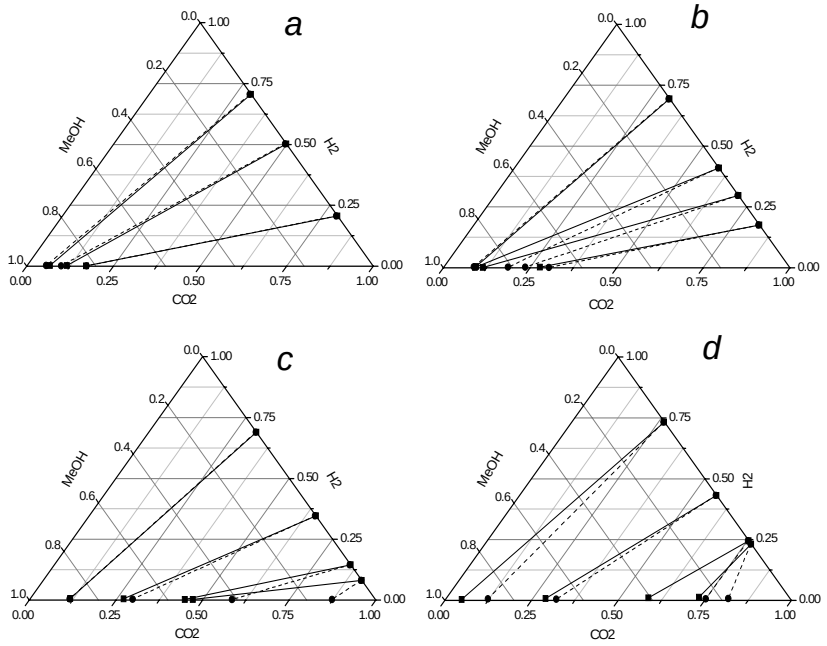

Fig. A.8. Vapor-liquid equilibrium for CO_2-H_2-MeOH system (T=278 K): a) P=20 bar, b) P=30 bar, c) P=39.5 bar, d) P=50 bar; --- Peng-Robinson, — experimental[10].

T [K]	P [bar]	$x_{CO2,exp}$	$x_{H2,exp}$	$x_{MeOH,exp}$	$x_{CO2,calc}$	$x_{H2,calc}$	$x_{MeOH,calc}$
278	20	0.065	0.0033	0.9317	0.0553	0.0025	0.9421
		0.1142	0.0028	0.883	0.0983	0.0019	0.8998
		0.1701	0.0012	0.8287	0.1721	0.0009	0.8270
278	30	0.0904	0.0019	0.9077	0.1849	0.0027	0.8124
		0.0916	0.0052	0.9032	0.0861	0.0039	0.9100
		0.1134	0.0015	0.8851	0.2351	0.0021	0.7628
		0.2779	0.0022	0.7199	0.3038	0.0014	0.6948
278	39.5	0.1143	0.007	0.8787	0.1143	0.0052	0.8805
		0.2697	0.0052	0.7251	0.2969	0.0035	0.6995
		0.4478	0.0031	0.5491	0.5837	0.0025	0.4138
		0.471	0.002	0.527	0.8725	0.0027	0.1249
278	50	0.0466	0.0046	0.9488	0.1211	0.0070	0.8719
		0.2867	0.0086	0.7047	0.3192	0.0057	0.6752
		0.5828	0.0101	0.4071	0.7493	0.0071	0.2436
		0.7272	0.0134	0.2594	0.8141	0.0079	0.1780
313	25	0.06	0.0039	0.9361	0.0532	0.0031	0.9437
		0.07	0.0034	0.9266	0.0617	0.0027	0.9356
		0.1	0.0019	0.8981	0.0960	0.0015	0.9025
313	60	0.08	0.0092	0.9108	0.0868	0.0086	0.9046
		0.21	0.0067	0.7833	0.2048	0.0054	0.7897
		0.23	0.0052	0.7648	0.2435	0.0044	0.7521
		0.31	0.0022	0.6878	0.3281	0.0024	0.6696
313	90	0.14	0.012	0.848	0.1704	0.0130	0.8166
		0.22	0.0127	0.7673	0.2316	0.0119	0.7565
		0.26	0.0118	0.7282	0.3262	0.0102	0.6636
		0.3	0.012	0.688	0.3504	0.0099	0.6397
		0.44	0.0084	0.5516	0.5321	0.0085	0.4594
		0.5	0.0064	0.4936	0.6897	0.0098	0.3005
		0.54	0.0058	0.4542	0.8747	0.0157	0.1097
		0.59	0.0054	0.4046	0.8979	0.0164	0.0857

Table A.6. Experimental and calculated liquid phase composition for CO_2-H_2-MeOH mixture at a temperature of 313.15[9] and 278 K[10]

	%AARD		
T [K]	x_{CO2}	x_{H2}	x_{MeOH}
313.15	25.30	38.83	19.00
278	19.49	38.75	15.97

Table A.7. %AARD calculated for CO_2-H_2-MeOH mixture at a temperature of 313.15 and 278 K.

For both systems, liquid phase composition as calculated by the Peng-Robinson EoS, doesn't perfectly fit experimental data for every condition; however this can be attributed to the error at the highest pressures. Indeed for CO_2-H_2-MeOH system, the worst predictions are at 50 e 90 bar and for high CO_2 concentrations (Figures A.7 and A.8), and similar considerations can be made for CO_2-O_2-MeOH system (Figure A.6, P=50 bar). A possible explanation may be searched in binary data interpolation, particularly for high CO_2 concentrations in the liquid phase of the CO_2-MeOH system, where Peng-Robinson equation doesn't perfectly predict vapor-liquid equilibrium.
However, even though CO_2 concentration in the liquid phase is not perfectly predicted, H_2 and O_2 concentrations are of major interest for the purpose of this study, and those are satisfactory predicted. Specifically, for pressure conditions around 20 bar, and for low CO_2 concentrations in the liquid phase (reaction conditions of this study), AARD relative to x_{CO2} and x_{O2} is around 15%.
Thus, for vapor-liquid equilibrium calculation of CO_2-O_2-MeOH-H_2 system at 263.15 K, binary parameters reported in Table A.8 and derived from Eq. 8-12 are used.

Components	T [K]	k_{ij}	Comment
CO_2-MeOH	263.15	0.0339	Interpolated – Eq. 8
O_2-MeOH	263.15	-0.0549	Extrapolated – Eq. 11
O_2-CO_2	263.15	0.0984	Interpolated – Eq.12
H_2-CO_2	263.15	0.1568	Extrapolated – Eq. 10
H_2-MeOH	263.15	-0.4964	Extrapolated – Eq. 9

Table 8. Binary interaction parameters for CO_2-O_2-MeOH-H_2 system @ T=263.15 K.

The model is now complete, and can be used to predict the system composition at equilibrium, following the algorithm for calculations reported in Figure A.9.

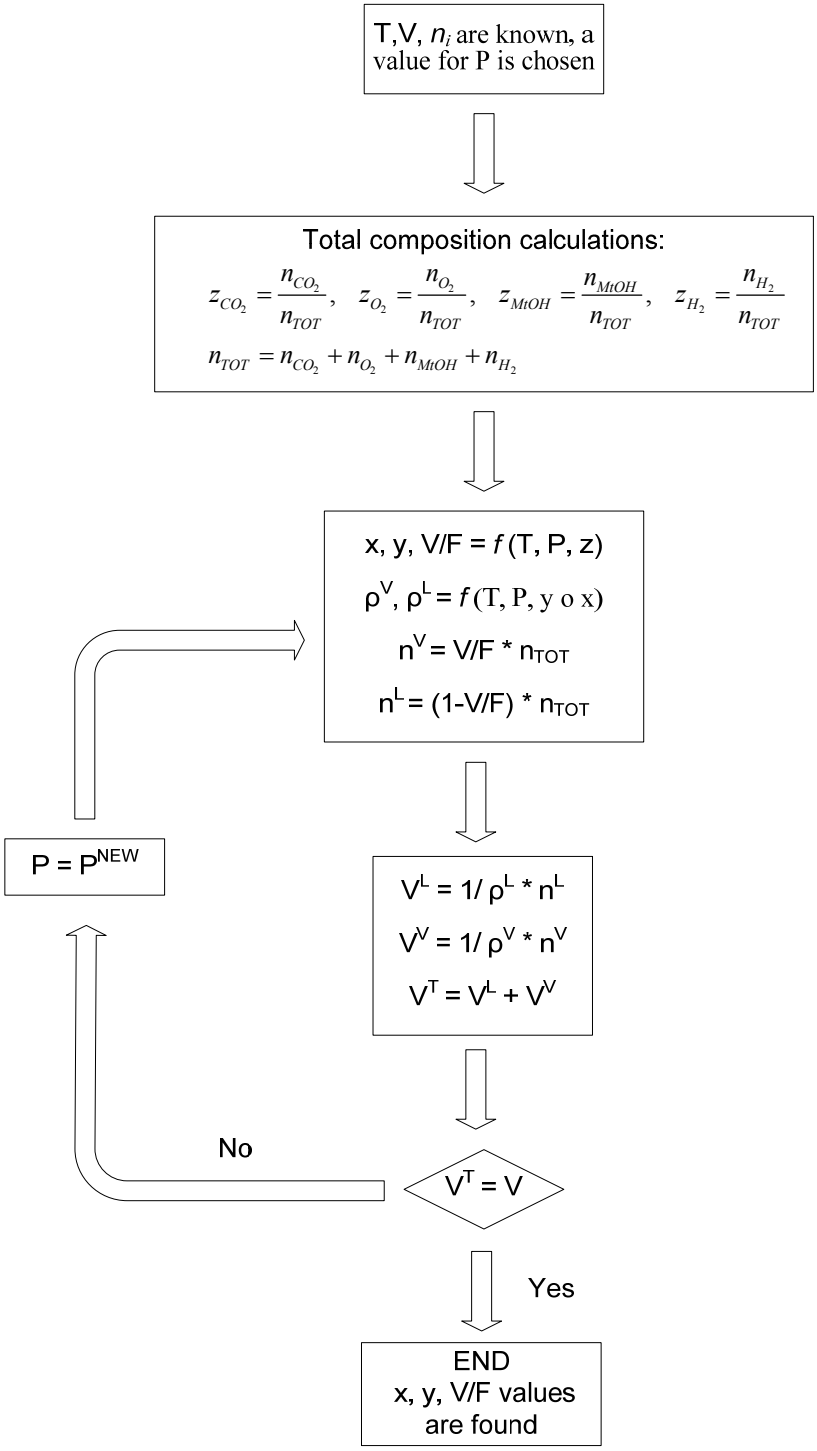

Fig. A.9. Algorithm for calculating CO_2-O_2-MeOH-H_2 compositions at equilibrium.

A.4 References

[1] Bezanehtak, K.; Combes, G. B.; Dehghani, F.; Foster, N. R.; Tomasko, D. L. Vapor-liquid equilibrium for binary systems of carbon dioxide plus methanol, hydrogen plus methanol, and hydrogen plus carbon dioxide at high pressures. *J. Chem. Eng. Data* 2002, *47*, 161-168.

[2] Brunner, E.; Hultenschmidt, W.; Schlichtharle, G. Fluid Mixtures at High Pressure. 4. Isothermal Phase Equilibria in Binary Mixtures Consisting of (Methanol + Hydrogen or Nitrogen or Methane or Carbon Monoxide or Carbon Dioxide). *J. Chem. Thermodyn.* 1987, *19*, 273-291.

[3] Hong J.H., Kobayashi R., Vapor—liquid equilibrium studies for the carbon dioxide-methanol system. *Fluid Phase Equilibria*, 1988, 41, 269-276.

[4] Bass D. G., J. K. Ferrell, R. W. Rousseau , The Solubility of Acid Gases in Methanol. - Final rept. Oct 76-Sep 78. *Technical report*, 1979,1-40.

[5] Seung Nam Joung, Chang Woo Yoo, Hun Yong Shin, Sun Young Kim, Ki-Pung Yoo, Chul Soo Lee, Wan Soo Huh, Measurements and correlation of high-pressure VLE of binary CO2–alcohol systems (methanol, ethanol, 2-methoxyethanol and 2-ethoxyethanol). *Fluid Phase Equilibria*, 2001, 185, 219-230

[6] Fredenslund, A., and G. A. Sather, ‘‘Gas-Liquid Equilibrium of the Oxygen-Carbon Dioxide System,’’ *J. Chem. Eng. Data*, 1970, 15, 17.

[7] Fischer, K.; Wilken, M. Experimental determination of oxygen and nitrogen solubility in organic solvents up to 10 MPa at temperatures between 298 and 398 K. *J. Chem. Thermodyn.*, 2001, *33*, 1285-1308.

[8] Zulema K. Lopez-Castillo, Sudhir N. V. Aki, Mark A. Stadtherr, Joan F. Brennecke, Enhanced Solubility of Oxygen and Carbon Monoxide in CO_2-Expanded Liquids, *Ind. Eng. Chem. Res.*, 2006, 45, 5351-5360.

[9] Zulema K. Lopez-Castillo, Sudhir N. V. Aki, Mark A. Stadtherr, Joan F. Brennecke, Enhanced Solubility of Hydrogen in CO_2-Expanded Liquids, *Ind. Eng. Chem. Res.*, 2008, 47, 570-576.

[10] Bezanehtak, K.; Dehghani, F.; Foster, N. R. Vapor-Liquid Equilibrium for the Carbon Dioxide + Hydrogen + Methanol Ternary System. *J. Chem. Eng. Data*, 2004, *49*, 430-434.